

THESIS

NORTH-NORTHWEST SHORTENING ACROSS LARAMIDE STRUCTURES
IN THE SOUTHEASTERN UINTA MOUNTAINS, COLORADO AND UTAH

Submitted by

Joe Denny Gregson

Department of Earth Resources

In partial fulfillment of the requirements

for the Degree of Master of Science

Colorado State University

Fort Collins, Colorado

Fall, 1994

COLORADO STATE UNIVERSITY

September 28, 1994

WE HEREBY RECOMMEND THAT THE THESIS PREPARED UNDER OUR SUPERVISION BY JOE D. GREGSON ENTITLED NORTH-NORTHWEST SHORTENING ACROSS LARAMIDE STRUCTURES IN THE SOUTHEASTERN UINTA MOUNTAINS, COLORADO AND UTAH BE ACCEPTED AS FULFILLING IN PART REQUIREMENTS FOR THE DEGREE OF MASTER OF SCIENCE.

Committee on Graduate Work

[Redacted]

[Redacted]

[Redacted]

[Redacted]

Adviser

[Redacted]

Department Head

ABSTRACT OF THESIS

NORTH-NORTHWEST SHORTENING ACROSS LARAMIDE STRUCTURES IN THE SOUTHEASTERN UINTA MOUNTAINS, COLORADO AND UTAH

The Rocky Mountain foreland consists of a series of anastomosing structural arches that vary greatly in trend. Several previous studies of Laramide faulting document predominantly northeast-southwest shortening that is independent of arch orientation. Laramide faults and folds in the southeastern Uinta arch, however, suggest a north-northwest shortening direction.

Laramide structures in the Dinosaur National Monument area were examined to investigate the possibility of north-northwest shortening. Eigenvector, M-plane, conjugate fracture, octahedra, and direct stress inversion analyses of 1206 slickensided minor faults give slip and σ_1 trends averaging N22°W. Although the slip and σ_1 trends are nearly perpendicular to individual structural trends, suggesting local control of stress and strain fields by the structures, a consistent component of northwesterly slip indicates north-northwest compression.

To test this unusual Laramide σ_1 direction, a 3-D restoration of the compressional Yampa graben area was

constructed. The optimum restoration gave similar slip trends (N48°W-N25°W) with clockwise rotations of 1° to 4° for the deformed blocks.

The north-northwest shortening and σ_1 trends in the Dinosaur area are highly oblique to the northeasterly trends elsewhere in the foreland. Hypotheses explaining the σ_1 and shortening trends in the study area include: 1) north-south contraction from bending in the thrust slab over a south-dipping listric ramp during northeasterly thrusting of the range, 2) right lateral shear due to the complex transition in structural vergence between the northeast-directed Uinta arch and southwest-directed White River uplift, and/or 3) eastward translation of the Uinta structural block due to impingement of the Sevier thrusts from the west. A combination of hypotheses 1 and 2 appear to best explain the observations and are favored as more proximal deformation mechanisms. The diverse structural trends in the study area probably resulted from both local and regional Laramide stresses, neither of which can be ignored in kinematic studies of foreland deformation.

Joe D. Gregson
Department of Earth Resources
Colorado State University
Fort Collins, CO 80523
Fall 1994

ACKNOWLEDGEMENTS

I want to express my appreciation for the funding that made my graduate study and thesis possible. The College of Natural Resources and Department of Earth Resources provided generous support through a Colorado Graduate Fellowship, Lary Kent Burns Memorial Scholarship, and Oscar and Isabel Anderson Graduate Fellowship. Field work and research support came from the Petroleum Research Fund of the American Chemical Society, the Geological Society of America, Four Corners Geological Society, Colorado Science Society, and Chevron Corporation. The cooperation of the staff at Dinosaur National Monument was invaluable.

I wish to thank my adviser, Dr. Eric Erslev, for this unique research opportunity and the critical insight to complete this project. Much appreciation also goes to the Earth Resources staff and my fellow students for their help, interest, and moral support. My heartfelt thank you goes out to my parents, Thelma and Harmon Gregson, who are not here to witness this event, but gave their all for me to have this opportunity. Most importantly, I wish to thank my lovely wife, Janet, for standing by me, listening to me, and sharing my dreams.

TABLE OF CONTENTS

	<u>Page No.</u>
Chapter 1 Introduction	1
Chapter 2 Geological Setting	8
Regional Tectonics	8
Model Predictions	10
Laramide Structure of the Uinta Arch	11
Structural Evolution of the Uinta Arch	14
Dinosaur National Monument Study Area	18
Stratigraphic Summary	19
Chapter 3 Methods	22
Field Methods	22
Minor Fault Data	25
Minor Fault Analysis Methods	26
Eigenvectors	27
Conjugate Fracture Method	28
M-Plane Method	29
Right (PT) Dihedra Method	29
Octahedra Method	31
Direct Inversion Method	31
Chapter 4 Field Obs. and Analyses of Minor Fault Data	34
Split Mountain	35
Split Mountain South - Dakota Hogback	36
Split Mountain South - Red Wash	38
Split Mountain Northwest	40
Split Mountain North - Little Rainbow Park	43
Section Ridge Anticline	45
Cliff Ridge Northeast	45
Cliff Ridge Southwest	47

Willow Creek Fault - Blue Mountain	49
Island Park Fault	52
Jones Hole North	52
Jones Hole South	54
Island Park South	55
Mitten Park Fault	58
Mitten Park Northeast - Warm Springs Monocline	59
Mitten Park - North of Green River	61
Mitten Park - South of Green River	63
Mitten Park Southwest	65
Red Rock Anticline	67
Yampa Monocline and Fault	69
Yampa Monocline West	70
Yampa Fault - Hell's Canyon	72
Hell's Canyon West	73
Hell's Canyon East	75
Johnson Draw	75
Yampa Fault East	78
Wolf Creek Fault - Mud Springs Monocline	80
Wolf Creek Fault	81
Cross Mountain	83
Chapter 5 Composite Paleostress Analyses	86
Slickenlines E_1 Stress Solutions	86
M-Plane Stress Solutions	88
Conjugate Stress Solutions	91
Combined M-Plane and Conjugate Stress Solutions	91
Direct Stress Inversion	91
Octahedra Method Stress Composites	95
Interpreted Stress Solutions	95
Comparison of Structural and Slip Orientations .	98
Discussion	101
Chapter 6 Structural Surface Modeling	103
Computer-Aided Structural Modeling	103
Data Acquisition and Preparation	105
Data Entry and Spatial Attribution	107

Preprocessing, Modeling, and Graphics Output . . .	107
Chapter 7 Three-Dimensional Restoration	112
Criteria for 3-D Restoration	112
Method	113
Application to the Yampa Graben Structure . . .	114
Discussion	127
Chapter 8 Tectonic Interpretations	129
Hypothesis 1: Bending in the Thrust Slab	130
Hypothesis 2: Interplay in Laramide Structures	131
Hypothesis 3: Interaction with the Thrust Belt .	134
Discussion	135
Implications for Laramide Tectonic Models . . .	135
Chapter 9 Discussion and Conclusions	137
Suggestions for Future Work	139

LIST OF FIGURES

		<u>Page No.</u>
Figure 1.1	Rocky Mountain Foreland of Wyoming . . .	2
Figure 1.2	Structural Location Map	3
Figure 1.3	Block Model of the Laramide Orogeny . .	4
Figure 1.4	Laramide Structure - Eastern Uinta Arch	6
Figure 2.1	Tectonic Map of the Uinta Mountains Area	13
Figure 2.2	Compound Structure of the Uinta Arch . .	14
Figure 2.3	Laramide Structure of Northwest Colorado	15
Figure 2.4	N-S Cross Section - Eastern Uinta Arch .	17
Figure 2.5	Stratigraphic Diagram - Eastern Uinta Mtns.	20
Figure 2.6	Stratigraphic Column of the Study Area .	21
Figure 3.1	Slickenline Location and Orientation Data	23
Figure 3.2	Minor Fault Surface Orientation Data . .	24
Figure 3.3	Riedel Shear Morphology	25
Figure 3.4	Octahedra Method	32
Figure 3.5	Direct Stress Inversion Method	33
Figure 4.1	Dinosaur Area Paleostress Summary . . .	35
Figure 4.2	Split Mountain South - Dakota Hogback .	37
Figure 4.3	Split Mountain South - Red Wash	39
Figure 4.4	Split Mountain Northwest	41
Figure 4.5	Split Mountain - Little Rainbow Park . .	44
Figure 4.6	Cliff Ridge Northeast	46
Figure 4.7	Cliff Ridge Southwest	48
Figure 4.8	Blue Mountain South - Willow Creek Fault	50
Figure 4.9	Jones Hole North	53
Figure 4.10	Jones Hole South	56
Figure 4.11	Island Park South	57
Figure 4.12	Mitten Park Northeast - Warm Springs . .	60
Figure 4.13	Mitten Park - North of Green River . . .	62
Figure 4.14	Mitten Park - South of Green River . . .	64

Figure 4.15	Mitten Park Southwest	66
Figure 4.16	Red Rock Anticline	68
Figure 4.17	Yampa Monocline	71
Figure 4.18	Hell's Canyon West	74
Figure 4.19	Hell's Canyon East	76
Figure 4.20	Johnson Draw	77
Figure 4.21	Yampa Fault East	79
Figure 4.22	Wolf Creek Fault - Mud Springs Monocline	82
Figure 4.23	Cross Mountain	84
Figure 5.1	Composite Slickenline Analysis	87
Figure 5.2	Slickenline Orientation Analysis	89
Figure 5.3	Composite M-Plane Analysis	90
Figure 5.4	Composite Conjugate Fracture Analysis .	92
Figure 5.5	Combined M-Plane and Conjugate Analysis	93
Figure 5.6	Composite Stress Inversion Analysis . .	94
Figure 5.7	Composite Octahedra Analysis	96
Figure 5.8	Composite Interpreted Stresses	97
Figure 5.9	Graph of Bed Strike vs. Striae E_3 Trend	99
Figure 5.10	Graph of Structural Trend vs. Striae E_3	100
Figure 5.11	Stereonet of Actual vs. Predicted Slip	101
Figure 6.1	Location Map of the Yampa Graben Area .	104
Figure 6.2	Location of Weber Tops Elevation Data .	106
Figure 6.3	Three-Dimensional TIN Views	108
Figure 6.4	Structure Contour Map from ARC/INFO . .	110
Figure 7.1	Structural Location of Yampa Graben Area	115
Figure 7.2	Locations of Gridded Cross Sections . .	116
Figure 7.3	North-South Cross Sections	117
Figure 7.4	North-South Cross Sections	118
Figure 7.5	East-West Cross Sections	119
Figure 7.6	East-West Cross Sections	110
Figure 7.7	Structural Domain Boundaries	122
Figure 7.8	Restored Structural Domains	123
Figure 7.9	Dip-Slip Restoration	124
Figure 7.10	Oblique-Slip Restoration	126
Figure 7.11	Final Restoration with Paleostresses . .	128

Figure 8.1 Slab Bending Model for the Uinta Arch . 130
Figure 8.2 East-West Section across Northern Colorado 132
Figure 8.3 Right-Wrench Strain Ellipse 132
Figure 8.4 Laramide Models for Study Area 133

LIST OF TABLES

		<u>Page No.</u>
Table 4.1	Split Mountain South - Dakota Hogback . .	36
Table 4.2	Split Mountain South - Red Wash	38
Table 4.3	Split Mountain Northwest	42
Table 4.4	Split Mountain - Little Rainbow Park . .	43
Table 4.5	Cliff Ridge Northeast	47
Table 4.6	Cliff Ridge Southwest	49
Table 4.7	Blue Mountain South - Willow Creek Fault	51
Table 4.8	Jones Hole North	54
Table 4.9	Jones Hole South	55
Table 4.10	Island Park South	58
Table 4.11	Mitten Park Northeast - Warm Springs . .	59
Table 4.12	Mitten Park - North of Green River . . .	61
Table 4.13	Mitten Park - South of Green River . . .	63
Table 4.14	Mitten Park Southwest	67
Table 4.15	Red Rock Anticline	69
Table 4.16	Yampa Monocline	72
Table 4.17	Hell's Canyon West	73
Table 4.18	Hell's Canyon East	75
Table 4.19	Johnson Draw	78
Table 4.20	Yampa Fault East	80
Table 4.21	Wolf Creek Fault - Mud Springs Monocline	81
Table 4.22	Cross Mountain	85
Table 5.1	Summary of Composite Stress Analyses . .	102

Chapter 1

INTRODUCTION

The Laramide foreland province of the western United States provides an excellent example of basement-involved foreland deformation. The central Rocky Mountain foreland consists of a series of anastomosing structural arches with a mean trend of N36°W in Wyoming (Fig. 1.1, Erslev, 1993). The interconnected Laramide basement arches vary greatly in orientation, however, from east-west trends (e.g., Uinta, Granite, and Owl Creek arches) to more north-south orientations (e.g., Front Range, Park-Gore Range, Rock Springs, and Douglas Creek arches) (Figs. 1.1, 1.2). Although horizontal contraction and basement-involved thrusting have been documented for Laramide structures of all trends (Berg, 1962; Gries, 1983; Stone, 1986a, 1993), differences among regional tectonic models still remain. In addition, paleomagnetic evidence for a 5° to 10° clockwise rotation of the minimally-deformed Colorado Plateau adds complexity to Laramide tectonics (Steiner, 1986; Hamilton, 1988, Bryan and Gordon, 1990). The goal of this thesis is to determine the kinematics of the diversely-trending Laramide structures in the southeastern Uinta arch and their implications for regional tectonic models.

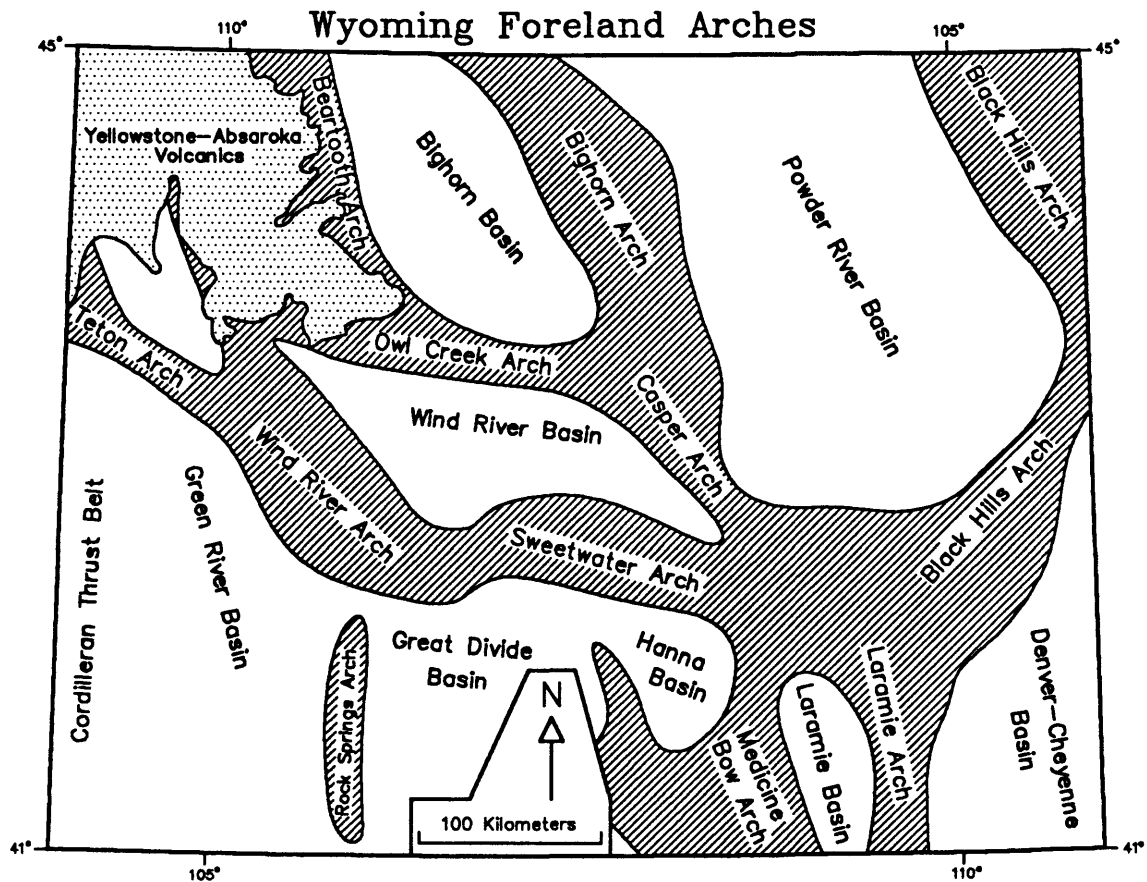


Figure 1.1 Arches and basins in Wyoming illustrating the connections between Rocky Mountain foreland culminations (from Erslev, 1993).

Brown (1988) and Erslev (1993) postulated an extended, single phase of northeast-southwest Laramide contraction that produced the diversely-trending foreland structures. In this model, dip-slip shortening occurred across northwest-trending arches while oblique- to lateral-slip occurred across structures whose trends were not perpendicular to a northeast-southwest maximum horizontal stress (σ_1) direction. This model predicts left-oblique slip for east-trending arches and right-oblique slip on

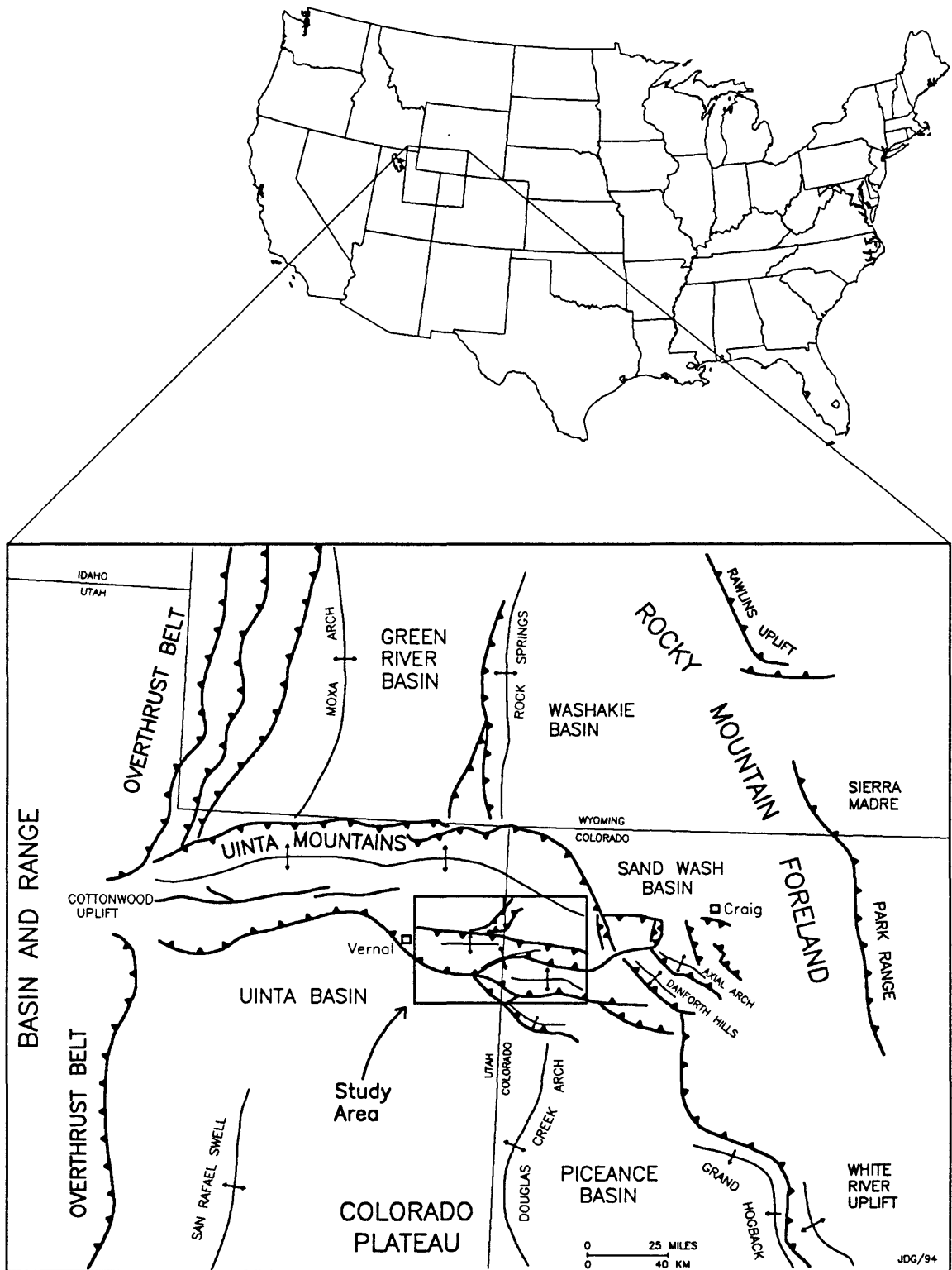


Figure 1.2 Location and generalized tectonic map of the northern Colorado Plateau margin (modified from Gries, 1983; Rowley et al., 1985; Stone, 1986a; Morel et al., 1986).

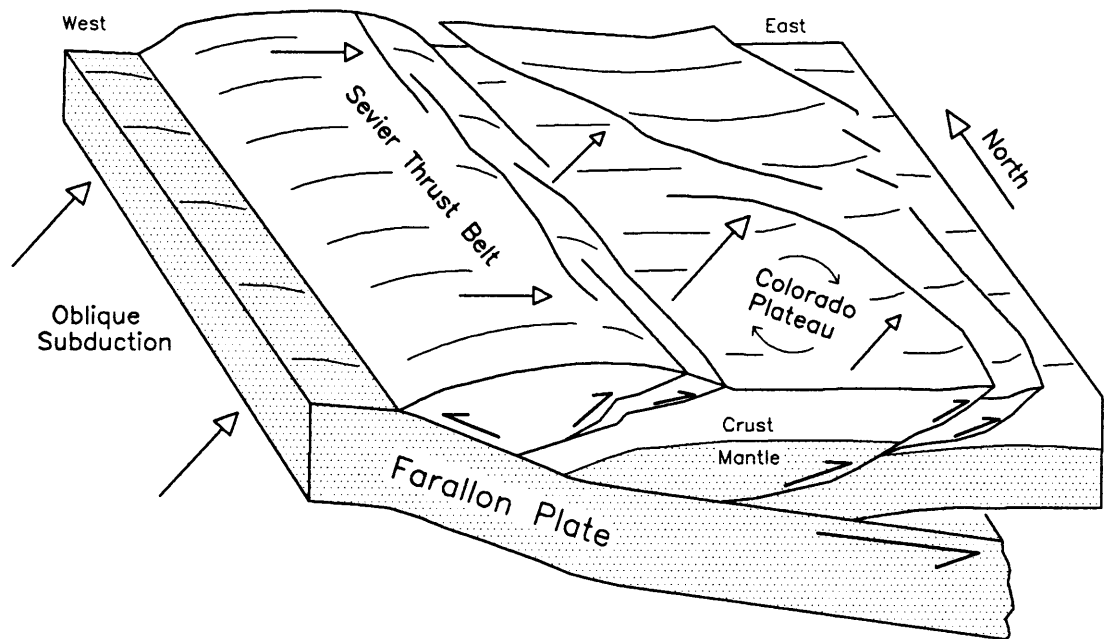


Figure 1.3 Schematic block diagram showing Laramide northeast-directed crustal detachment during low angle subduction. Variable slip on the detachment explains rotation of the Colorado Plateau (from Erslev, 1993).

north-south structures. Erslev (1993) explained rotation of the Colorado Plateau as the result of variable slip along an underlying, northeast-directed, crustal detachment with greater shortening to the north in Wyoming (Fig. 1.3; Erslev, 1993). Alternatively, Gries (1983) used drill hole and seismic evidence for large thrust overhangs on arches of all orientations to postulate 3 phases of Laramide deformation. Gries (1983) suggested that the early contraction and σ_1 direction rotated from an east-west trend in the Late Cretaceous to northeast-southwest in the mid-Laramide. A proposed north-south σ_1 in the Eocene produced

east-trending structures without oblique slip (Gries, 1983). Exposed structures on east-trending Laramide arches, such as the southeastern Uinta arch, provide an opportunity to test regional tectonic models.

Because the kinematics of east-trending arches and the role of the Colorado Plateau in Laramide tectonics are still poorly understood, exposed structures in the southeastern Uinta arch are the focus of this paper. Structures in the study area form a generally east-trending, anastomosing array of faults with two anomalous northeast-trending splays (Fig. 1.4). Field work collected minor fault orientation data from these Laramide structures in the Dinosaur National Monument area of Colorado and Utah.

To examine the local kinematics and test regional tectonic models, this study:

- 1) estimated paleostress tensor and slip vector orientation(s) using fracture geometry and stress inversion of minor fault data from 22 sites in the study area,
- 2) constructed a structure surface model on the top of the Pennsylvanian-Permian Weber Sandstone from cross sections, field reconnaissance, and mapped outcrop data, and
- 3) restored the Weber Sandstone structure surface in three dimensions to generate an independent estimate of the Laramide shortening directions(s) in the Yampa graben area,
- 4) compared paleostress and slip estimates from the minor fault analyses to the strain predicted by Laramide models.

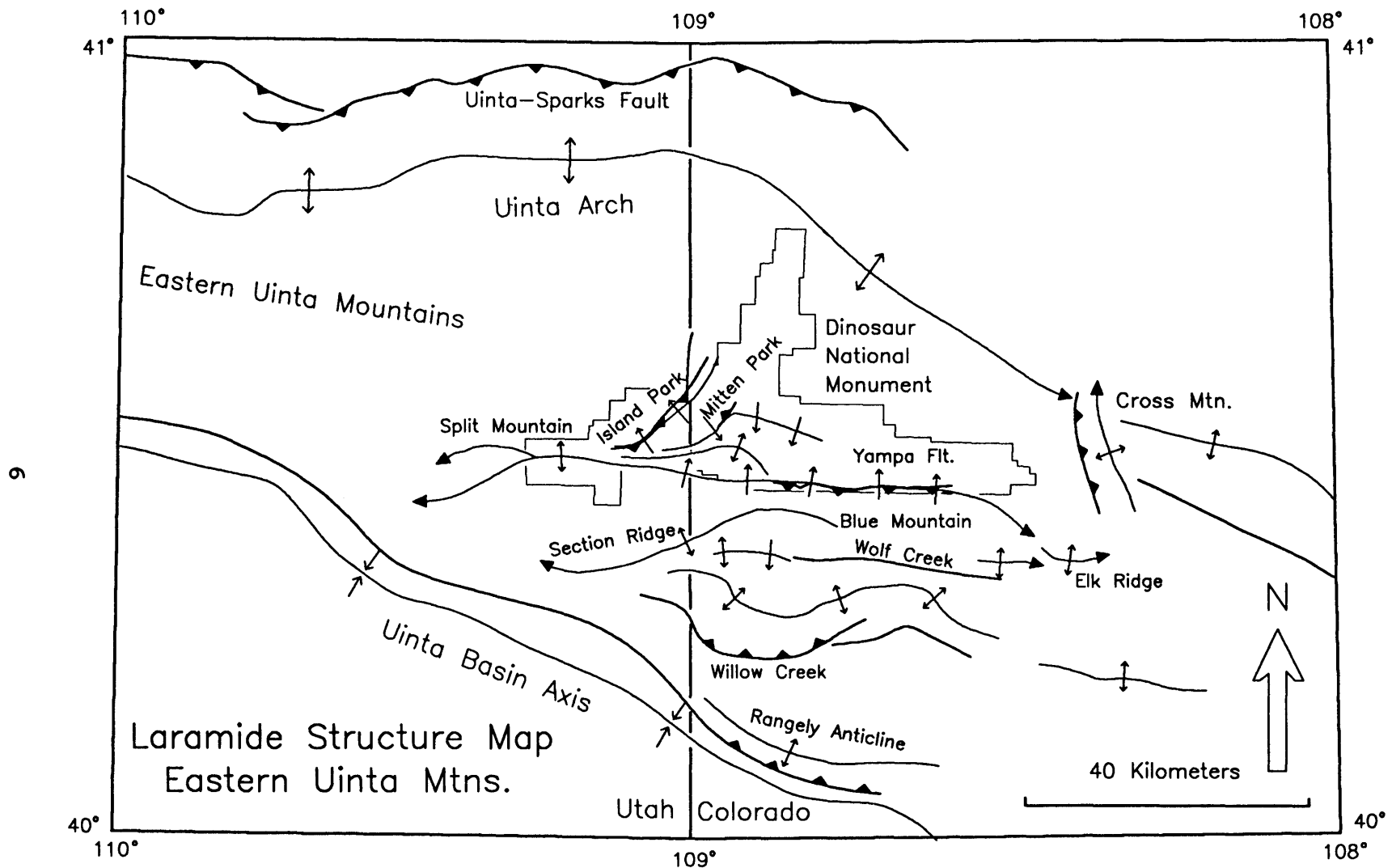


Figure 1.4 Location map of Laramide structures in the eastern Uinta arch and the Dinosaur National Monument study area.

Chapter 2

GEOLOGICAL SETTING

Regional Tectonics

Recent work has documented evidence for northeasterly slip and σ_1 trends during Laramide contraction (Robbins, 1987; Erslev, 1993; Erslev and Rodgers, 1993; Molzer, 1993; Paylor and Yin, 1993; Selvig, 1993; Wise and Obi, 1992). Molzer (1993) used slickenside and conjugate minor fault data to determine sinistral-oblique shortening oriented N37°E to N65°E along the southeastern Owl Creek arch. Paylor and Yin (1993) used fault striations, tension fractures, and fold orientations to support a model of left-oblique slip on the northern Owl Creek fault system. In addition, slickenline and fold trend data from the Beartooth arch indicates N22°E to N28°E (Wise and Obi, 1992) and N30°E to N40°E (Robbins, 1987) Laramide contraction. Slickenside data from the north-central Uinta arch near Flaming Gorge reservoir also indicate northeasterly slip and σ_1 (Gregson and Erslev, 1994).

Other single-phase models call for direct involvement of the Colorado Plateau in Laramide deformation. Based on deformation patterns in plaster analog models of transpressive strike-slip, Sales (1968) suggested that

eastward translation of the Colorado Plateau and a left-lateral shear-couple across the Uinta arch caused the observed Laramide trends. Noting the arcuate array of Laramide structures bounding the Colorado Plateau to the north and east, Hamilton (1988) proposed that the plateau converged and rotated clockwise (relative to the North American craton) about an Euler pole in central New Mexico.

Other tectonic models employed polyphase contraction to explain the diversity of foreland structures (Chapin and Cather, 1983; Gries, 1983). Chapin and Cather (1983) used evidence from north-trending, elongate basins of possible dextral strike-slip origin to propose a two-stage Laramide orogeny. Their model suggested that an early Laramide $N70^{\circ}E$ trending σ_1 direction shifted to $N45^{\circ}E$ in the Eocene and resulted in north-northeastward transpression in the Rocky Mountain foreland and northward translation of the Colorado Plateau (Chapin and Cather, 1983). As previously discussed, Gries (1983) extended these ideas and proposed a three-stage Laramide model with Eocene uplift of the Uinta arch during north-south shortening. Bergh and Snoke (1993) utilized structural overprinting relationships to infer similar polyphase Laramide deformation in the Shirley Mountains of south-central Wyoming.

Sedimentation patterns, dating of synorogenic sedimentation, and paleogeographic reconstructions, however, do not support the timing of the polyphase models (Hansen,

1986b; Johnson and Finn, 1986; Dickinson et al., 1988; Perry et al., 1992). For example, isopach trends of Paleocene sedimentation in the Piceance basin indicate early Laramide uplift of the southeastern Uinta arch (Johnson and Finn, 1986). Thrusting on the Uinta basin boundary fault preceded deposition of the Lower to Middle Eocene Wasatch Formation (Hansen, 1986b). On the north flank of the Uinta arch, major thrusting and overturning of the Late Cretaceous Ericson Sandstone occurred on the Uinta-Sparks fault zone prior to deposition of the Middle Paleocene Fort Union Formation (Hansen, 1986b). Subsequent thrust displacements of the Fort Union, Wasatch, and Green River formations indicate an extended deformation history along the north-central Uinta arch (Hansen, 1986b).

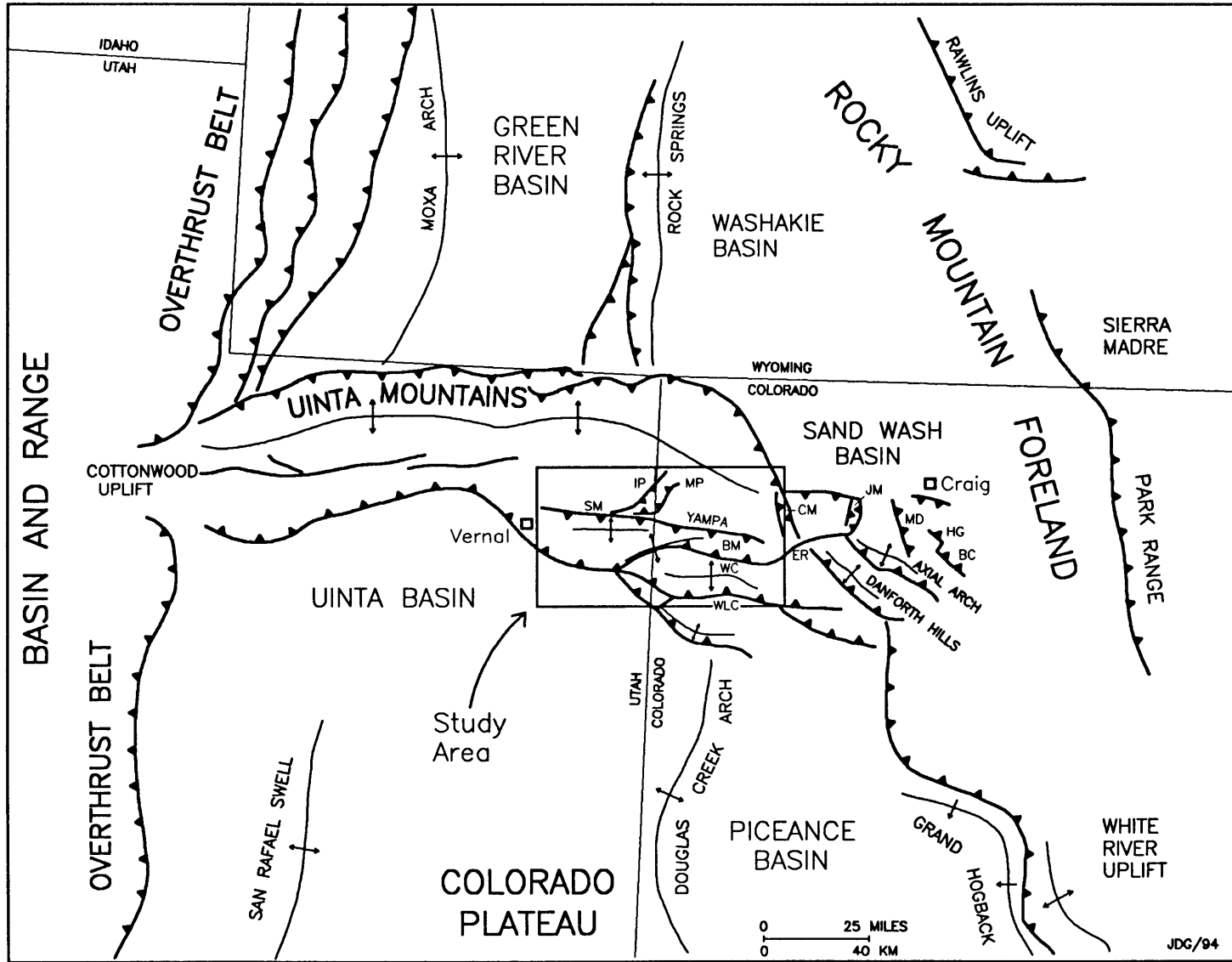
Model Predictions

Many Laramide tectonic models place the northern margin of the Colorado Plateau along the southeastern Uinta arch, but the kinematics of each model predict different slip vectors along this boundary. A single stage of uniform northeasterly contraction (Brown, 1988) suggests oblique-sinistral transpression along the south side of the Uinta arch. Polyphase models imply dip-slip shortening across the Uinta arch (Chapin and Cather, 1983; Gries, 1983). The left-lateral shear couple model of Sales (1968) suggests sinistral-wrenching along the southern Uinta arch boundary.

Laramide Structure of the Uinta Arch

The Uinta arch forms a major east-striking structural anticline that extends into the Sevier thrust belt on the west and is bounded by Laramide thrust faults on the north, northeast, and south (Fig. 2.1). The Uinta arch consists of western and eastern elongate domes (Fig. 2.2) whose culminations coincide with the north-south trending Moxa arch and Rock Springs/Douglas Creek arches, respectively (Fig. 2.1; Ritzma, 1969; Hansen, 1986a, 1986b). In the westernmost Uintas, the Cottonwood uplift and the Wasatch fault effectively truncate the mountain range, but the anticlinal axis of the Uinta arch can be traced westward through the Wasatch range to the Oquirrh Mountains in the Basin and Range province (Ritzma, 1969; Hansen, 1986b). The surface expression of the easternmost Uinta arch axis disappears under the Miocene basin fill of the Browns Park Formation but probably continues eastward through the Cross and Juniper Mountains pop-up structures that expose Uinta Mountain Group strata (Ritzma, 1969; Hansen, 1986b, Stone 1986b). The Uinta arch trend may continue into the White River uplift to the southeast of Juniper Mountain as the Danforth Hills/Axial arches (Hansen, 1986b), but these structures display a southwest vergence direction opposite that of the adjacent northeast-directed Uinta thrust margin (Figs. 2.1, 2.3).

Figure 2.1 Tectonic map of the Uinta Mountains area. Features marked on the map include Split Mountain (SM), Island Park (IP), Mitten park (MP), Blue Mountain (BM), Willow Creek (WLC), Wold Creek (WC), Elk Ridge (ER), Cross Mountain (CM), Juniper Mountain (JM), Moffat Dome (MD), Horse Gulch (HG), and Beaver Creek (BC), (modified from Gries 1983; Rowley et al., 1985; Stone 1986a; Morel et al., 1986).



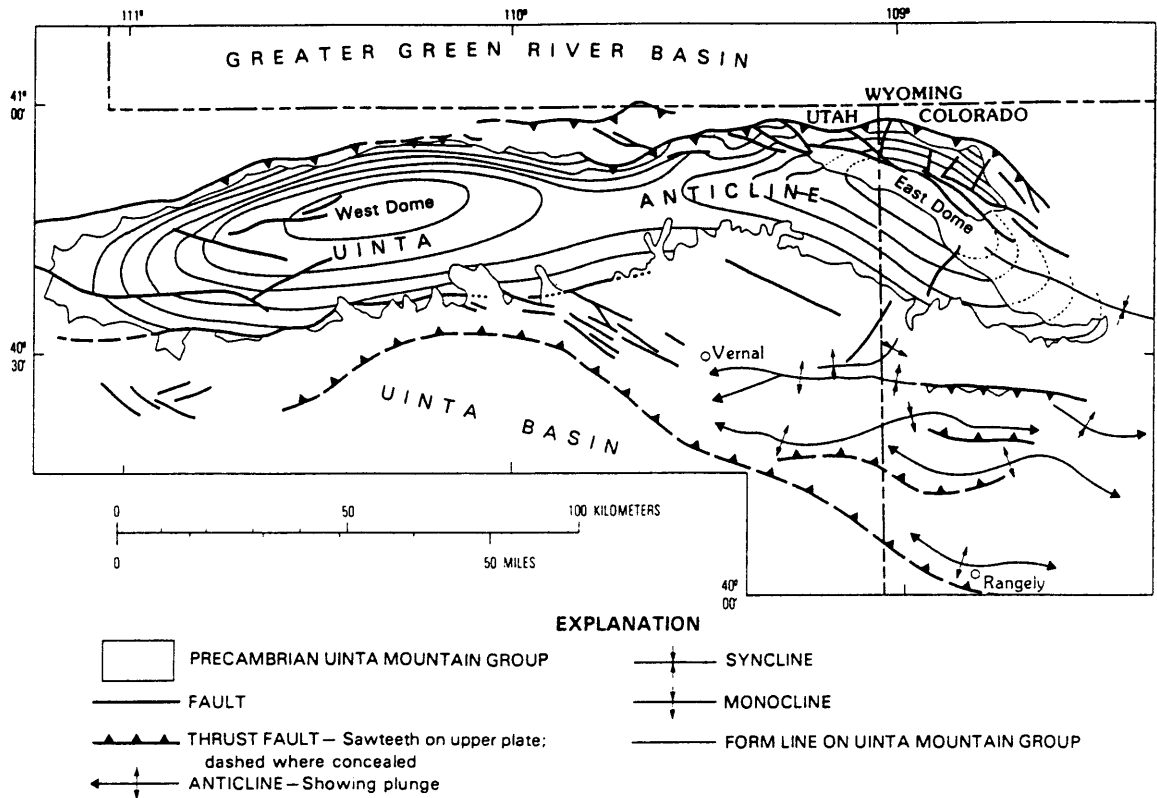


Figure 2.2 Generalized structure map of the Uinta Mountains showing the compound form of the Uinta anticline (from Hansen, 1986a).

Structural Evolution of the Uinta Arch

The area the Uinta arch coincides with the late Precambrian, east-trending structural trough that accommodated 8-11 km (24-35,000 feet) of Proterozoic Uinta Mountain Group sediments (Hansen, 1986b; Stone, 1993a). The coincidence of the late Precambrian basin with Laramide structures has been documented through surface outcrop, seismic, and drill hole data, but the exact extent of the

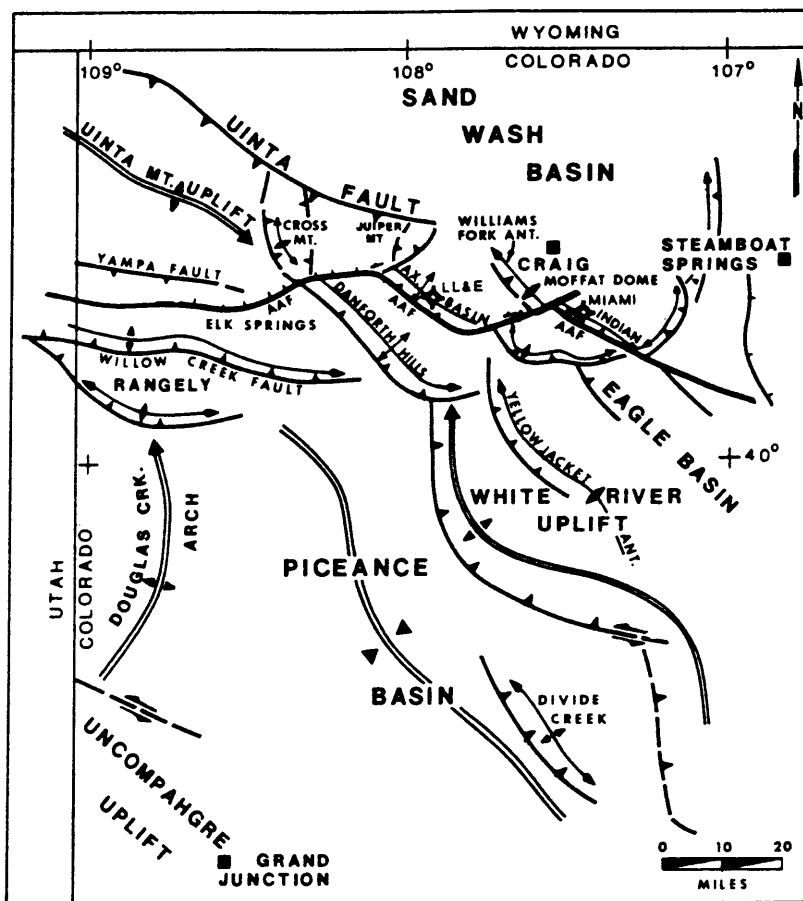


Figure 2.3 Structural index map of northwest Colorado (from Stone, 1986b).

Uinta trough is not well defined (Hansen, 1986b; Stone, 1986b, 1993a). The Upper Cambrian Ladore Formation was deposited on an angular unconformity on top of the Uinta Mountain Group (Hansen, 1986b; Stone, 1993a). Seismic and drill hole data indicate that Precambrian Uinta Mountain Group rocks are preserved in the upthrown blocks of Laramide thrusts in the Axial, Beaver Creek, and Rangely anticlines

but not in the footwalls (Stone, 1986, 1993a; Morel, 1986). Inversion of the Precambrian structures occurred on the Axial and Beaver Creek thrusts east of the study area during the Ancestral Rocky Mountain orogeny, as evidenced by thinning of Pennsylvanian strata in the hanging wall blocks (Stone, 1986b; Morel, 1986). Seismic and drill hole evidence also shows that the Pennsylvanian structures became reactivated during the Laramide (Stone, 1986b, 1993a; Morel, 1983). Laramide movement on pre-existing and newly-formed structures contributed to the complex kinematics observed in the study area. Lack of deformation in Cambrian through Cretaceous strata, however, indicates that the area east of the White River uplift was tectonically quiet until major structural inversion in the Laramide (Hansen, 1986b).

Laramide uplift of the Uinta arch produced 11-13 km of structural relief with the surrounding basins (Sales, 1971) with the greatest structural relief in the eastern Uintas (Fig. 2.4; Ritzma, 1969; Hansen, 1986b). Laramide structures exposed in the eastern Uinta Mountains occur under the Gilbert Peak erosion surface that is often marked as an angular unconformity under the Oligocene Bishop Conglomerate (Hansen, 1986a, 1986b). Offsets of the Gilbert Peak unconformity and the Bishop Conglomerate indicate post-Laramide regional northeastward tilting, subsidence, and the formation of the Browns Park graben northeast of the study area (Hansen, 1986a, 1986b).

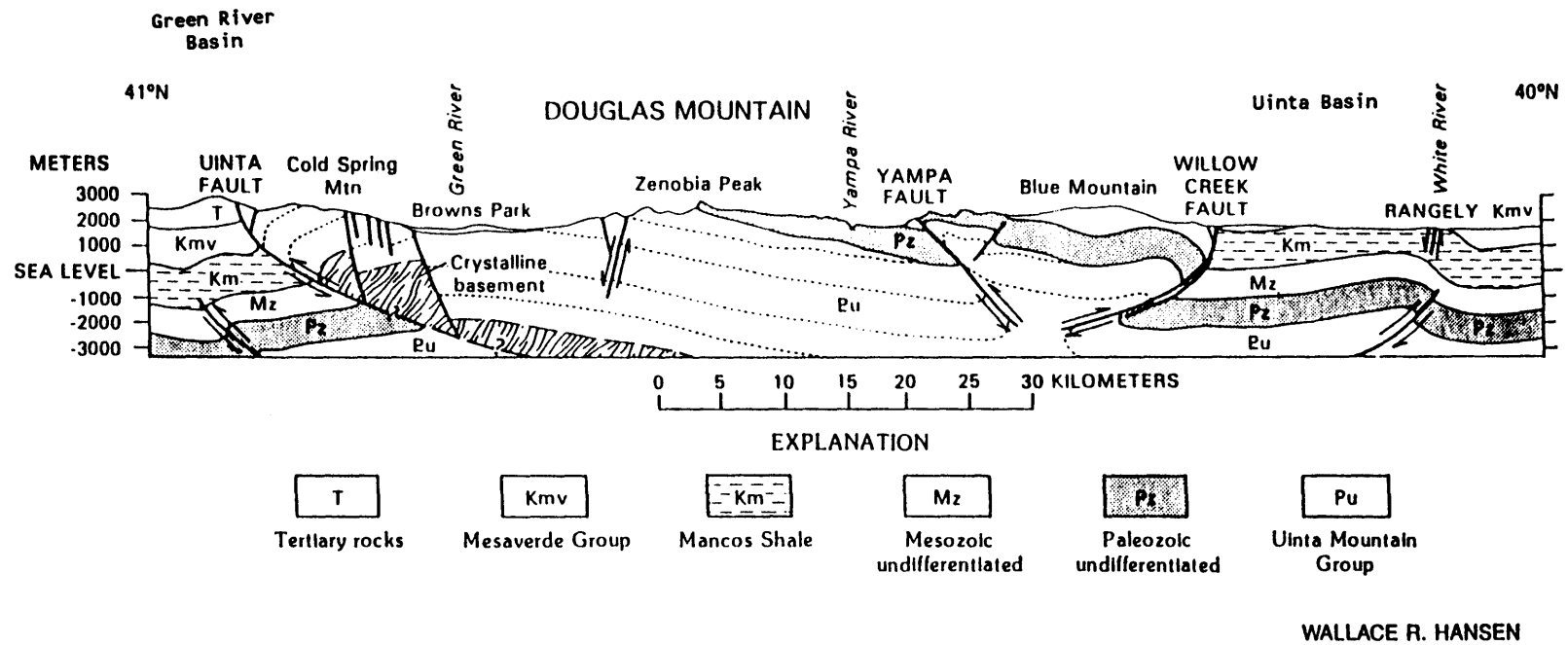


Figure 2.4 Structural cross section across the eastern Uinta arch and the study area showing the structural relief between the arch and the Green River basin to the north and the Uinta basin to the south (from Hansen, 1986b).

Dinosaur National Monument Study Area

The Dinosaur National Monument study area is located along the southeastern Uinta arch in Colorado and Utah (Fig. 2.1). The study area provides excellent exposure of Laramide structures with minor faults for slip vector and paleostress estimation. Canyons cut by the Green and Yampa rivers expose Precambrian strata as well as the Island Park, Mitten Park, and Yampa faults.

Located on the 5°-10° south-southwestward dipping backlimb of the eastern Uinta arch, structures in the Dinosaur National Monument area display a complex anastomosing pattern (Figs. 2.1, 1.4). The Split Mountain, Yampa, Wolf Creek, and Willow Creek fault systems are generally east-west trending. The western end of the Wolf Creek fault system splays into the south Split Mountain structure and the west-southwest trending Section Ridge anticline at Cliff Ridge. The generally northeast-trending Mitten Park and Island Park structures curve into east-west alignment and merge with the Yampa/Split Mountain system to the southwest. The predominance of east-west structures in the study area suggest overall north-south shortening, whereas the northeasterly trends of the Mitten Park, Island Park, and Section Ridge structures as well as Juniper Mountain to the east of the study area suggest a component of northwest-southeast shortening.

Stratigraphic Summary

This study did not include a detailed examination of the stratigraphy and sedimentology of the deformed strata. Published map descriptions of sedimentary strata provided adequate detail for discriminating rock units in the field (Figs. 2.5, 2.6). Primary rock units that provided minor fault data included sandstones and orthoquartzites of the Late Proterozoic Uinta Mountain Group, the Cambrian Lodore Formation sandstones, the Pennsylvanian Weber Sandstone, the conglomeratic Gartra Member of the Upper Triassic Chinle Formation, the Lower Cretaceous(?) Buckhorn Conglomerate Member of the Cedar Mountain Formation, the Lower Cretaceous Dakota Sandstone, and the Upper Cretaceous Castlegate Sandstone. The conglomeratic strata provided the best overall minor fault data.

A generalized stratigraphic column illustrated for the Dinosaur National Monument study area (Fig. 2.6) contains thicknesses from cross sections drawn from published maps and field observations in the study area. Detailed stratigraphic descriptions for the Uinta Mountains and surrounding basins are provided by Rowley et al. (1985).

GENERAL STRATIGRAPHY – EASTERN UINTA MOUNTAINS		
	NORTHEAST FLANK	SOUTH FLANK
MIOCENE	Browns Park Formation	
OLIGOCENE	Bishop Conglomerate	
EOCENE	Bridger Formation	Duchesne River Formation Uinta Formation
	Green River Formation	
	Wasatch Formation	
	? — — ?	
PALEOCENE	Fort Union Formation	
CRETACEOUS	Mesaverde Group	
	Hilliard Shale	Mancos Shale
	Frontier Formation	Frontier Member
	Mowry Shale	Mowry Member
	Dakota Sandstone	
	Cloverly Formation	Cedar Mountain Formation
JURASSIC	Morrison Formation	
	Stump Formation	
	Entrada Sandstone	
	Carmel Formation	
TRIASSIC	Glen Canyon Sandstone	
	Chinle Formation Gartra Member, at base	
	Moenkopi Formation	
PERMIAN	Park City Formation	
PENNSYLVANIAN	Weber Sandstone	
	Morgan Formation	
	Round Valley Limestone	
MISSISSIPPIAN	Doughnut Formation	
	Humbug Formation	
	Madison Limestone	
CAMBRIAN	Lodore Formation	
PROTEROZOIC ? — — ?	Uinta Mountain Group	
ARCHEAN	Red Creek Quartzite	(Unexposed)
	Owiyukuts Complex	

Figure 2.5 Stratigraphic summary after Hansen (1986b).

GENERAL PRE-LARAMIDE STRATIGRAPHY IN THE DINOSAUR NATIONAL MONUMENT AREA

SYSTEM	STRATIGRAPHIC UNIT	LITHOLOGY	THICKNESS (FEET)
Upper Cretaceous	Mesaverde Group		2600
	Sego Sandstone, at base		0-250
	Buck Tongue, Mancos Shale		200-500
	Castlegate Sandstone		0-100
	Mancos Shale		4800-5600
	Frontier Sandstone		100-300
L. Cretaceous	Mowry Shale		30-200
	Cedar Mountain Formation		30-250
	Dakota Sandstone		0-200
Jurassic	Morrison Formation		500-1200
	Stump Formation Entrada Sandstone Carmel Formation		100-800
	Glen Canyon Sandstone (Navajo/Nugget equivalent)		500-600
Triassic	Chinle Formation Gardiner Member, at base		200-500
	Moenkopi Formation		500-1000
Permian	Park City Formation		100-200
Pennsylvanian	Weber Sandstone		1000
	Morgan Formation		1000
	Round Valley Limestone Doughnut Shale/Humbug Fm.		150-500
Mississippian	Madison Limestone (Leadville equivalent)		600
Cambrian	Lodore Formation		600
Proterozoic Y	Uinta Mountain Group		Bottom not exposed. Up to 7000 in adjacent areas.

JDG/94

Figure 2.6 Stratigraphic column of study area.

Chapter 3

METHODS

FIELD METHODS

During the summer of 1993, field investigations consisted of a reconnaissance of the major structures in the Dinosaur area, scouting each structure for minor fault exposures, and measurements of minor fault surfaces, lineations, and bedding attitudes with a Brunton compass. Slickensided minor fault data were collected from 22 sites in the Dinosaur National Monument area. 1206 minor fault surfaces and 1202 striae were measured. Sampling locations are illustrated in Figures 3.1 and 3.2 along with plots of slickenline and minor fault orientations. More detailed structural descriptions are included in Chapter 4.

Bedding attitudes were recorded using the right-rule (i.e. dip direction 90° clockwise from strike direction) in strike azimuth (i.e. 360°) and dip format. Minor fault attitudes were recorded as the strike and dip of the plane along with the trend and plunge of lineations. The sense of slip determined from Riedel shear fractures (Petit, 1987) was also recorded. Minor fault surfaces were subdivided into areas of approximately 160 cm^2 (25 in^2) per measurement for consistency in sampling over larger areas. The scarcity

Slickenline Orientation Data

Dinosaur National Monument
Southeastern Uinta Mountains

22

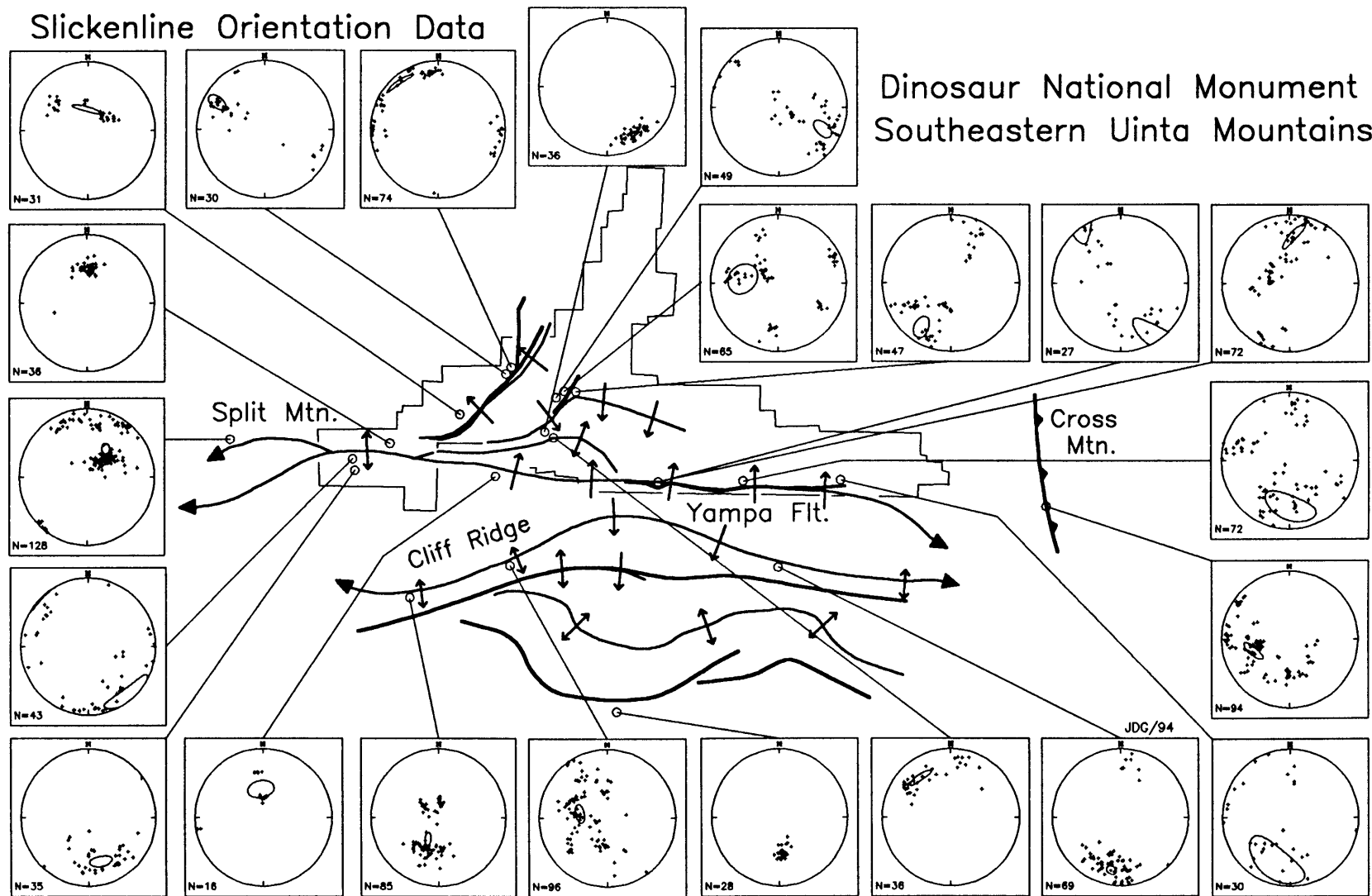


Figure 3.1 Minor fault striae from 22 sample sites. Ellipses indicate the 95% confidence interval (C.I.) of the first eigenvector (E_1) (Vollmer, 1989).

Minor Fault Orientation Data

Dinosaur National Monument
Southeastern Uinta Mountains

23

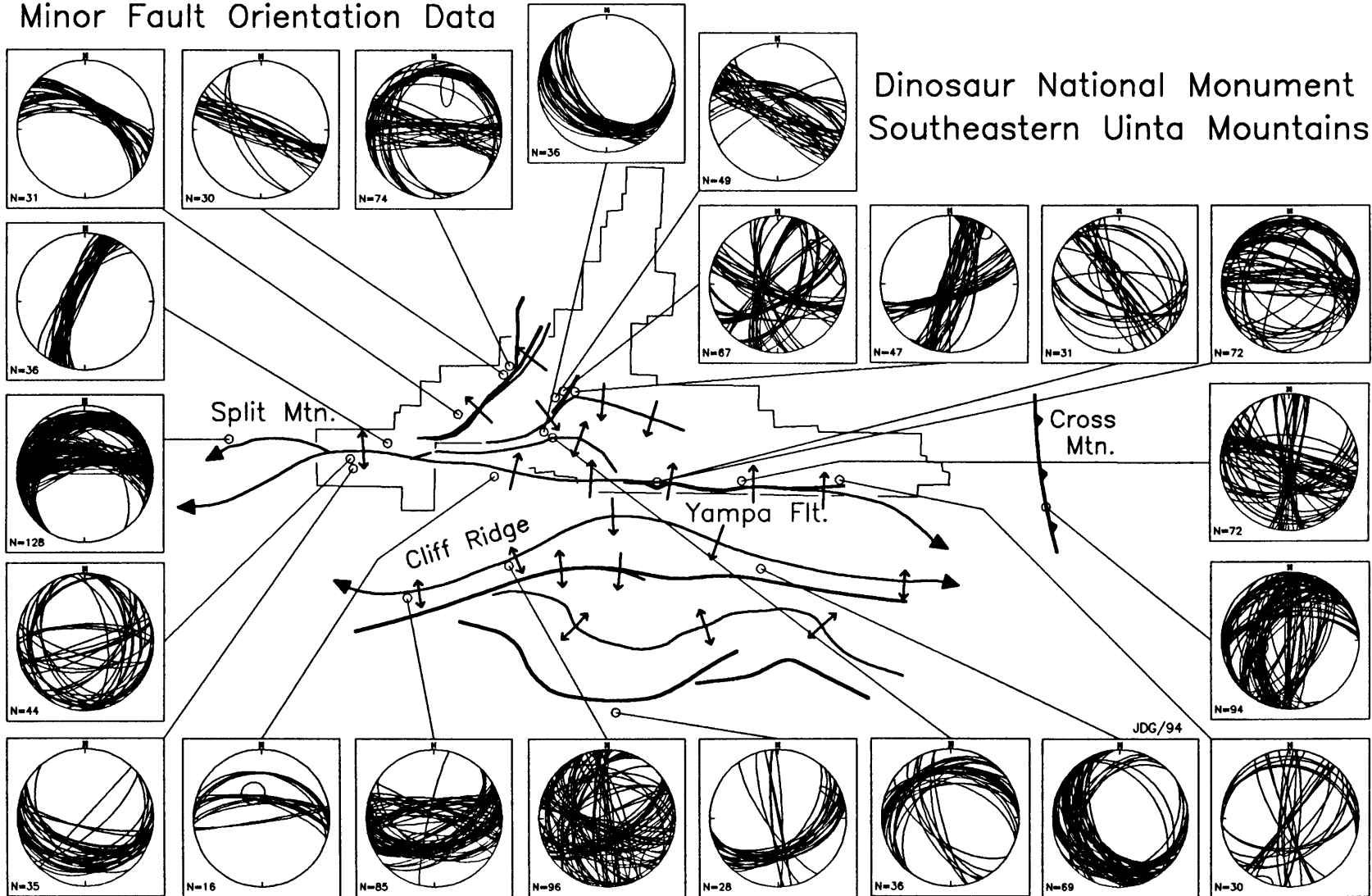


Figure 3.2 Minor fault surfaces from 22 sample sites. Ellipses indicate the 95% confidence interval (C.I.) of the second eigenvector (E_2) (Vollmer, 1989).

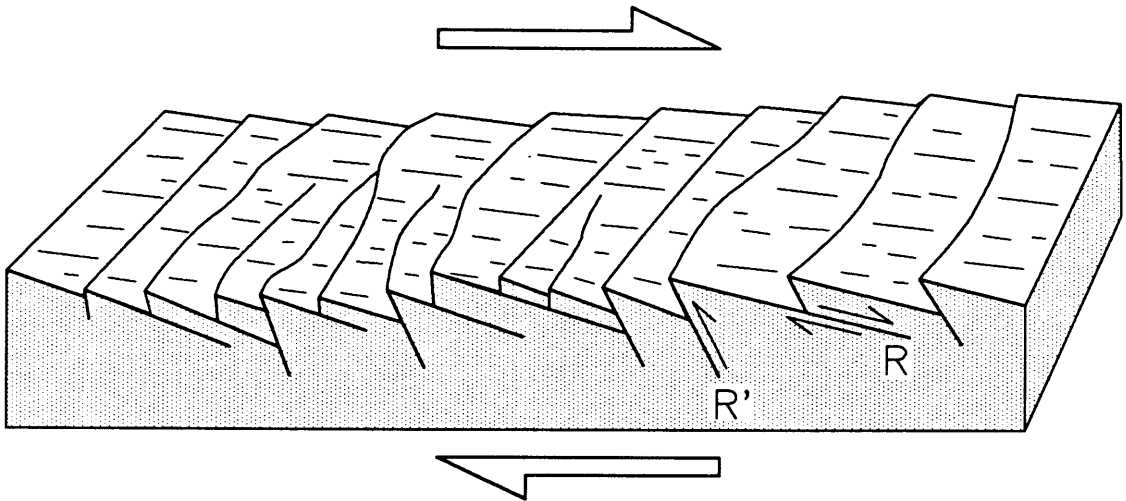


Figure 3.3 Block cartoon of a striated fault surface illustrating the stepped, Riedel shear morphology. The missing top section moved to the right (modified from Allmendinger et al., 1989).

of striated minor faults limited sample sizes and prohibited the use of a randomized sampling plan.

Minor Fault Data

Minor fault exposures were examined closely to determine the slip sense of the slickenside surfaces. Allmendinger et al. (1989) illustrated the morphological features of slickensides using criteria described by Petit (1987). Figure 3.3 displays the relationship of synthetic R and antithetic R' shears on a slickensided fault surface.

In the study area, minor faults most commonly consisted of polished, quartzose surfaces with stepped Riedel shear fractures. Occasionally, minor faults displayed various combinations of calcite growth fibers and/or Riedel shears on adjacent surfaces. In this study, mainly quartzose slickenside surfaces with distinct Riedel shear steps and

lineations were used to determine shear sense. In several locations, more than one direction and/or sense of slip appeared on the same minor fault surfaces. When possible, the multiple lineations were measured and recorded.

MINOR FAULT ANALYSIS METHODS

Numerous techniques are available for estimation of the paleostress tensor from minor fault data. Methods used in this study include eigenvector analysis of slickenlines, M-plane and conjugate fracture techniques, the direct stress inversion method of Angelier (1990), and the right octahedra (PT) technique of Lisle (1987).

The stress estimation methods are based on the premise that slickensided faults have a direct relationship to paleostress conditions during the time of deformation. Slickenlines record the direction of movement along a fault induced by the stress tensor. If produced in a uniform stress field, the direction and sense of slip on faults of all orientations should correlate with a single stress tensor (Angelier, 1990). The orientation and relative magnitude of the stress tensor may be subsequently estimated from fault and slip orientation data. Although individual slip vectors on interacting/intersecting faults may vary significantly from resolved shear stress directions, the variations tend to follow a Gaussian distribution with the mean centered near the "true" maximum principle stress (σ_1) orientation (Dupin et al., 1993; Pollard et al., 1993).

In this study, minor faults were divided into fault types (i.e., thrust, left, right, normal) on the basis of slip sense determined in the field and the calculated rake angle of the striae. The rake angle was computed in a LOTUS spreadsheet from the strike and dip of the fault plane and the trend or plunge of the slickenline. Use of the trend provided more accurate rake values for faults dipping less than 45°, whereas the plunge was used for steeper dips. Average orientations of the fault types were obtained with eigenvector analysis.

Eigenvectors

Eigenvectors are mutually perpendicular lines of best fit through the N directions of maximum variance in an N-dimensional data set. With 3-D lineation data, the orientation of first eigenvector (E_1) is such that "the sum of the squared distances from the tips of the vectors to the first eigenvector is the maximum possible" (Davis, 1986). The second eigenvector (E_2) is orthogonal to E_1 in the direction the greatest remaining variation in the data set. The third eigenvector (E_3) is perpendicular to the first two and represents the direction of least variation of the data as well as the mean lineation trend. Note that in this study and in the ORIENT computer program (Vollmer, 1989) used to analyze the lineation data, this convention is reversed, and E_1 parallels the mean lineation direction.

Eigenvalues represent the proportion of the total variance of a data set accounted for by their respective

eigenvectors (Davis, 1986). Normalized eigenvalues are obtained by dividing the individual eigenvalues by the total eigenvalue and sum to 1.0. A normalized eigenvalue of 1.0 indicates that all of the data are coaxial, whereas normalized eigenvalues of less than 1.0 reflect increasing dispersion in the data set. With 3-D directional data, normalized eigenvalues of 0.333 reflect uniform dispersion.

Conjugate Fracture Method

Rock mechanics research indicates that conjugate fractures form by brittle failure under triaxial stress conditions (e.g., Donath, 1970). In many circumstances, the fractures are inclined symmetrically to the σ_1 direction at an average angle of 25-30° (Donath, 1970). Observations of natural minor faults display a range of conjugate angles, however, and the estimated σ_1 can be approximated as the acute bisector of a fault pair if they do not represent pre-existing planes of weakness.

In practice, possible conjugate minor fault data sets may be analyzed with eigenvector techniques. The poles to the conjugate planes are used in the calculation, and the orientation of the second eigenvector (E_2) approximates the orientation of the acute bisector. However, eigenvector analysis requires samples of roughly equal size from both conjugates for an unbiased estimate of the acute bisector. Analyses of synthetic data indicate that the normalized eigenvalues for conjugate fracture sets with 60° between the fault planes are $E_1 = 0.75$, $E_2 = 0.25$, and $E_3 = 0$. Conjugate

slickenlines on minor faults provide the same eigenvalues, but the estimated σ_1 orientation lies along the first eigenvector (E_1). Moreover, analysis of synthetic data also shows that the slickenline eigenvalues are the same even with a mix of conjugate faults centered on σ_1 (e.g., a mixed data set with both thrust and lateral conjugate geometries). Possible conjugate slickenline data sets may be identified from the normalized eigenvalues.

M-plane Method

A movement plane or M-plane is orthogonal to the fault plane and contains the slip lineations (Goldstein and Marshak, 1988). The M-plane method used in this study combines eigenvector analysis of minor fault types with the plotting of the composite fault data as M-planes on an equal area stereonet. In this analysis, σ_1 is assumed to lie within the movement plane at a 30° angle to the fault. After construction of M-planes for each site, eigenvectors of the combined M-plane σ_1 orientations provide a composite estimate the average regional σ_1 (Chapter 5).

Right (PT) Dihedra Method

A fault plane and a plane perpendicular to the fault/slickenline intersection divide 3-D space into four dihedra, where two are in compression (P, pressure) and two are in extension (T, tension) at the time of faulting (Angelier and Mechler, 1977). The maximum principal stress (σ_1) lies within the P quadrants, and the least principal stress (σ_3) falls within the T quadrants. Data from

striated faults are compiled to estimate an overall stress tensor. Two common PT methods are used to extract the best-fit stress tensor orientation (Allmendinger et al., 1989).

In the original PT method (Angelier and Mechler, 1977), lines bisecting the P and T dihedral angles along the movement plane estimate the greatest and least principal stress directions, respectively (Allmendinger, 1989). These lines are plotted on a stereonet, and the principal stress orientations are found by either density contouring or calculating the eigenvectors of the lineation estimates. Although precise and easily applied, one drawback to this method is that the σ_1 estimate for each fault datum is restricted to the movement plane at an angle of 45° from the fault (Allmendinger et al., 1989). This assumption is correct only when the fault plane and its conjugate normal plane are planes of maximum shear stress and is incompatible with triaxial fracture mechanics discussed above (Donath, 1970).

Another PT method overlays successive derivations of PT dihedral angles and determines the region of overlap on the lower hemisphere of a stereonet (Angelier and Mechler, 1977). Density contouring of the overlapping data provides an estimate of the principal stress orientations. This method only restricts the σ_1 estimate for each minor fault to the P dihedral angle region and is more compatible with conjugate fracture mechanics.

More than one density maxima often occur with the PT methods. This may reflect the presence of more than one

stress tensor and deformation phase (Charlesworth et al., 1993) or may represent a simple data set with a large resolved area of possible stress orientations.

Alternatively, several maxima may reflect interaction between multiply-oriented faults under a single stress tensor (Pollard et al., 1993). Multiple maxima may prevent a unique stress tensor estimate from a fault data set.

Octahedra Method

The octahedra method of Lisle (1987) extends the PT dihedra method. The dihedra are divided into octants along the movement plane (M-plane). The octahedra technique adds more constraint to the possible position of σ_3 in the final analysis because σ_3 must lie on the same side of the M-plane as σ_1 (Allmendinger, 1989). The SLICK CONTOUR program of Vollmer (1993; Fig. 3.4) implements the octahedra method for directed-slip fault data. The best solution is determined by maximizing the product (P) of the percentages of the fault data in the test dihedra (Vollmer, 1993). In this study, the automatic search routine was augmented by contouring the data and manually searching, adjusting, and centering the stress axes for best fit and maximum P.

Direct Inversion Method

The direct inversion method uses directed-slip data from minor faults to calculate the orientation of the principal stresses and a ratio of relative stress magnitudes [$\Phi = (\sigma_2 - \sigma_3)/\sigma_1 - \sigma_3$]. Values for the ratio Φ range from 0 to 1. Small values of Φ correspond to a prolate stress

SLICK CONTOUR - OCTAHEDRA METHOD

Maxima Estimate

○	X = estimate of Sigma1	: 25.1, 318.6
□	Y = estimate of Sigma2	: 0.81, 052.4
△	Z = estimate of Sigma3	: 63.5, 159.1

P1 = % data with X in Sigma1 dihedra	: 79.7%
P2 = % data with Z in Sigma3 dihedra	: 89.1%
P3 = % with X & Z in opposing AB dihedra	: 95.3%
P = PROB(X=Sigma1) = P1*P2*P3	: 67.6%

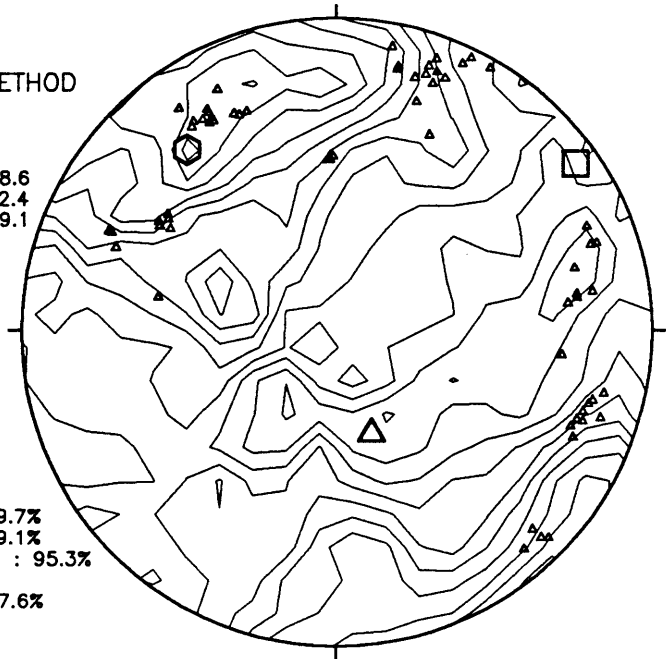


Figure 3.4 Paleostress tensor determination from the SLICK CONTOUR program (Vollmer, 1993) showing lineation orientations, contours, and stress tensor axes.

ellipsoid, whereas values close to 1 indicate a highly oblate stress ellipsoid.

The direct inversion method (Angelier, 1990) assumes that motion on faults of all orientations result from a single stress tensor. Ideally, the resolved shear stress direction on each plane should correspond to the observed striae. After stress directions are computed for the data, the orientation of the stress tensor is calculated with a least-squares procedure that minimizes the sum of the angles between the calculated slip vectors and the slickenlines (Charlesworth et al., 1993). This method is implemented in the STRESS computer program by Villemin and Charlesworth (1991; Fig. 3.5).

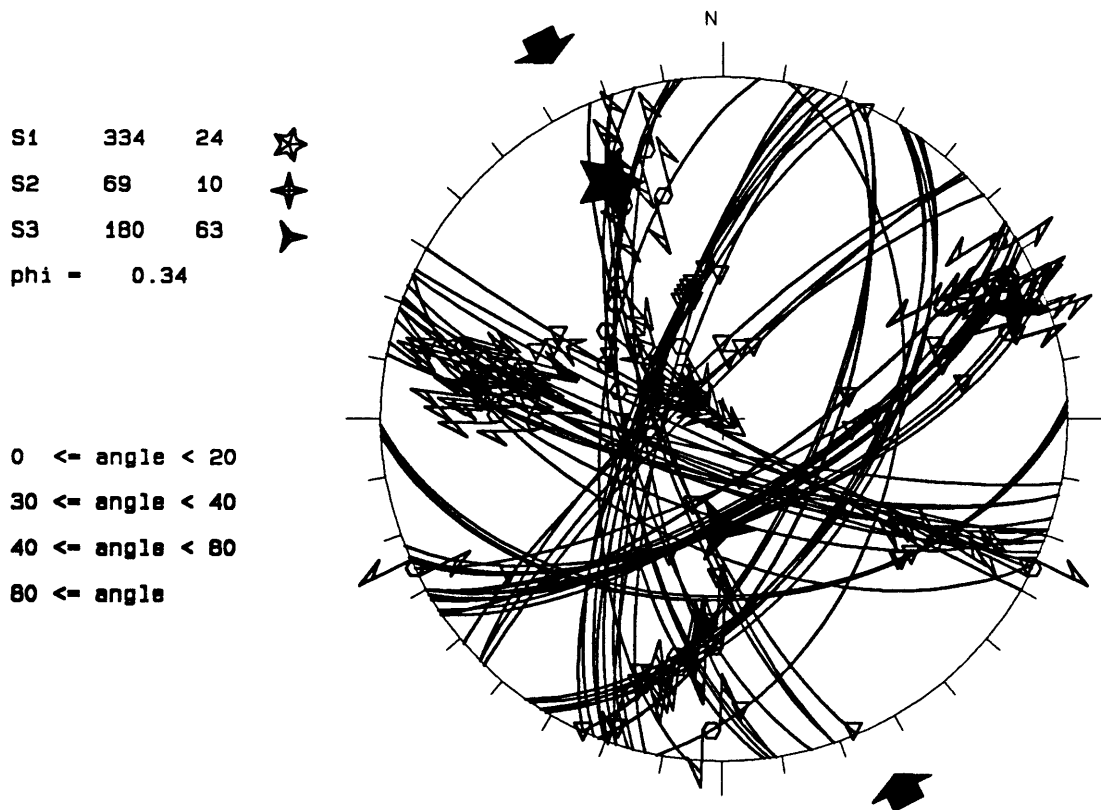


Figure 3.5 Paleostress tensor determination from the STRESS program (Villemain and Charlesworth, 1991) showing minor faults, slip linears, and stress tensor axes.

One drawback to the direct inversion method is the least squares estimation of the stress tensor. Least squares methods can place undue weight on rogue data, and a few errant data values can result in significant errors in the inverted stress tensor. Direct stress tensor inversion works best with fault-slip data of multiple orientations. A perfectly conjugate fault system makes the determination of ϕ effectively impossible (Angelier, 1990).

Chapter 4

FIELD OBSERVATIONS AND ANALYSES OF MINOR FAULT DATA

The Dinosaur National Monument study area contains significant structural relief and folded strata, but most of the Laramide faults are either not emergent or covered. In many places, large blocks of strata rotated coherently, apparently without significant internal faulting and brecciation. Consequently, minor faults were most often found in close proximity to mapped or inferred major faults, which resulted in most data coming from steeply-dipping or overturned strata. In general, the slickenside data exhibit considerable dispersion both within and between the 22 sampled sites (Figs. 3.1, 3.2). Most of the dispersion is probably attributed to the high dips of the deformed strata.

This chapter discusses the local structure and field observations of each data site. Field data and minor fault analyses are presented in both tabular and graphical equal-area stereonet form. Generalized sketches of data field sites summarize associated fault/fold geometries. Results of minor fault analyses are discussed and qualitatively interpreted for each site. Figure 4.1 summarizes the interpreted paleostress tensor σ_1 trends for each site.

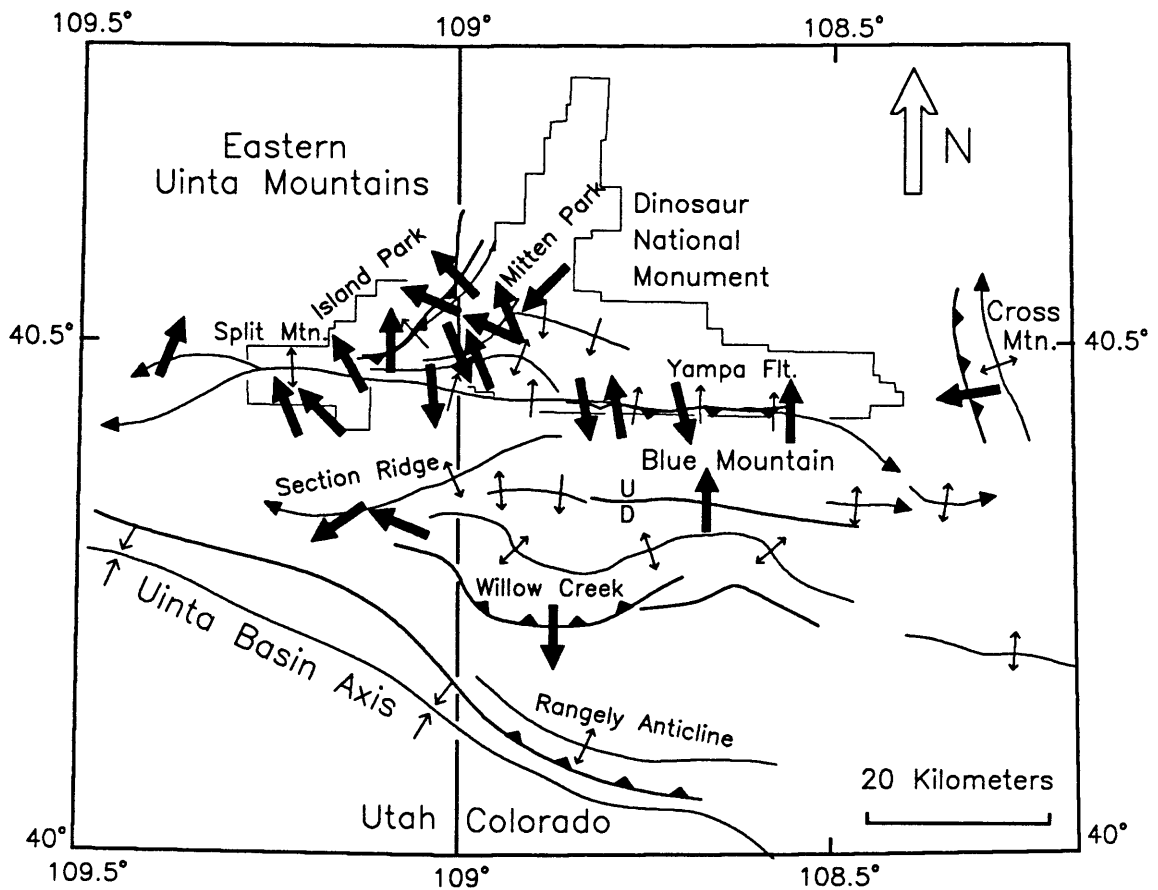


Figure 4.1 Index map of 22 sample sites and interpreted σ_1 trends from minor fault data in the Dinosaur area.

SPLIT MOUNTAIN

The Split Mountain structure is a narrow anticline that merges with the Blue Mountain highland (Fig. 2.1) to the east and attenuates into several splays that step down to the Uinta basin boundary fault on the west (Stone, 1993). Split Mountain anticline is bounded by an east-west trending segment of the Island Park fault on the north and by a steep monocline on the south.

Table 4.1 Split Mountain South - Dakota Hogback

PALEOSTRESS TENSOR σ_1 ESTIMATES (n = 36)			
<u>METHOD</u>	<u>TREND-PLUNGE</u>	<u>SENSE</u>	<u>\$/PROB./EIGEN.</u>
Direct Inversion	021-65	All	0.26
Octahedra Method	152-59	All	59.7%
Slickenlines E ₁	164-34	All	0.7746
M-Plane(s)	001-03	Thrust	
	133-65	Normal	
Bedding Attitude	099-60		

Split Mountain South - Dakota Hogback

A faulted, offset structure on the south side of Split Mountain displays associated slickensides in a footwall exposure. The structure is exposed in an east-trending double hogback of the Cretaceous Dakota Sandstone, Mowry Shale, and Frontier Sandstone (Fig. 4.2; NE, NE, NE, SEC. 36, T4S, R23E, Uintah County, Utah; Rowley et al., 1978). The measured orientation of the hogback strata averaged about 099-60 (Table 4.1). The Frontier Sandstone displays a stratigraphic separation of about 100-200 meters on the west that attenuates completely to no offset about 200-300 meters to the east. The exposed footwall of the fault extends from the top of the Dakota hogback, through locally drag-folded and overturned Mowry Shale and Frontier Sandstone (i.e. up section) and into the Mancos Shale to the south. The surface slope of the exposed footwall suggests a southward fault dip of roughly 30°. With bedding rotated back to horizontal, however, this attitude becomes a south-directed thrust dipping about 30° to the north. Most of the 36 minor faults are predominantly dip-slip (Fig. 4.2) and oriented

Minor Fault Data Analysis – Split Mountain South (Dakota)

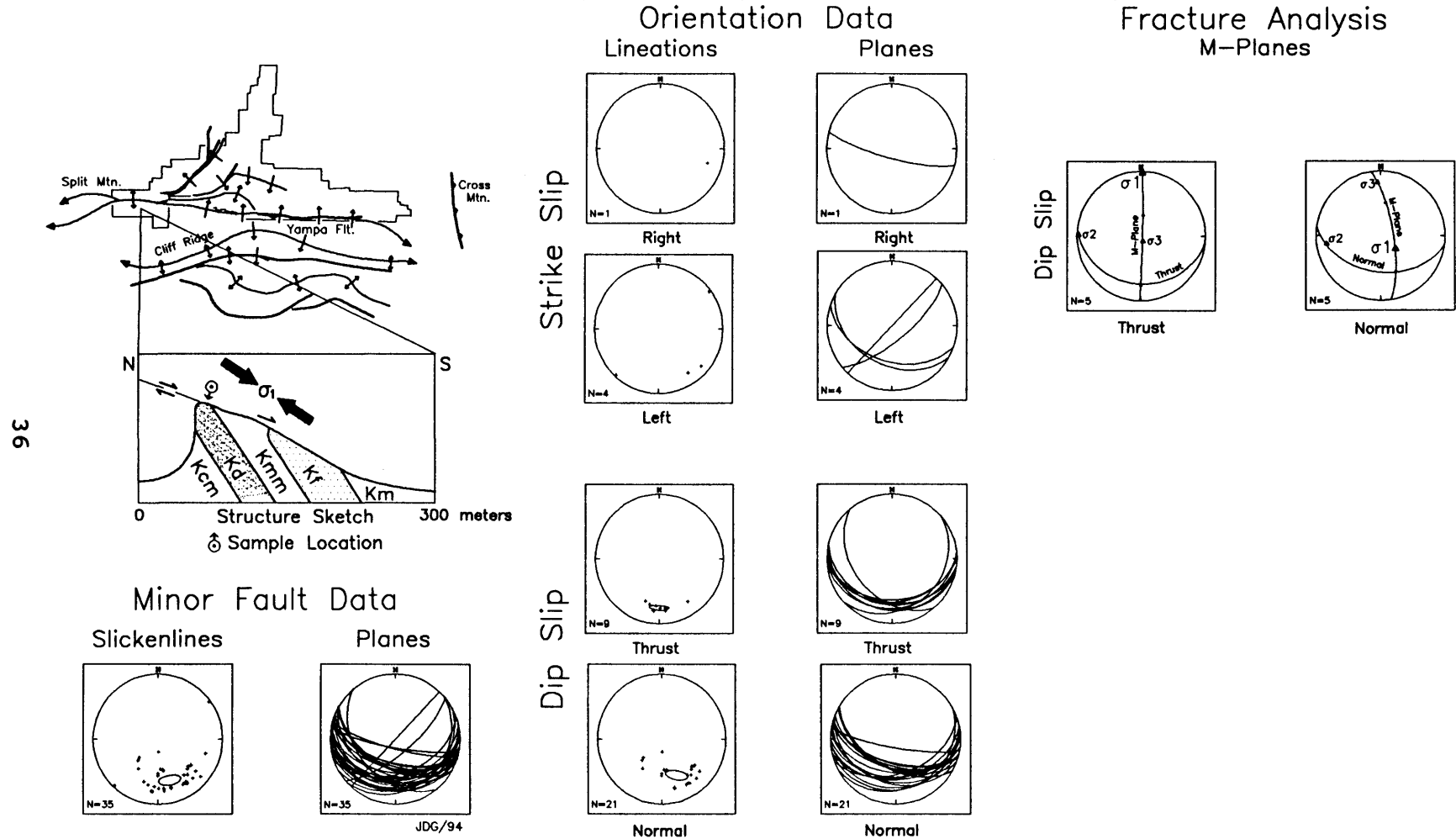


Figure 4.2 Site data summary. Ellipses represent 95% C.I. of E_1 (lineations). Solid arrows indicate apparent plunge of σ_1 in plane of section.

Table 4.2 Split Mountain South - Red Wash

PALEOSTRESS TENSOR σ_1 ESTIMATES (n = 44)			
<u>METHOD</u>	<u>TREND-PLUNGE</u>	<u>SENSE</u>	<u>\$/PROB./EIGEN.</u>
Direct Inversion	114-09	All	0.30
Octahedra Method	118-23	All	75.3%
Slickenlines E_1	140-08	All	0.5690
M-Plane(s)	136-29	Left	
	291-10	Right	
	178-42	Normal	
Conjugate Faults E_2	113-12	Thrust	0.2882
	155-39	Lateral	0.3123
Conjugate Lines E_1	129-09	Thrust	0.7486
	297-05	Lateral	0.7286
Bedding Attitude	100-54		

subparallel to the larger fault. Paleostress tensor estimates are summarized in Table 4.1.

Direct stress inversion and the octahedra method gives a relatively high plunge angle for σ_1 . M-Planes indicate thrust and normal σ_1 orientations, whereas the slickenlines E_1 has a thrust orientation. When restored to horizontal, the σ_1 orientation is nearly horizontal and oriented north-northwest.

Split Mountain South - Red Wash

The second site on the south side of Split Mountain was located in the Gartra Member of the Triassic Chinle Formation about 1.6 km north-northwest of the previous site (Fig. 4.3; SE, SE, NW, SEC. 25, Uintah County, Utah; Rowley et al., 1978). The site is north of the Red Wash trail in Dinosaur National Monument. At this site, the Gartra forms a prominent hogback oriented about 100-54 (Table 4.2) which curves to the northwest around the end of the anticline.

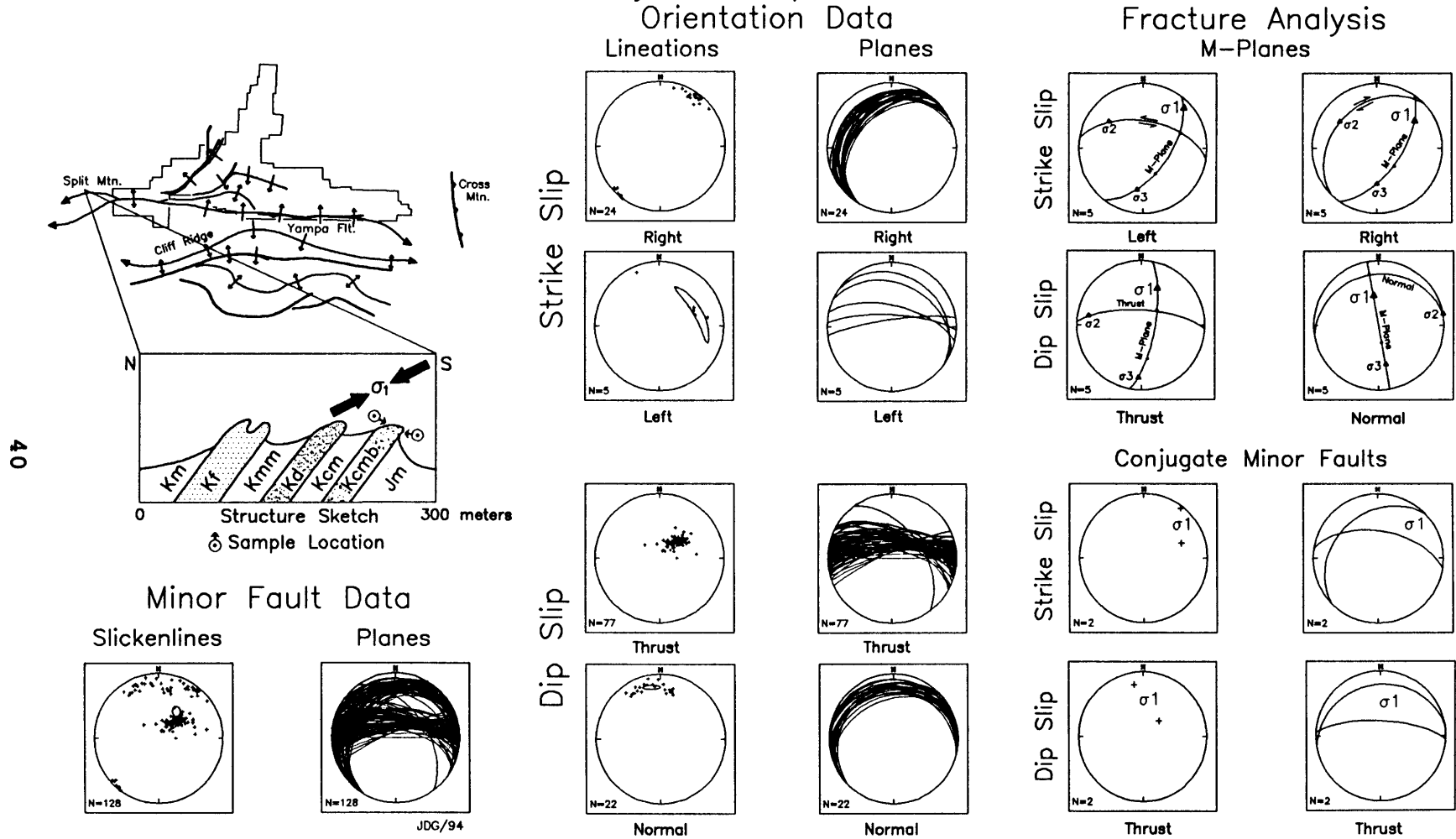
The Red Wash site displayed a zone of diverse minor faults between large relatively undeformed sandstone slabs. The zone was highly weathered, however, and only 44 measurements were collected. The diverse data required additional σ_1 estimates (Table 4.2), but the results suggest a σ_1 oriented toward the northwest. The agreement between the direct inversion, PT octahedra, and conjugate thrust methods is quite close, and the Red Wash strata appear to have been deformed by a single stress tensor.

Split Mountain Northwest

The Split Mountain northwest site is located west of Dinosaur National Monument in a triple hogback of the Cretaceous Cedar Mountain Formation, Dakota Sandstone, and Frontier Sandstone (Fig. 4.4; SE, NE, SW, SEC. 6, T4S, R23E, Uintah County, Utah; Rowley et al., 1978). Situated in the northernmost of three anticlinal splays on the west end of Split Mountain, the Cedar Mountain hogback dips about 273-55. The Dakota hogback displayed few minor faults, but the Cedar Mountain hogback contained the most slickensides found in the study area. The 128 minor faults form a conjugate fracture set, but many striae are highly oblique (Fig. 4.4).

Direct inversion of all the minor faults gives an east-northeast σ_1 orientation--very much in contrast to the general structural attitude (Table 4.3). The octahedra method calculates a north-northwest σ_1 (an 84° difference). The discrepancy in the two methods probably results from the almost perfect conjugate geometry of the minor faults and

Minor Fault Data Analysis – Split Mountain Northwest



40

Figure 4.4 Site data summary. Ellipses represent 95% C.I. of E_1 (lineations). Solid arrows indicate apparent plunge of σ_1 in plane of section.

Table 4.3 Split Mountain Northwest

PALEOSTRESS TENSOR σ_1 ESTIMATES (n = 128)			
<u>METHOD</u>	<u>TREND-PLUNGE</u>	<u>SENSE</u>	<u>Φ/PROB./EIGEN.</u>
Direct Inversion	074-08	All	0.73
	007-43	Thrust-Normal	0.18
	071-12	Lateral	0.54
Octahedra Method	347-30	All	66.9%
Slickenlines E_1	034-49	All	0.7437
M-Plane(s)	024-38	Thrust	
	046-13	Left	
	054-30	Right	
	350-52	Normal	
Conjugate Faults E_2	011-46	Thrust-Normal	0.1765
	048-23	Lateral	0.1272
Conjugate Striae E_1	008-44	Thrust-Normal	0.7743
	051-21	Lateral	0.8588
Bedding Attitude	273-55		

the oblique slips. The high stress ratio value in the direct inversion method suggests an oblate stress ellipsoid. When the data are sorted into dip-slip and lateral-slip subsets, the direct stress inversions show lower Φ values and better agreement with the other methods. Indeed, direct inversion of the dip-slip data coincides closely with the conjugate fracture method.

The conjugate method applied to the dip-slip data set (99 measurements) gives similar σ_1 orientations ($\approx 010-45$), and high eigenvalues. In addition, the overall slickenlines E_1 exhibits an eigenvalue consistent with conjugate faulting (≈ 0.7500). When considered with the results of the M-plane constructions, the overall σ_1 is interpreted to trend north-northeastward with a plunge of about 30° .

Table 4.4 Split Mountain North - Little Rainbow Park

PALEOSTRESS TENSOR σ_1 ESTIMATES (n = 36)			
METHOD	TREND-PLUNGE	SENSE	$\frac{\$}{\text{PROB./EIGEN.}}$
Direct Inversion	346-04	All	0.70
Octahedra Method	232-39	All	69.7
Slickenlines E_1	001-48	All	0.9475
M-Plane(s)	332-32	Left	
Bedding Attitude	297-48		

Split Mountain - Little Rainbow Park

Little Rainbow Park is located on the north side of Split Mountain just to the west of the head of Green River canyon which cuts through the anticline (Fig. 4.5; NW, NE, NW, SEC. 11, T4S, R24W, Uintah County, Utah; Rowley and Hansen, 1979). The Island Park fault trends west-northwest through the area but is mostly covered or not emergent.

Few minor faults are exposed on the west side of the Green River in the mouth of the Split Mountain Canyon and in Little Rainbow Park. Although well-exposed, the Glen Canyon Sandstone did not reveal any minor faults, and only a small data set of 36 measurements was collected from two small exposures in the Chile Gartra. The minor faults have left-thrust orientations (Fig. 4.5).

The similar orientations of the minor fault data results in diverse σ_1 orientations (Table 4.4). Direct inversion yields a relatively oblate stress ellipsoid. Although the octahedra method gives a fair probability estimate, the σ_1 trend differs 114° from direct inversion and 129° from the slickenlines E_1 . The high eigenvalue for

Minor Fault Data Analysis – Split Mountain/Rainbow Park

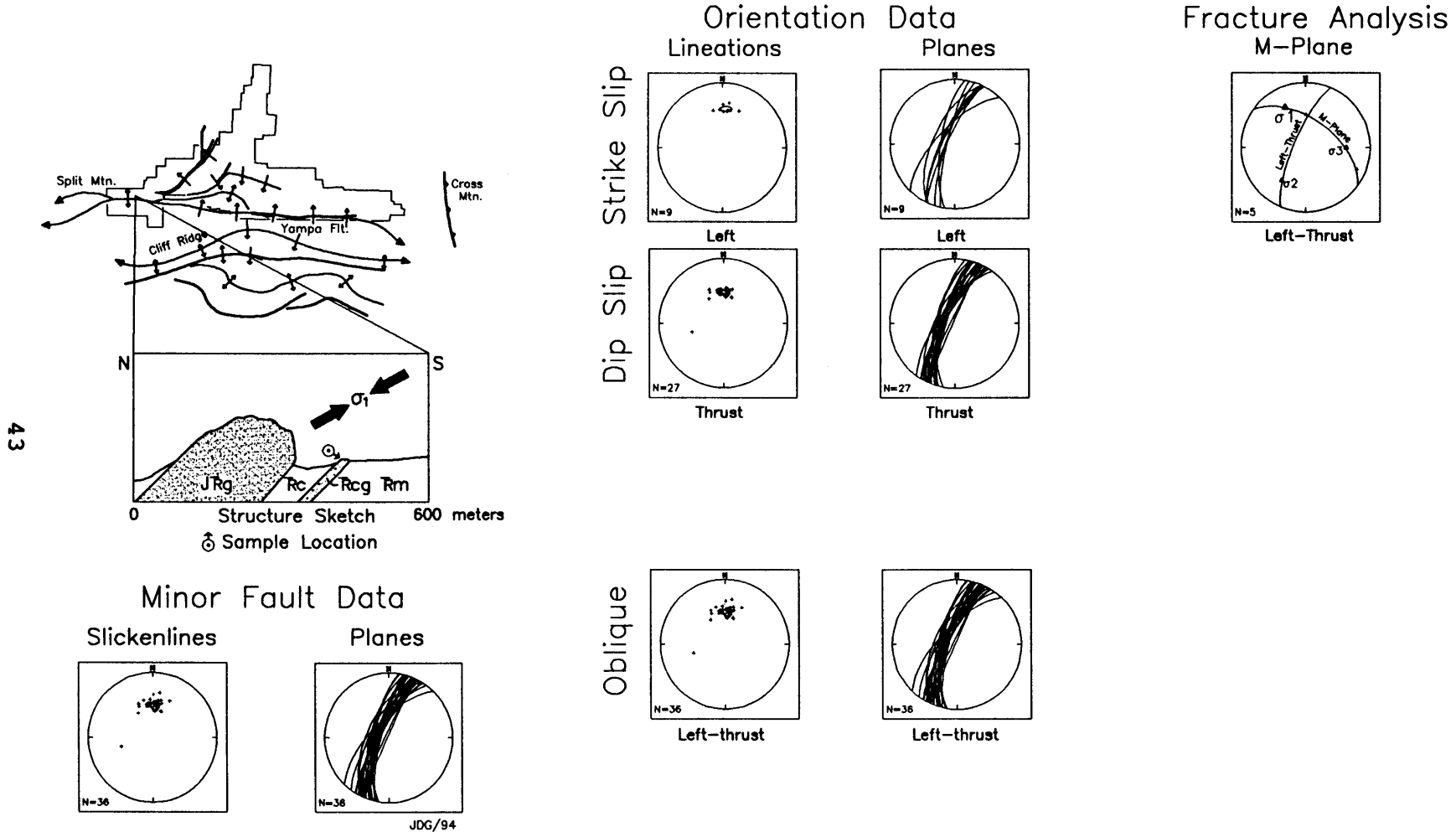


Figure 4.5 Site data summary. Ellipses represent 95% C.I. of E_1 (lineations). Solid arrows indicate apparent plunge of σ_1 in plane of section.

the slickenlines E_1 indicates a single minor fault population, however, and the M-plane construction probably provides the most reasonable σ_1 estimate.

SECTION RIDGE ANTICLINE

The Section Ridge anticline is a major west-southwest trending, south-verging structure and may partially coincide with the Uinta Basin boundary fault. Topographically, Cliff Ridge is the massive exposure of folded Weber Sandstone that forms the prominent mountain north of highway U.S. 40 just west of Dinosaur, Colorado.

Cliff Ridge Northeast

The Cliff Ridge northeast site is located on the south side of the Section Ridge anticline (Fig. 4.6) and north of the Moffat County 16 road (NW, NW, NW, SEC. 33, T1S, R25E, Uintah County, Utah; Rowley et al., 1985). A traverse up a canyon through the forelimb of the fold revealed no emergent thrusts. Most of the strata south of the Weber outcrop are covered with only a few hogbacks of more resistant strata exposed. Minor faults were found along the top of a double hogback in the Cretaceous Cedar Mountain Formation ($n = 34$) and Dakota Sandstone ($n = 61$, Fig. 4.6).

Although the overall dip of the strata from the Weber outcrop southward is nearly vertical, the dip along the top of the Dakota hogback varies from vertical to locally overturned (to $\approx 245-38$ OT). Local deviations from the overall vertical dips may reflect drag-folding in the footwall of an offset structure as seen at Split Mountain.

Minor Fault Data Analysis – Cliff Ridge Northeast

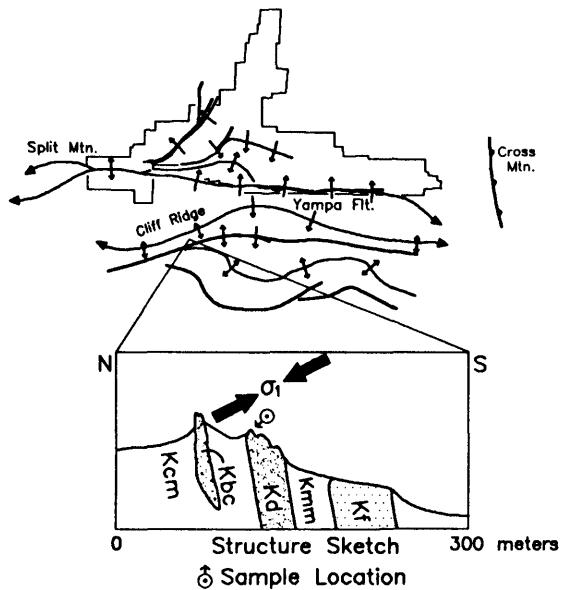
Orientation Data

Fracture Analysis

Lineations

Planes

M-Planes

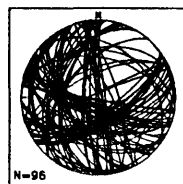
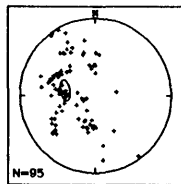


45

Minor Fault Data

Slickenlines

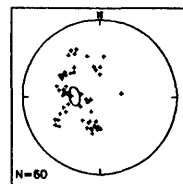
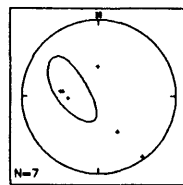
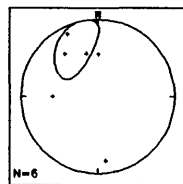
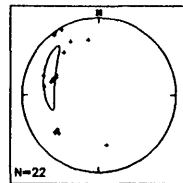
Planes



JDG/94

Strike Slip

Dip Slip

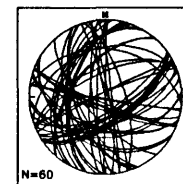
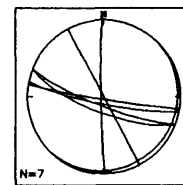
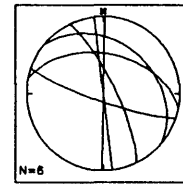
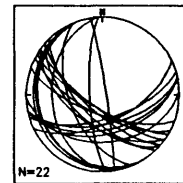


Right

Left

Thrust

Normal



Right

Left

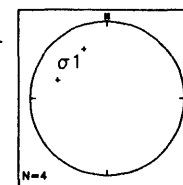
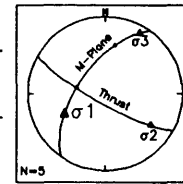
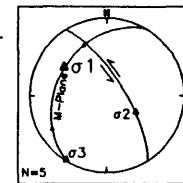
Thrust

Normal

Strike Slip

Dip Slip

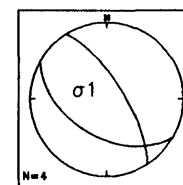
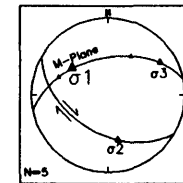
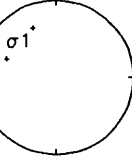
Strike Slip



Left

Thrust

Conjugate Minor Faults



Right

Figure 4.6 Site data summary. Ellipses represent 95% C.I. of E_1 (lineations). Solid arrows indicate apparent plunge of σ_1 in plane of section.

Table 4.5 Cliff Ridge Northeast - Section Ridge Anticline

PALEOSTRESS TENSOR σ_1 ESTIMATES (n = 96)			
<u>METHOD</u>	<u>TREND-PLUNGE</u>	<u>SENSE</u>	<u>‡/PROB./EIGEN.</u>
Direct Inversion	303-74	All	0.17
Octahedra Method	225-84	All	54.9%
Slickenlines E_1	280-56	All	0.6787
M-Plane(s)	243-40	Thrust	
	303-34	Left	
	306-41	Right	
Conjugate Faults E_2	289-65	Lateral	0.2845
Conjugate Striae E_1	313-33	Lateral	0.8921
Bedding Attitude	065-90		

Direct inversion gives a highly-plunging σ_1 and a prolate stress ellipsoid (Table 4.5). The octahedra method also yields a high plunge for σ_1 , but the probability is not very high. The high plunge contrasts with the other methods, however, and is probably lower. The concurrence of trends and range of plunges suggest a σ_1 that trends west-northwest and plunges about 50°.

Cliff Ridge Southwest

The Cliff Ridge southwest site is about 4.8 km west-southwest of the northeast site (Fig. 4.7; NW, NW, SW, SEC. 1, T1S, R24E, Uintah County, Utah; Rowley et al., 1985). The structural and stratigraphic location is similar except that outcrops are less prominent. Cedar Mountain and Dakota strata dip at a high angle without overturning ($\approx 90-78$ average). The Buckhorn Conglomerate yielded 85 minor faults with a conjugate relationship (Fig. 4.7).

Direct inversion of the data gives a steeply plunging σ_1 and prolate stress ellipsoid (Table 4.6). The direct

Minor Fault Data Analysis – Cliff Ridge Southwest

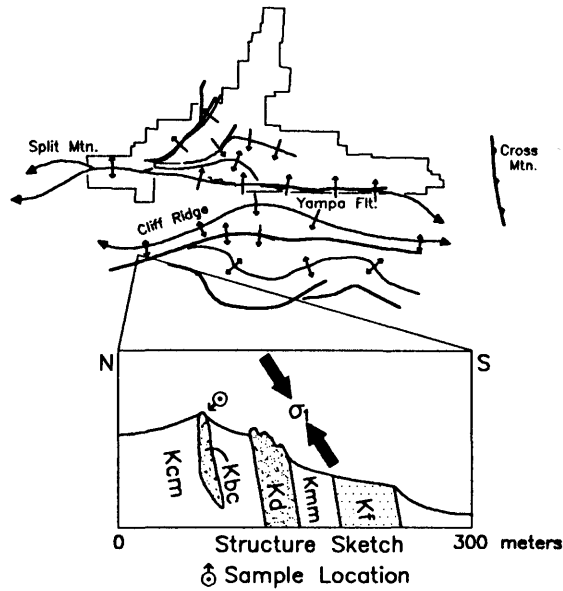
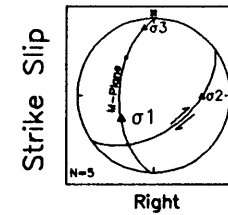
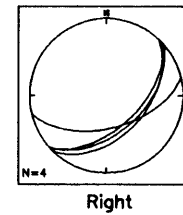
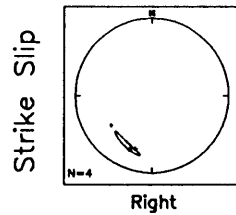
Orientation Data

Fracture Analysis

Lineations

Planes

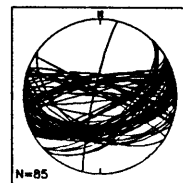
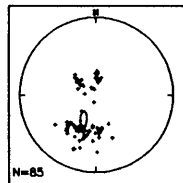
M-Plane



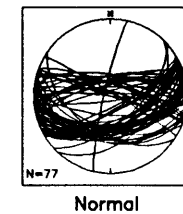
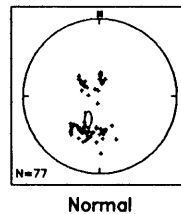
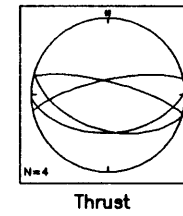
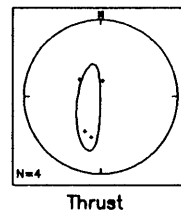
Minor Fault Data

Slickenlines

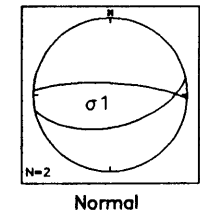
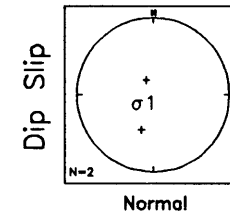
Planes



Dip Slip



Conjugate Minor Faults



47

Figure 4.7 Site data summary. Ellipses represent 95% C.I. of E_1 (lineations). Solid arrows indicate apparent plunge of σ_1 in plane of section.

Table 4.6 Cliff Ridge Southwest - Section Ridge Anticline

PALEOSTRESS TENSOR σ_1 ESTIMATES (n = 85)			
<u>METHOD</u>	<u>TREND-PLUNGE</u>	<u>SENSE</u>	<u>W/PROB./EIGEN.</u>
Direct Inversion	245-74	All	0.34
Octahedra Method	175-87	All	72.2%
Slickenlines E_1	207-61	All	0.7829
M-Plane(s)	234-48	Right	
Conjugate Faults	232-70	Normal	0.1727
Conjugate Striae	225-74	Normal	0.8010
Bedding Attitude	090-78		

inversion is similar to the conjugate interpretations, and the trend also corresponds to the right-lateral M-plane construction. The divergence of the octahedra and slickenlines E_1 estimates reflects the concentration of data on the south-dipping conjugate (Fig. 4.7). The estimates suggest an overall σ_1 trending about 235° and dipping 70-75°. The high plunge of this σ_1 estimate may reflect extension in the steeply-dipping forelimb, early thrusting and subsequent rotation, or normal faulting in response to a northeasterly regional σ_1 . With the bedding rotated back to horizontal, σ_1 would be close to horizontal with a north-northeast trend.

Willow Creek Fault - Blue Mountain

The Blue Mountain site is in the Upper Cretaceous Castlegate and Segó Sandstone (Mesa Verde Group) hogbacks about 1.6 km south of the town of Blue Mountain, Colorado. Two stations in the footwall block of the Willow Creek thrust fault yielded 28 minor fault measurements (Fig. 4.8; SW, NE, SE, and SW, SW, SW, SEC. 8, T3N, R102W, Moffat

Minor Fault Data Analysis – Blue Mountain Central

Orientation Data

Fracture Analysis

M-Planes

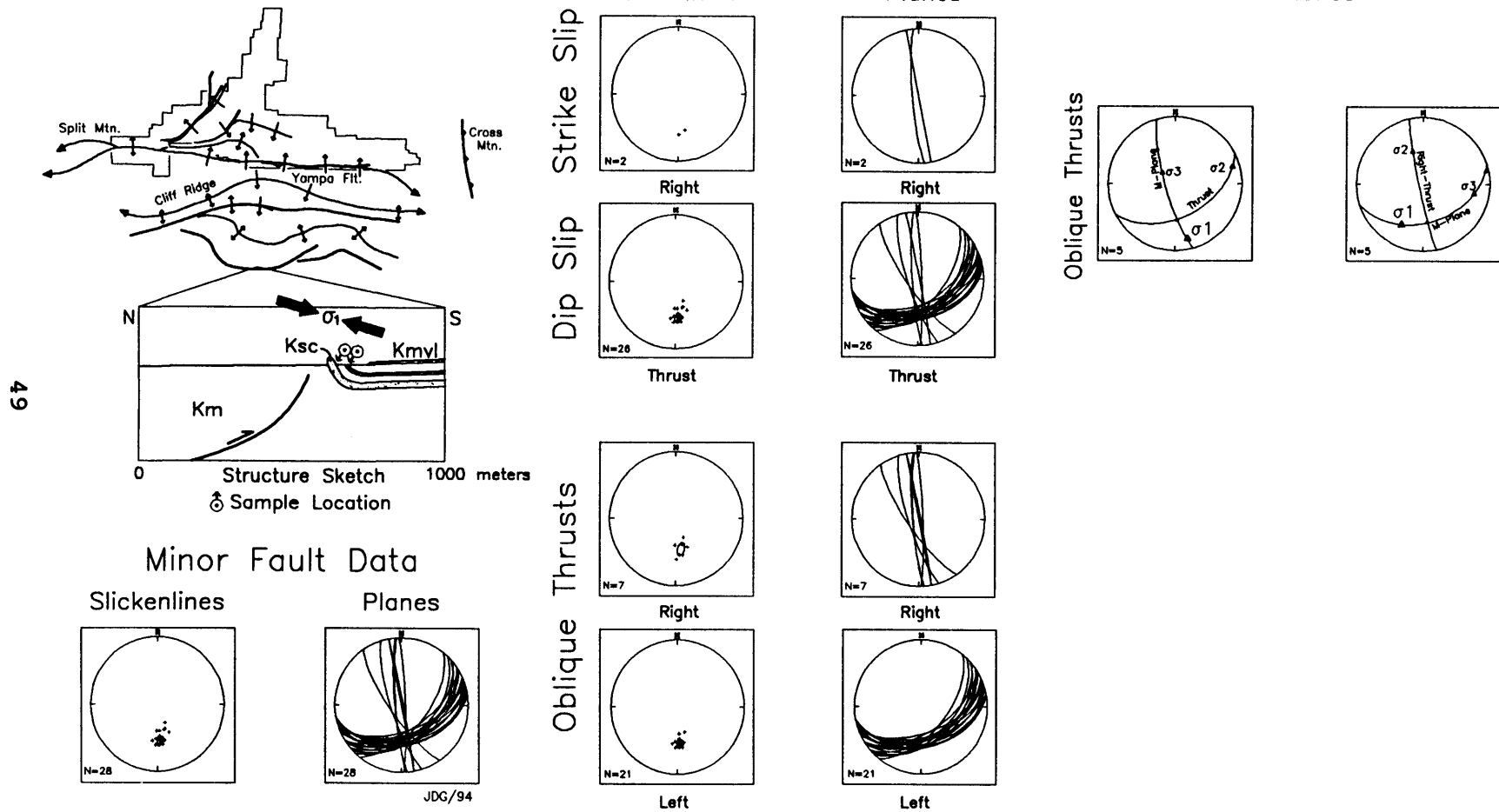


Figure 4.8 Site data summary. Ellipses represent 95% C.I. of E_1 (lineations). Solid arrows indicate apparent plunge of σ_1 in plane of section.

Table 4.7 Blue Mountain South - Willow Creek Fault

PALEOSTRESS TENSOR σ_1 ESTIMATES (n = 28)			
<u>METHOD</u>	<u>TREND-PLUNGE</u>	<u>SENSE</u>	<u>‡/PROB./EIGEN.</u>
Direct Inversion	008-00	All	0.60
Octahedra Method	357-00	All	96.4‡
Slickenlines E_1	175-47	All	0.9802
M-Plane(s)	168-16	Left-Thrust	
	208-32	Right-Thrust	
Bedding Attitude	075-49 to 067-69		

County, Colorado; Rowley et al., 1985). The first station is located just west of the Blue Mountain-Rangely road in poorly exposed Sego Sandstone with bedding oriented about 075-49, and the other station occurs about 1.6 km to the west in a prominent Castlegate Sandstone hogback (\approx 067-69). The covered trace of the Willow Creek thrust was mapped in the Mancos Shale flats just to the north (Cullins, 1969). The Willow Creek thrust may be an emergent segment of the Uinta basin boundary fault (Stone, 1993).

Although the direct stress inversion gives a somewhat oblate stress ellipsoid, the octahedra method exhibits a similar σ_1 orientation with a high probability (Table 4.7). However, the M-plane constructions suggest that the plunge is not horizontal; the horizontal plunge from the direct inversion and octahedra methods probably results from the tightly clustered slickenlines with a 47° plunge. The average paleostress results suggest that the σ_1 orientation trends southward (180-190°) and plunges about 15-20°.

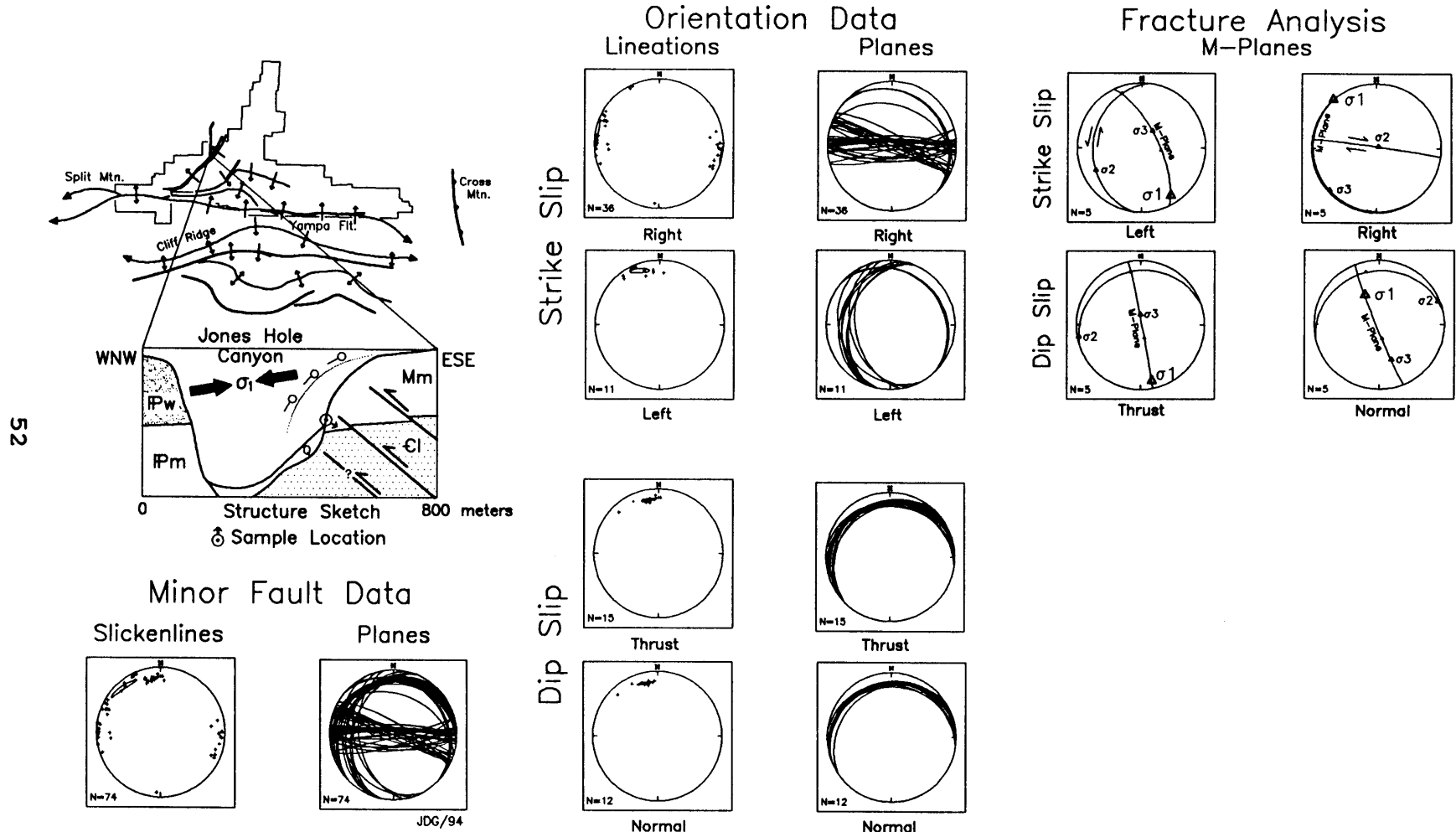
ISLAND PARK FAULT

The Island Park fault bounds the western side of the Mitten Park block. The Mitten Park block is a north-northeast trending pop-up structure between the Mitten Park and Island Park faults (Fig. 1.4). As mapped by Hansen et al. (1983), the Island Park fault forms the east-west trending northern boundary of Split Mountain anticline, curves into a northeast trend along the western margin of the Mitten Park block, and dies out north of Jones Hole in a north-south splay. In Jones Hole canyon, Cambrian and Precambrian strata are exposed in the hanging wall block. Although field observations indicate that the master fault zone in Jones Hole canyon is high angle ($\approx 75^\circ$), the hanging wall exposes several imbricate thrusts in the Mississippian Madison Limestone that dip 20-70°. Two exposures of the Cambrian Ladore Formation yielded minor fault data.

Jones Hole North

The Jones Hole north site is located up a steep box canyon to the northeast of the creek in upper Jones Hole canyon where erosion has exposed the top of Ladore sandstone in the hanging wall of the fault (Hansen, 1977a). The site occurs near the branch of the fault splays at the north end of the Island Park fault (Fig. 4.9; NE, NE, NE, SEC. 12, T3S, R25E, Uintah County, Utah). The cliff wall on the northwest side of the box canyon exposes a complexly faulted and brecciated fold in the Madison Limestone. Two exposed imbricate thrusts may correspond with mapped fault splays

Minor Fault Data Analysis – Jones' Hole North



52

Figure 4.9 Site data summary. Ellipses represent 95% C.I. of E_1 (lineations). Solid arrows indicate apparent plunge of σ_1 in plane of section.

Table 4.8 Jones' Hole North - Island Park Fault

PALEOSTRESS TENSOR σ_1 ESTIMATES (n = 74)			
METHOD	TREND-PLUNGE	SENSE	\$/PROB./EIGEN.
Direct Inversion	318-07	All	0.14
Octahedra Method	304-16	All	44.4%
Slickenlines E_1	320-11	All	0.6720
M-Plane(s)	168-12	Thrust	
	148-14	Left	
	318-00	Right	
	332-48	Normal	
Bedding Attitude	190-17		

with the lower one oriented about 335-43 and the upper one oriented about 030-32. The upper thrust was mapped up the ridgeline by Hansen (1977a). Difficult access limited data collection to 74 minor fault measurements (Fig. 4.9). A poorly exposed, low-angle minor fault displayed both thrust and normal Riedel shears on the same surface.

The σ_1 estimates range in trend from 304° to 348° (Table 4.8). Direct stress inversion gives a prolate stress ellipsoid, and agrees well with the average M-plane (\approx 331-12) and slickenlines E_1 . The σ_1 from the octahedra method yields a low probability (44.4%). The results suggest a σ_1 with a northwesterly trend and almost horizontal plunge.

Jones Hole South

The Jones Hole south site is located about one km south of the northern site (Fig. 4.10; NW, NE, SW, SEC. 12, T3S, R25E, Uintah County, Utah; Hansen, 1977a). Minor faults (n = 30) occur in the middle Ladore sandstone exposed in the hanging wall near a covered section of the fault.

Table 4.9 Jones' Hole South - Island Park Fault

PALEOSTRESS TENSOR σ_1 ESTIMATES (n = 30)			
<u>METHOD</u>	<u>TREND-PLUNGE</u>	<u>SENSE</u>	<u>%/PROB./EIGEN.</u>
Direct Inversion	297-18	All	0.42
Octahedra Method	115-14	All	48.7%
Slickenlines E ₁	299-21	All	0.7767
M-Plane(s)	238-52	Thrust	
	267-04	Left	
	328-19	Right	
Bedding Attitude	176-20		

Direct stress inversion gives a west-northwest trending prolate stress ellipsoid that corresponds well with the slickenlines E₁ (Table 4.9). The octahedra method estimates a similar σ_1 axial trend that plunges in opposite direction. The M-plane average trends more westerly. The results suggest a west-northwest trending σ_1 that plunges about 20°.

Island Park South

The Island Park south site is located near the end of the Island Park road and the mouth of Whirlpool Canyon in Dinosaur National Monument (Fig. 4.11; NE, SE, NW, SEC. 33, T3S, R25E, Uintah County, Utah; Hansen, 1979a). The southwestern end of the northeast-trending segment of the Island Park fault is generally delineated and mapped by the juxtaposition of the Weber Sandstone against Mesozoic strata (Hansen, 1979a). Footwall strata display little deformation and low bedding dips to within a few 10s of meters from the fault zone. Triassic Moenkopi and Chinle rocks in the hanging wall are sharply dragged into steep dips near the fault. Much of the fault trace is covered, however, and few

Minor Fault Data Analysis – Jones' Hole South

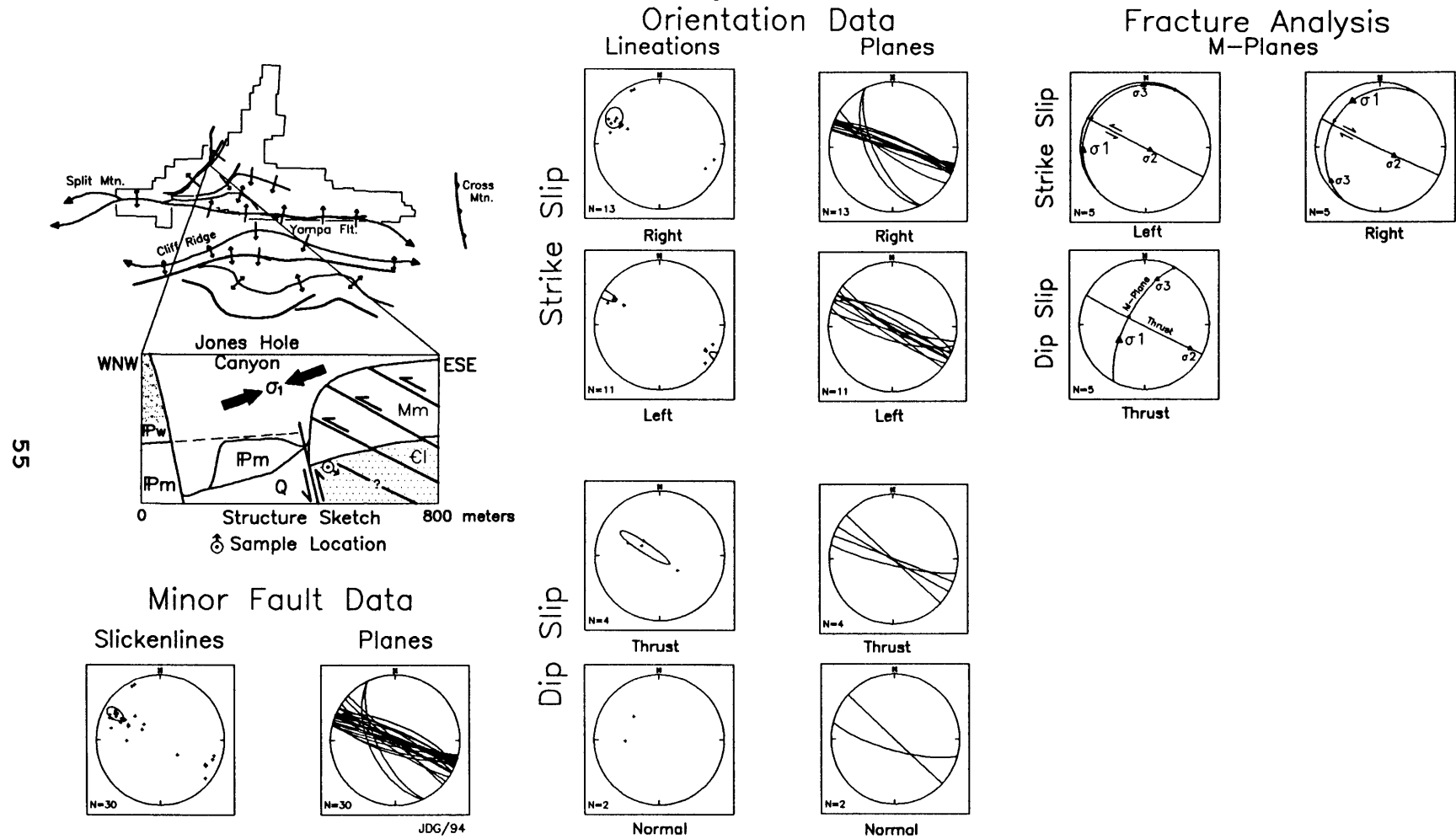
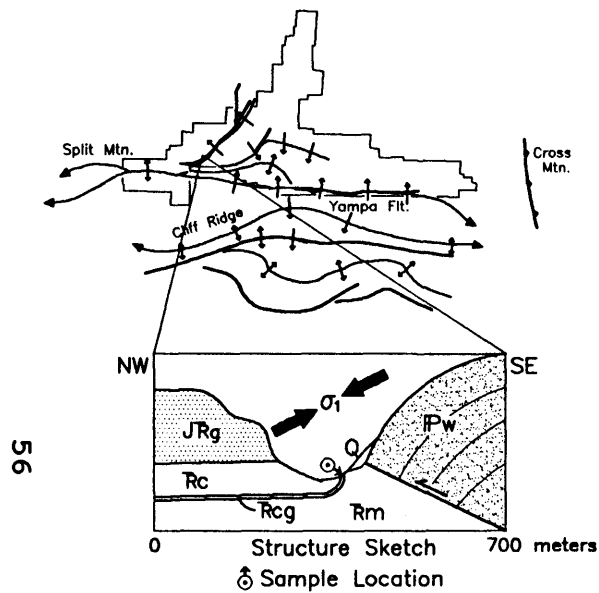


Figure 4.10 Site data summary. Ellipses represent 95% C.I. of E_1 (lineations). Solid arrows indicate apparent plunge of σ_1 in plane of section.

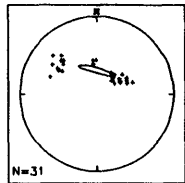
Minor Fault Data Analysis – Island Park South



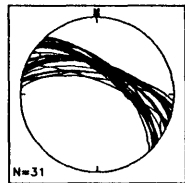
56

Minor Fault Data

Slickenlines



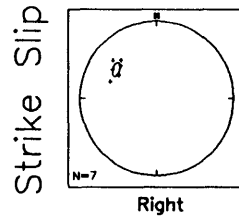
Planes



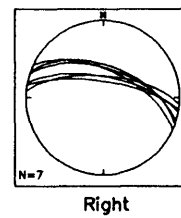
JDC/94

Orientation Data

Lineations

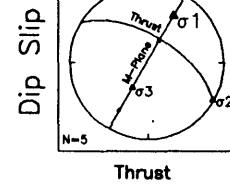
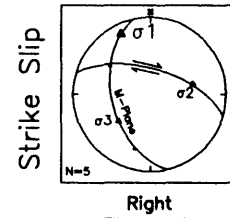


Planes



Fracture Analysis

M-planes



Dip Slip

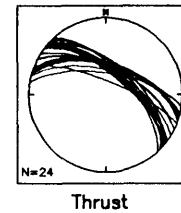
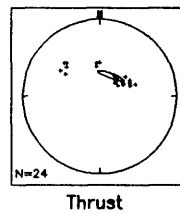


Figure 4.11 Site data summary. Ellipses represent 95% C.I. of E_1 (lineations). Solid arrows indicate apparent plunge of σ_1 in plane of section.

Table 4.10 Island Park Fault South

PALEOSTRESS TENSOR σ_1 ESTIMATES (n = 31)			
<u>METHOD</u>	<u>TREND-PLUNGE</u>	<u>SENSE</u>	<u>*/PROB./EIGEN.</u>
Direct Inversion	087-32	All	0.56
Octahedra Method	061-45	All	93.7%
Slickenlines E_1	358-65	All	0.7350
M-Plane(s)	030-32	Thrust	
	333-40	Right	
Bedding Attitude	226-85 to 038-60 OT		

minor faults were found in the area. Nearly vertical (226-85) to overturned (038-60 OT) Moenkopi and Chinle strata yielded 31 slickenside measurements over a large area.

Although direct inversion and the octahedra method exhibit somewhat similar σ_1 estimates, the lack of variability in the data set surely biased the estimates (Table 4.10). The slickenlines E_1 trend corresponds closely to the average M-plane, however, and the results suggest a northerly σ_1 trend that plunges about 30-40°.

MITTEN PARK FAULT

The Mitten Park fault bounds the eastern side of the Mitten Park block opposite the Island Park fault (Fig. 1.5). The Mitten Park fault and monocline trend northeast-southwest with dextral bends trending generally east-west on both ends. Structural offset on the northern end of the northeast-trending segment dies out rapidly after intersecting the east-trending Warm Springs monocline. The Green River meanders around the Mitten Park/Warm Springs intersection and exposes the Mitten Park fault at the head of Whirlpool Canyon. The southern end of the Mitten Park

Table 4.11 Mitten Park Northeast - Warm Springs Monocline

PALEOSTRESS TENSOR σ_1 ESTIMATES (n = 47)			
METHOD	TREND-PLUNGE	SENSE	Σ /PROB./EIGEN.
Direct Inversion	218-11	All	0.31
Octahedra Method	220-11	All	72.2%
Slickenlines E_1	214-33	All	0.6727
M-Plane(s)	115-48	Thrust	
	203-30	Left	
	241-04	Right	
	238-50	Normal	
Conjugate Faults E_2	040-00	Lateral	0.1031
Conjugate Striae E_1	218-14	Lateral	0.8782
Bedding Attitude	103-53		

monocline curves westward and merges into the western Red Rock anticline. Vertical structural relief on the Mitten Park structure approaches 900 meters (3000 feet).

Mitten Park Northeast - Warm Springs Monocline

The Warm Springs monocline is exposed in the Canyon of Ladore just east of its intersection with the Mitten Park fault (Hansen, 1977b). The fault underlying the monocline is not emergent in the canyon, and the strata in the forelimb of the fold are oriented about 103-53 at the level of the Green River. The site is located on the west side of the Green River in the fine-grained sandstones of the Mississippian Humbug Formation (Fig. 4.12; NW, NW, SW, SEC. 28, T7N, R104W, Moffat County, Colorado; Hansen, 1977b). The 47 minor faults display a conjugate relationship.

With the exception of the thrust M-plane construction, the stress tensor estimates exhibit a southwest trending σ_1 (Table 4.11). Overall, the results suggest a southwest trending σ_1 that plunges about 10-20°.

Minor Fault Data Analysis – Mitten Park/Warm Springs

Orientation Data

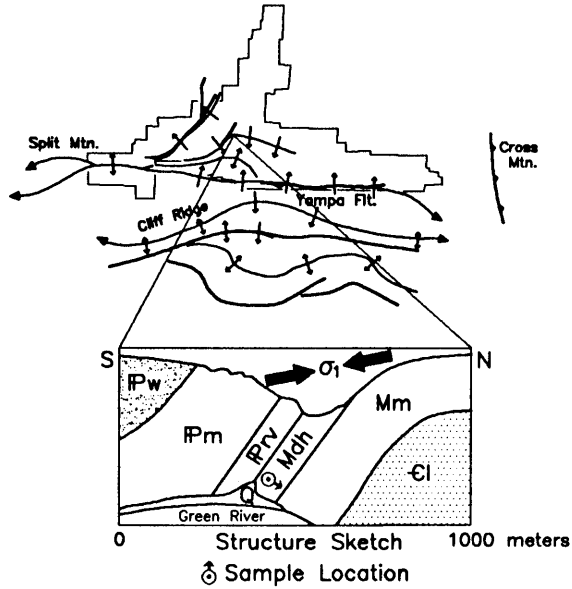
Fracture Analysis

Lineations

Planes

M-Planes

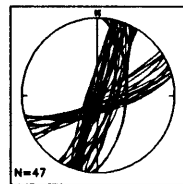
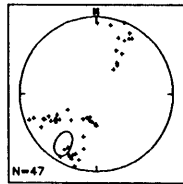
59



Minor Fault Data

Slickenlines

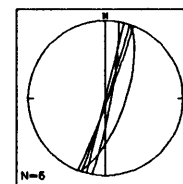
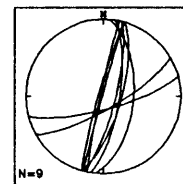
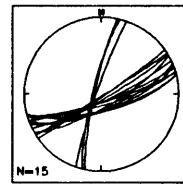
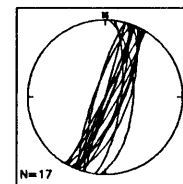
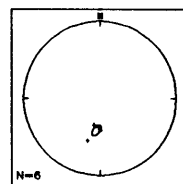
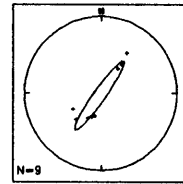
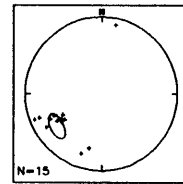
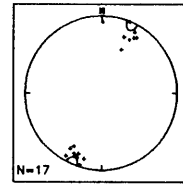
Planes



JDG/94

Strike Slip

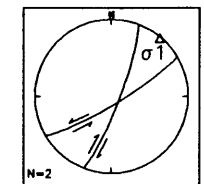
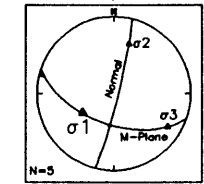
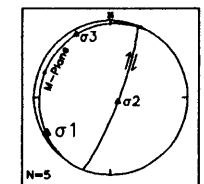
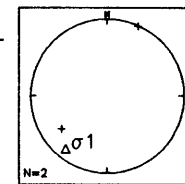
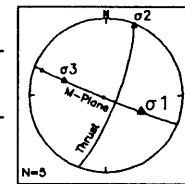
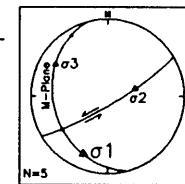
Dip Slip



Strike Slip

Dip Slip

Strike Slip



Conjugate Minor Faults

Figure 4.12 Site data summary. Ellipses represent 95% C.I. of E_1 (lineations). Solid arrows indicate apparent plunge of σ_1 in plane of section.

Table 4.12 Mitten Park Fault - North of Green River

PALEOSTRESS TENSOR σ_1 ESTIMATES (n = 64)			
METHOD	TREND-PLUNGE	SENSE	λ /PROB./EIGEN.
Direct Inversion	334-24	All	0.34
Octahedra Method	321-26	All	68.8%
Slickenlines E_1	276-44	All	0.4912
M-Plane(s)	296-44	Thrust	
	016-10	Left	
	324-23	Right	
Bedding Attitude	052-30 to 035-39		

Mitten Park - North of Green River

The Mitten Park north site is about 1.6 km downstream from Echo Park on the north side of the Green River at the head of Whirlpool Canyon (NW, NW, SE, SEC. 29, T7N, R104W, Moffat County, Colorado; Hansen, 1977b). The orientation of the Mitten Park fault across the canyon in the fault zone measures about 222-55. At the level of the Green River, the Mitten Park fault places Precambrian Uinta Group strata against upper Mississippian rocks. The Cambrian Ladore sandstones provided most of the exposed minor faults (n = 54), although some slickensides were found in the Pennsylvanian-age upper Morgan Formation sandstones (n = 10). Bedding attitudes range from 052-30 to 035-39 in the Ladore (hanging wall) adjacent to the fault and 071-87 in the Morgan (footwall). The minor faults display diverse attitudes and slip (Fig. 4.13).

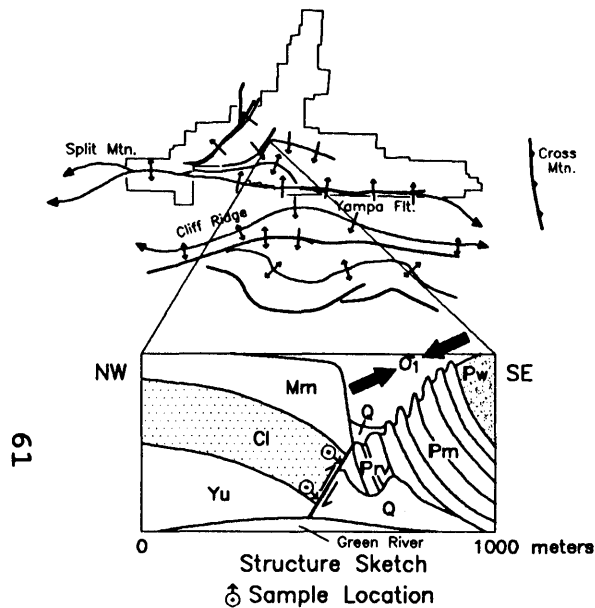
Direct inversion, the octahedra method, and the average M-plane all give a northwesterly orientation for σ_1 (Table 4.12). The low slickenlines E_1 eigenvalue indicates a poor

Minor Fault Data Analysis – Mitten Park North of Green River

Orientation Data

Fracture Analysis

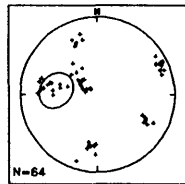
M-Planes



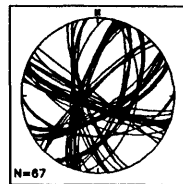
61

Minor Fault Data

Slickenlines



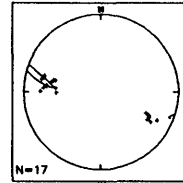
Planes



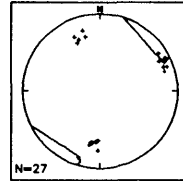
JDG/94

Strike Slip

Lneations

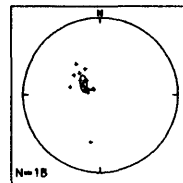


Right

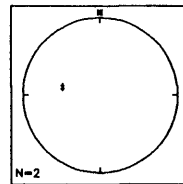


Left

Dip Slip

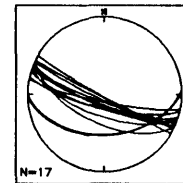


Thrust

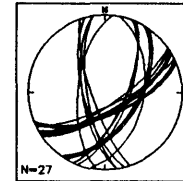


Normal

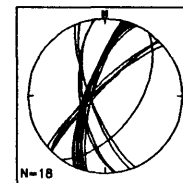
Planes



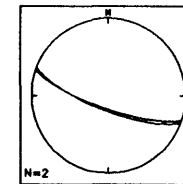
Right



Left

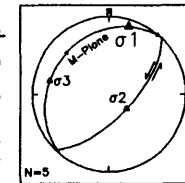


Thrust



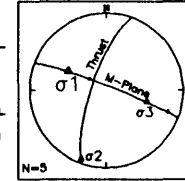
Normal

Strike Slip

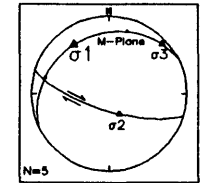


Left

Dip Slip



Thrust



Right

Figure 4.13 Site data summary. Ellipses represent 95% C.I. of E_1 (lineations). Solid arrows indicate apparent plunge of σ_1 in plane of section.

Table 4.13 Mitten Park Fault - South of the Green River

PALEOSTRESS TENSOR σ_1 ESTIMATES (n = 48)			
<u>METHOD</u>	<u>TREND-PLUNGE</u>	<u>SENSE</u>	<u>\$/PROB./EIGEN.</u>
Direct Inversion	118-15	All	0.27
Octahedra Method	295-13	All	54.7%
Slickenlines E_1	116-28	All	0.7009
M-Plane(s)	027-49	Thrust	
	094-12	Left	
	135-25	Right	
	058-52	Normal	
Conjugate Faults E_2	115-41	Lateral	0.0685
Conjugate Striae E_1	119-15	Lateral	0.9257
Bedding Attitude	050-20		

conjugate relationship. Overall, the results suggest a north-northwest σ_1 trend that plunges about 25°.

Mitten Park - South of Green River

The Mitten Park south site is located on the south side of the Green River opposite the site above (NE, SE, SW, SEC. 29, T7N, R104W, Moffat County, Colorado; Hansen, 1977b). The Mitten Park fault is well exposed, and in some places, the fault zone is less than 20 meters wide. All of the minor faults found at the south site occurred in the Cambrian Ladore Formation sandstones. The Ladore is exposed low on the hillside with an attitude of about 050-20 (Table 4.13). Rocks near the fault are highly fractured and display numerous silicified slip zones. Some minor faults exhibited gouge zones that were occasionally associated with poor slickensides. One such gouge zone was oriented about 240-80 with senseless slicks trending 334-80. Most of the 49 minor faults measured at the site came from a shear face in the hanging wall near the fault trace (Fig. 4.14).

Minor Fault Data Analysis – Mitten Park South of Green River

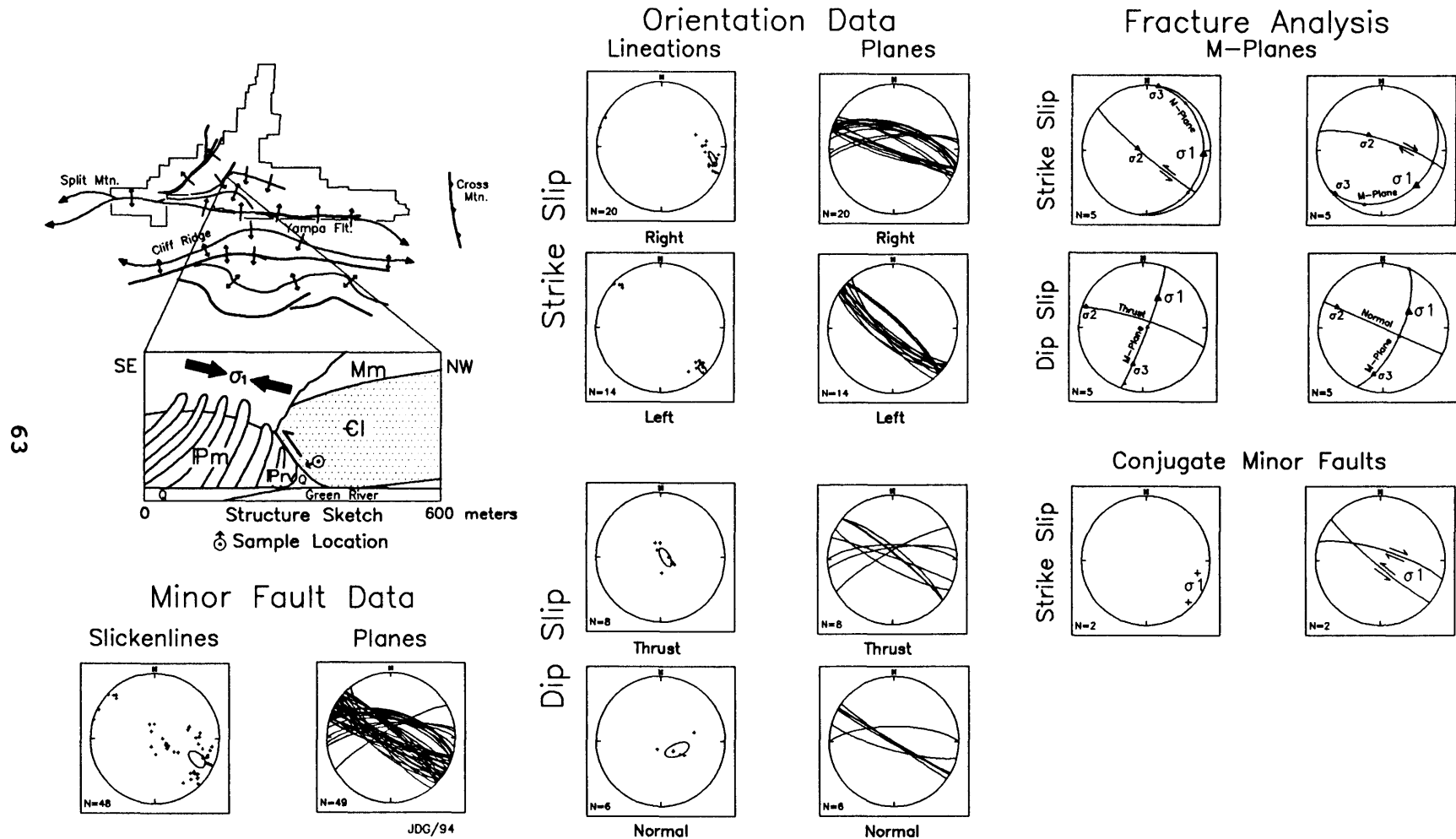


Figure 4.14 Site data summary. Ellipses represent 95% C.I. of E_1 (lineations). Solid arrows indicate apparent plunge of σ_1 in plane of section.

With the exception of the thrust and normal M-plane constructions, all the methods give similar σ_1 axial trends (Table 4.13). Although conjugate constructions did not exhibit eigenvalues consistent with conjugate faulting, the σ_1 orientations were close to the other methods. The thrust and normal M-plane estimates for σ_1 display an average trend toward the northeast and share a common axial trend with the σ_1 computed for the Mitten Park/Warm Springs site. The two sites are less than 1.6 km apart, and the common σ_1 trends may be related. This may reflect two stress tensors or complex local stresses across the structural corner between the Mitten Park and Warm Springs structures. The stress tensor estimates at the Mitten Park south site suggest a σ_1 trending to the west-northwest and plunging 10-20°.

Mitten Park Southwest

The Mitten Park southwest site is located near the axis of the Trail Draw syncline about 3.2 km west of the Chew ranch homestead and the Echo Park road (SW, NW, SE, SEC. 2, T6N, R104W, Moffat County, Colorado; Hansen and Rowley, 1980a). The sampling site is about 500 meters north of the Weber Sandstone outcrop in the forelimb of the north vergent Red Rock anticline. The minor faults occur in the south-southeast vergent Weber Sandstone forelimb of the Mitten Park monocline. The 36 minor faults measured at the site displayed similar orientations but different slip senses along the same trends (Fig. 4.15).

Minor Fault Data Analysis – Mitten Park Southwest

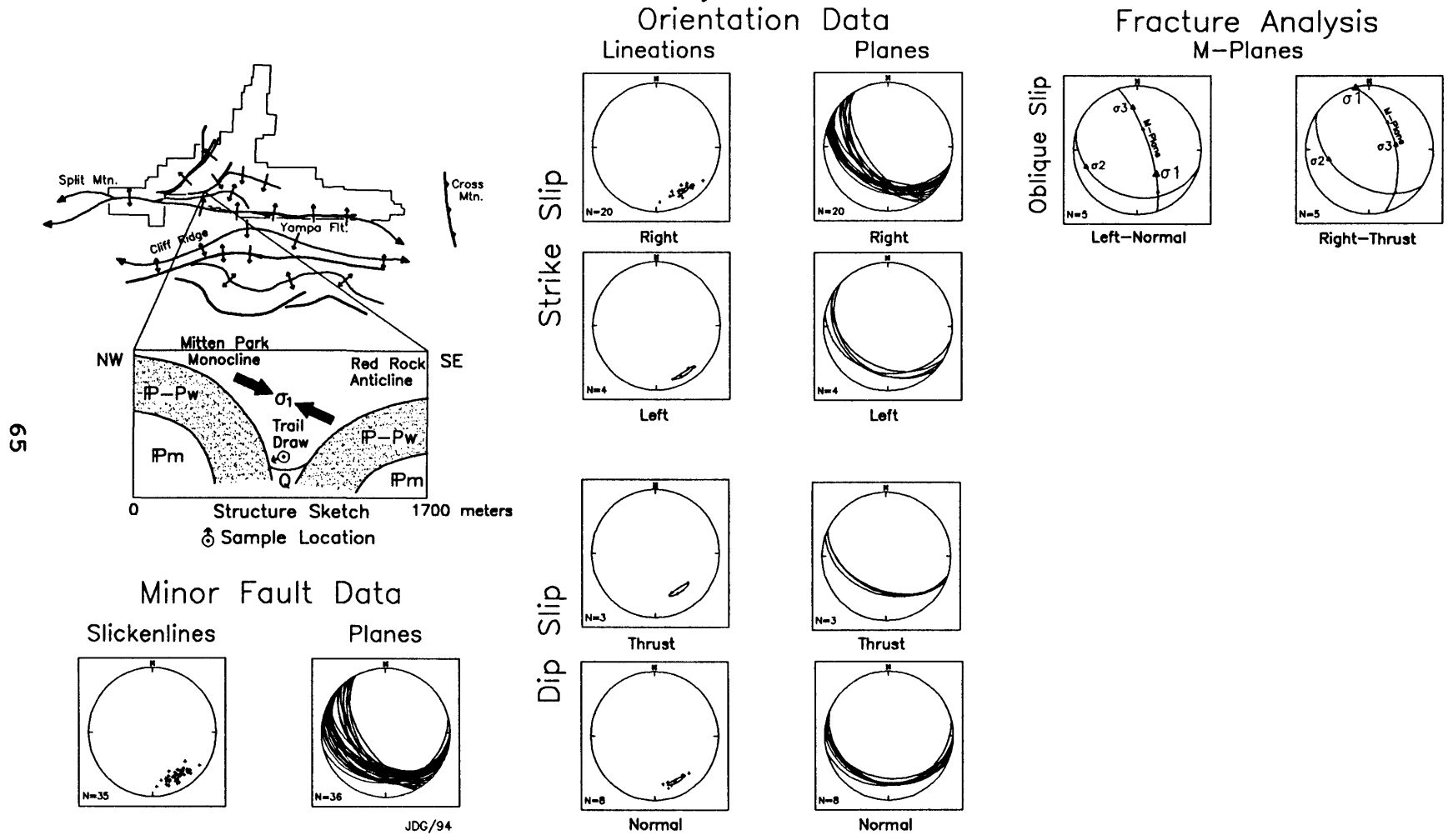


Figure 4.15 Site data summary. Ellipses represent 95% C.I. of E_1 (lineations). Solid arrows indicate apparent plunge of σ_1 in plane of section.

Table 4.14 Mitten Park Monocline Southwest

PALEOSTRESS TENSOR σ_1 ESTIMATES (n = 36)			
<u>METHOD</u>	<u>TREND-PLUNGE</u>	<u>SENSE</u>	<u>\$/PROB./EIGEN.</u>
Direct Inversion	213-34	All	0.26
Octahedra Method	193-31	All	78.4%
Slickenlines E_1	149-22	All	0.9549
M-Plane(s)	142-50	Left-Normal	
	347-02	Right-Thrust	
Bedding Attitude	051-75		

The small number of measurements and the low variety of minor fault orientations make each paleostress analysis suspect (Table 4.14). The direct inversion and octahedra methods suggest a south-southwest directed σ_1 . However, the slickenlines E_1 and the M-plane constructions suggest a more south-southeast trending σ_1 . Because the problems expressed above affect the first two methods the most, the slickenlines E_1 and M-plane constructions provide more reliable estimates and suggest a south-southeast trending σ_1 that dips 20-30°.

Red Rock Anticline

The Red Rock site is located south of the Mitten Park southwest site in the Weber Sandstone forelimb of the Red Rock anticline (Fig. 4.16; SE, SW, SE, SEC. 2, T6N, R104W, Moffat County, Colorado; Hansen and Rowley, 1980a). Although mapped as an almost continuous outcrop (Hansen and Rowley, 1980a), much of the Weber is covered at the site and is exposed as isolated flatirons. Pervasive fracturing in the lower part of the Weber flatiron made bedding difficult to distinguish and measurements difficult. Bedding

Minor Fault Data Analysis – Red Rock West

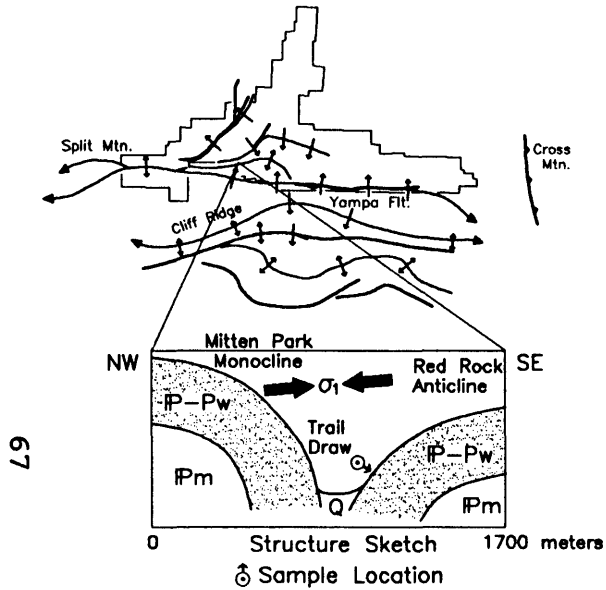
Orientation Data

Fracture Analysis

M-Planes

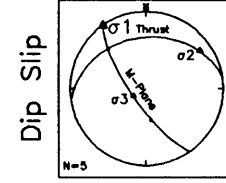
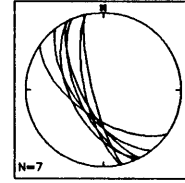
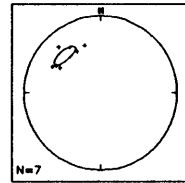
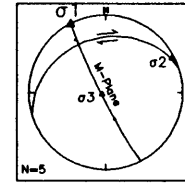
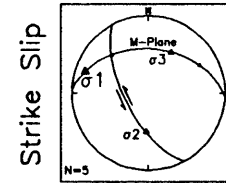
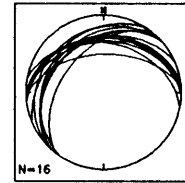
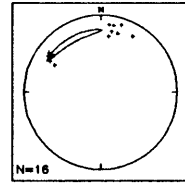
Lineations

Planes



67

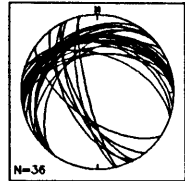
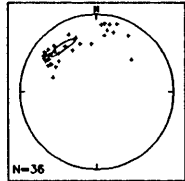
Strike Slip



Minor Fault Data

Slickenlines

Planes



JDC/94

Dip Slip

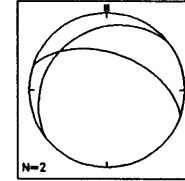
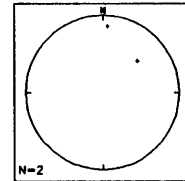
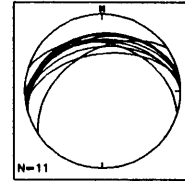
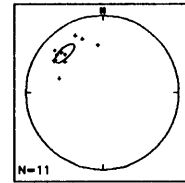


Figure 4.16 Site data summary. Ellipses represent 95% C.I. of E_1 (lineations). Solid arrows indicate apparent plunge of σ_1 in plane of section.

Table 4.15 Red Rock Anticline West

PALEOSTRESS TENSOR σ_1 ESTIMATES (n = 36)			
METHOD	TREND-PLUNGE	SENSE	\$/PROB./EIGEN.
Direct Inversion	092-12	All	0.36
Octahedra Method	300-05	All	86.6%
Slickenlines E_1	323-28	All	0.7875
M-Plane(s)	325-01	Thrust	
	288-14	Left	
	332-00	Right	
Bedding Attitude	255-25		

attitudes in the flatiron were diverse, however, and locally did not parallel the forelimb attitude. In the highly fractured sandstone, the bedding averaged about 255-25. Most of the 36 minor faults appeared to be nearly bedding parallel (Fig. 4.16).

Estimates of the σ_1 axial trend range from 272° to 332° with generally low plunge (Table 4.15). The direct inversion and octahedra methods give a prolate stress ellipsoid and a high probability, respectively. The slickenlines E_1 orientation agrees with the M-plane constructions. Overall, the σ_1 estimates suggest a north-northwest trend and almost horizontal plunge.

YAMPA MONOCLINE AND FAULT

The Yampa structure can be traced for about 80 km from the western end of Split Mountain almost to Cross Mountain on the east. The Yampa structure splays toward the west to produce the Red Rock anticline and then merges with the Red Rock, Mitten Park, and Island Park structures to form the northern margin of Split Mountain (Fig. 1.5). Along the

central part of the structure, the Yampa fault forms the northern boundary of the Blue Mountain highland. To the east, the Yampa structure splays into north and south monoclines before losing surface expression west of Cross Mountain. The Yampa/Wolf Creek structural trend aligns with the buried Elk Springs anticline, however, which may represent a subsurface continuation of the Blue Mountain structure to the east (Stone, 1986b; Rowley et al., 1985; Dyni, 1968).

Yampa Monocline West

The Yampa west site is located about 6.4 km west-southwest of the Red Rock and Mitten Park southwest site (Fig. 4.17; NW, NW, SW, SEC. 15, T1S, R25E, Uintah County, Utah; Hansen and Rowley, 1980a). The site is east of the Dinosaur National Monument overlook of Moonshine Draw and Vivas Cake Hill off of the Harper's Corner road (Hansen et al., 1983). The Weber Sandstone crops out east of the overlook with an orientation of about 275-68 (Table 4.16). Sixteen minor faults were found in the poorly exposed Weber strata near the top of the north-vergent forelimb of the Yampa monocline. The minor faults appear to form a crude conjugate set (Fig. 4.17).

With the exception of the direct inversion method, all of the σ_1 estimates are comparable (Table 4.16). Direct inversion yields an oblate stress ellipsoid. In contrast, the similar σ_1 estimates from the octahedra and slickenlines E_1 methods display a high probability and an eigenvalue

Minor Fault Data Analysis – Yampa Monocline West

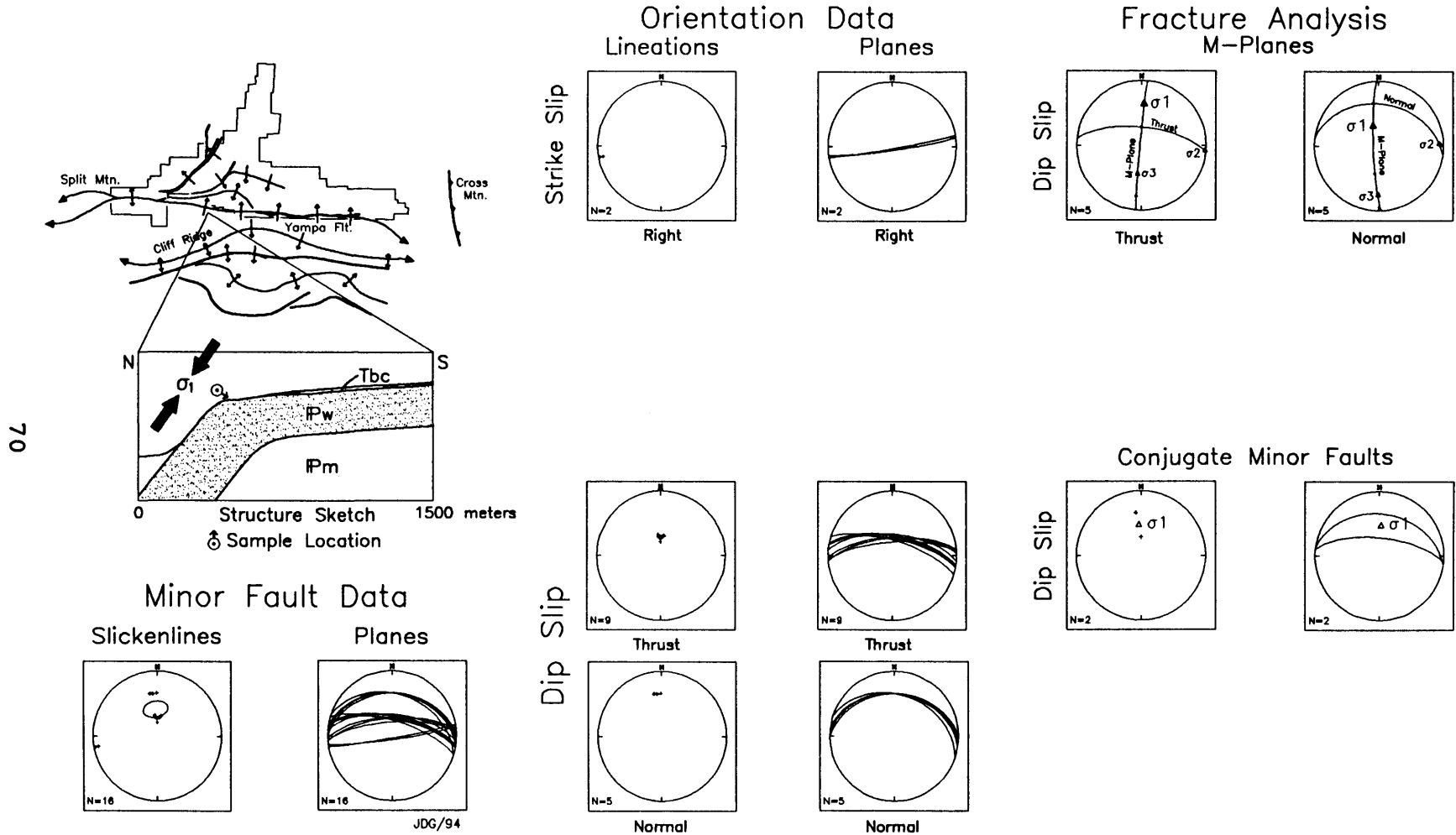


Figure 4.17 Site data summary. Ellipses represent 95% C.I. of E_1 (lineations). Solid arrows indicate apparent plunge of σ_1 in plane of section.

Table 4.16 Yampa Monocline West

PALEOSTRESS TENSOR σ_1 ESTIMATES (n = 16)			
METHOD	TREND-PLUNGE	SENSE	‡/PROB./EIGEN.
Direct Inversion	313-34	All	0.74
Octahedra Method	352-60	All	82.0%
Slickenlines E_1	356-56	All	0.8088
M-Plane(s)	003-37	Thrust	
	343-64	Normal	
Conjugate Faults E_2	003-51	Thrust-Normal	0.0761
Conjugate Striae E_1	355-51	Thrust-Normal	0.9181
Bedding Attitude	275-68		

consistent with conjugate faulting. Overall, the results suggest a σ_1 that trends about 355° and plunges about 50-60°. The overall orientation of the minor faults suggest almost bedding parallel thrusting with subsequent rotation. Rotating the bedding to horizontal results in a σ_1 trend of about 175° that plunges 10-20°.

Yampa Fault - Hells Canyon

Hells Canyon is located about 16 km east of the Yampa west site and 1.6 km south of the Yampa bench road in Dinosaur National Monument (Hansen et al., 1983). Hells Canyon is a deeply incised side canyon of the Yampa River that exposes the north-directed Yampa thrust fault. On the west side of Hells Canyon, the Yampa fault places the uppermost Precambrian Uinta Group into contact with the Triassic Chinle Formation. Across Hells Canyon, the exposed Yampa fault is oriented about 080-24 and displays about 1220 meters (4000 feet) of stratigraphic separation along the fault. Stratigraphic throw across the fault zone is about 1450 meters (4750 feet), however, which equates with a

Table 4.17 Hell's Canyon West - Yampa Fault

PALEOSTRESS TENSOR σ_1 ESTIMATES (n = 27)			
<u>METHOD</u>	<u>TREND-PLUNGE</u>	<u>SENSE</u>	<u>\$/PROB./EIGEN.</u>
Direct Inversion	171-11	All	0.25
Octahedra Method	155-14	All	52.8%
Slickenlines E_1	148-10	All	0.5736
M-Plane(s)	189-20	Thrust	
	287-15	Left	
	169-05	Right	
Bedding Attitude	311-25 to 295-65		

trigonometrically computed underlying fault dip of approximately 51°. A secondary fault observed on both sides of the canyon near the hinge in the upper forelimb exhibited an attitude of about 125-84. Most of the minor faults were found near the thrust in the Precambrian Uinta Group quartzites and Cambrian Ladore sandstones.

Hells Canyon West

The poorly exposed Uinta and Ladore rocks on the west side of Hells Canyon yielded 27 minor fault measurements (Fig. 4.18; NE, SE, SEC. 30, T6N, R102W, Moffat County, Colorado; Hansen and Rowley, 1980b). Most of the data came from high in the exposed forelimb of the fold. Bedding at the site ranged from about 311-25 to 295-65.

With exception of the left-lateral M-plane, all of the methods provide broadly similar σ_1 estimates (Table 4.17). Direct inversion gives a prolate stress ellipsoid, and the octahedra method has a high probability. The right-lateral M-plane is similar to the direct inversion. The results suggest a σ_1 trending about 170° and plunging 10-15°.

Minor Fault Data Analysis – Hell's Canyon West

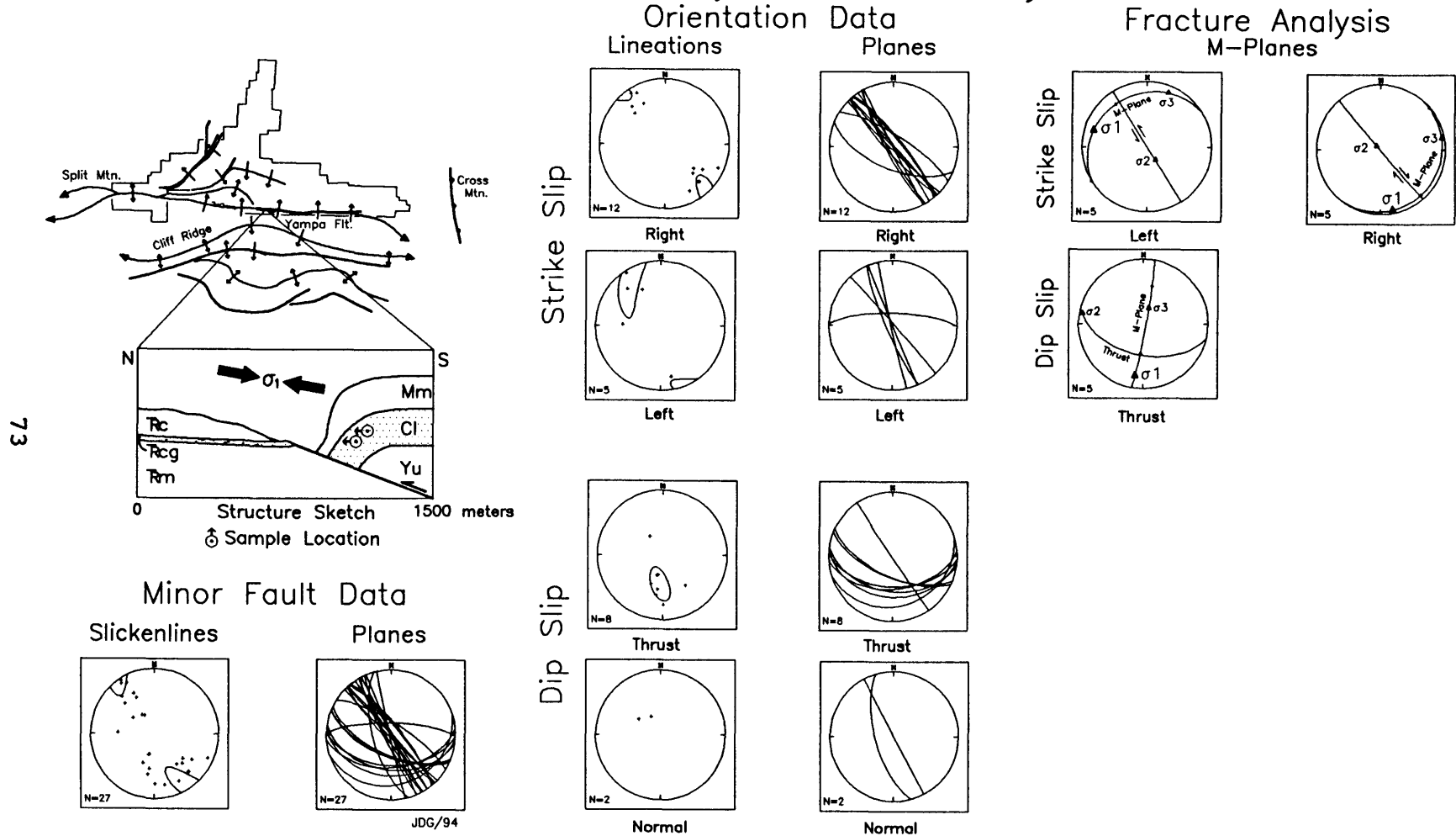


Figure 4.18 Site data summary. Ellipses represent 95% C.I. of E_1 (lineations). Solid arrows indicate apparent plunge of σ_1 in plane of section.

Table 4.18 Hell's Canyon East - Yampa Fault

PALEOSTRESS TENSOR σ_1 ESTIMATES (n = 72)			
<u>METHOD</u>	<u>TREND-PLUNGE</u>	<u>SENSE</u>	<u>#/PROB./EIGEN.</u>
Direct Inversion	355-05	All	0.45
Octahedra Method	340-08	All	57.7%
Slickenlines E_1	005-31	All	0.5954
M-Plane(s)	001-14	Thrust	
	234-55	Normal	
Bedding Attitude	239-70 to 289-05		

Hells Canyon East

Most of the minor fault data from the east side of Hells Canyon came from hanging wall outcrops close to the Yampa thrust fault (Fig.4.19) NW, SW, SEC. 29, T6N, R102W, Moffat County, Colorado; Hansen and Rowley, 1980b). The Cambrian Ladore Formation sandstones provided most of the data, but several measurements came from Precambrian Uinta Mountain Group quartzites. Bedding attitudes range from about 239-70 to 289-05. The 72 minor faults display a wide variety of attitudes, but the splay-like array of minor thrust faults appear to be the most representative.

With the exception of the normal M-plane construction, the paleostress estimates display a north to north-northwest σ_1 trend of low plunge (Table 4.18). In contrast, the normal M-plane construction is based on a small, diverse data set of only 5 measurements. The results suggest a σ_1 trending about 350° and plunging 10-15°.

Johnson Draw

Johnson Draw is located about 8 km east of Hells Canyon and 1.6 km south of the Yampa bench road (Fig. 4.20;

Minor Fault Data Analysis – Hell's Canyon East

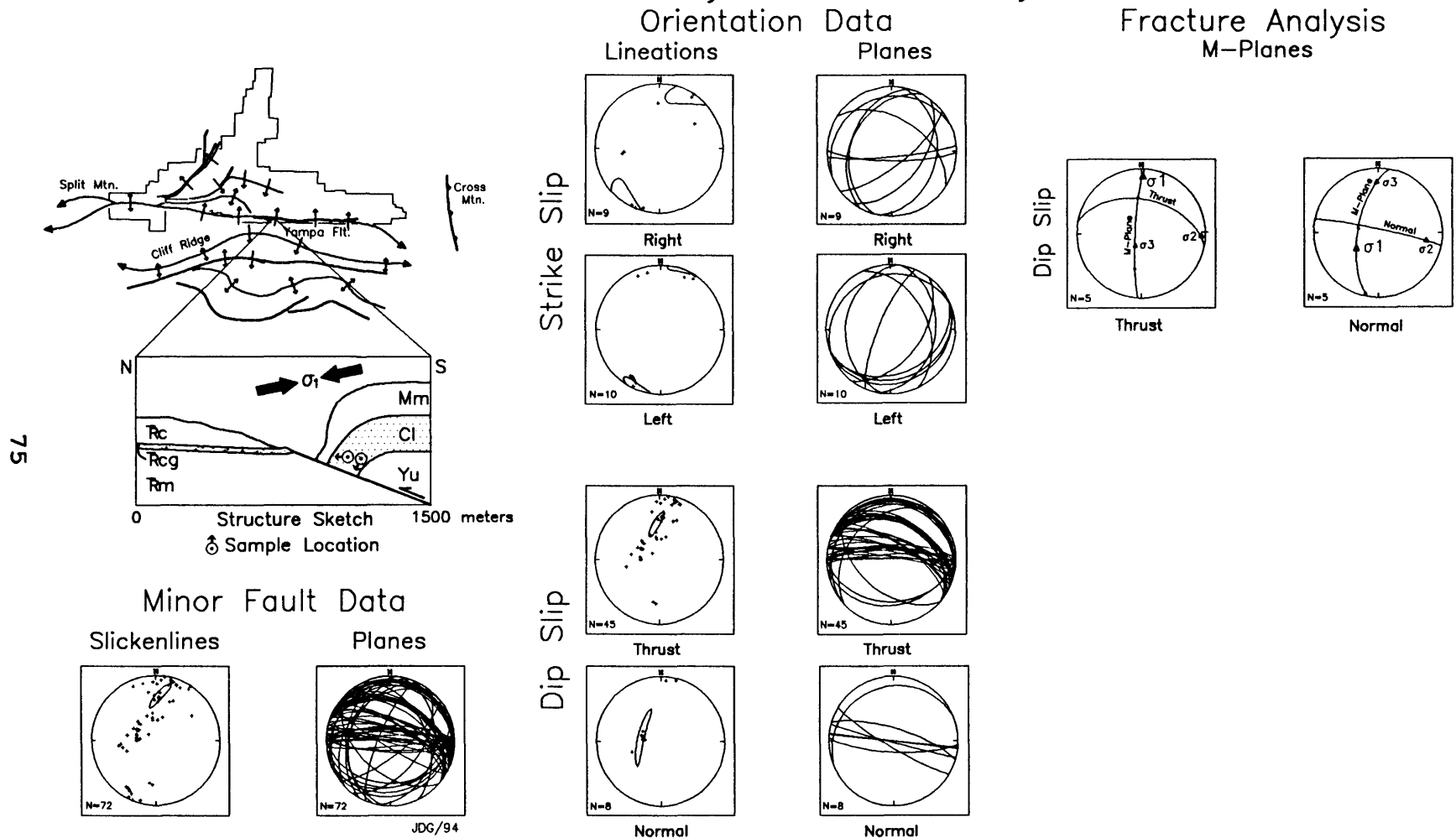
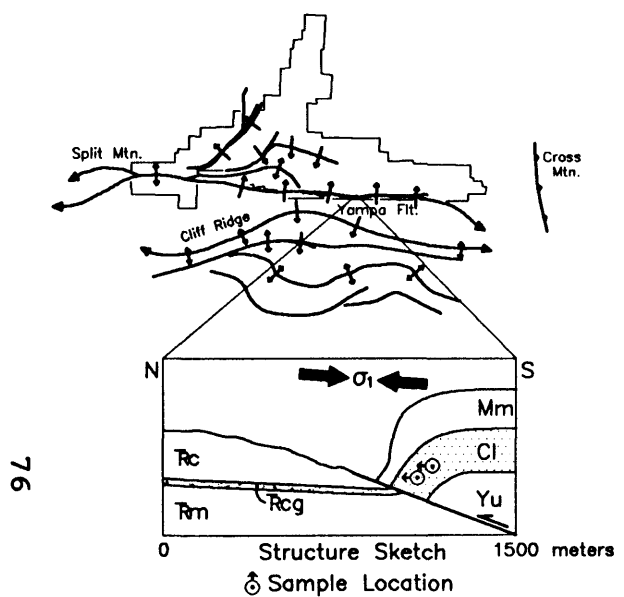


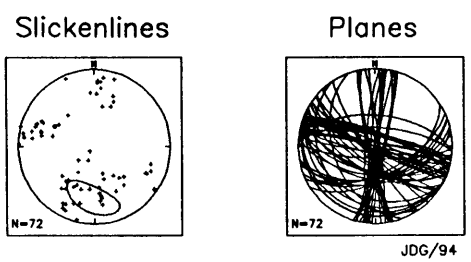
Figure 4.19 Site data summary. Ellipses represent 95% C.I. of E_1 (lineations). Solid arrows indicate apparent plunge of σ_1 in plane of section.

Minor Fault Data Analysis – Johnson Draw

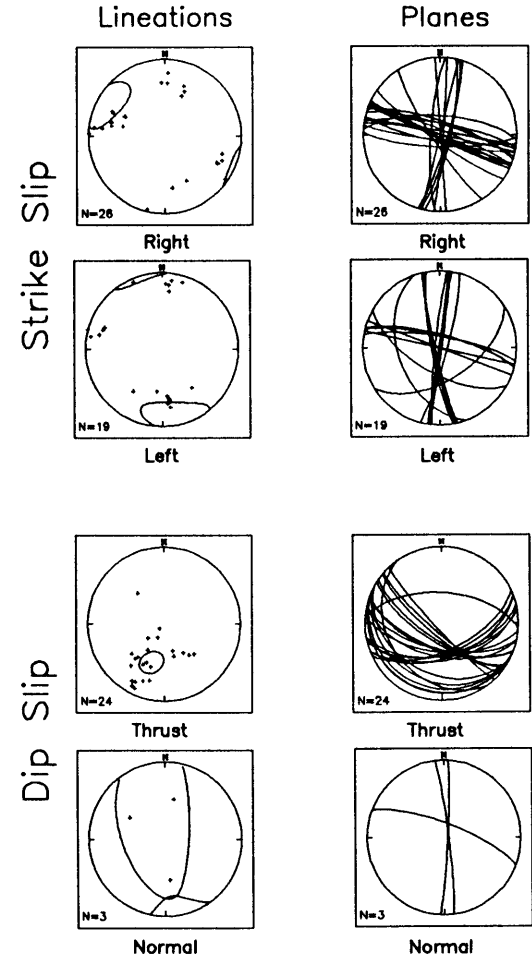


76

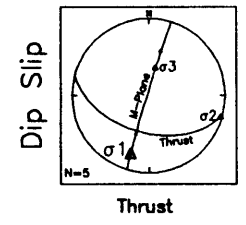
Minor Fault Data



Orientation Data



Fracture Analysis M-Plane



Possible Conjugate Minor Faults

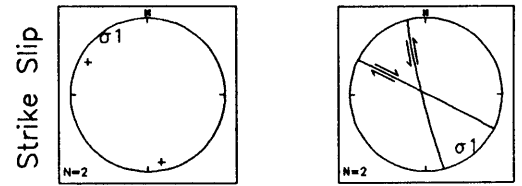


Figure 4.20 Site data summary. Ellipses represent 95% C.I. of E_1 (lineations). Solid arrows indicate apparent plunge of σ_1 in plane of section.

Table 4.19 Johnson Draw - Yampa Fault

PALEOSTRESS TENSOR σ_1 ESTIMATES (n = 72)			
<u>METHOD</u>	<u>TREND-PLUNGE</u>	<u>SENSE</u>	<u>§/PROB./EIGEN.</u>
Direct Inversion	167-00	All	0.64
Octahedra Method	163-08	All	49.5%
Slickenlines E_1	183-32	All	0.4569
M-Plane(s)	198-20	Thrust	
Conjugate Faults E_2	142-06	Lateral	0.1734
Conjugate Striae E_1	324-01	Lateral	0.7829
Bedding Attitude	258-55		

C, SW, SEC. 30, T6N, R101W, Moffat County, Colorado; Hansen and Carrara, 1980). The Yampa fault and fold at Johnson Draw is similar to Hells Canyon but is not as well exposed. The east side of Johnson Draw yielded 72 minor fault measurements from the Cambrian Ladore Formation sandstones. The diversely-oriented data came from the forelimb of the hanging wall fold with average bedding of about 258-55.

The paleostress tensor estimates exhibit a range of σ_1 axial trends from south-southeast to slightly south-southwest (Table 4.19), and the resolved stress tensors are generally poorly defined. Overall, the results suggest a σ_1 estimate that trends about 165° and plunges about 5°.

Yampa Fault East

The Yampa east site is located about 8 km east of Johnson Draw and marks the easternmost outcrop of the Cambrian Ladore Formation along the Yampa fault (Fig. 4.21; SW, NW, SEC. 25, T6N, R101W, Moffat County, Colorado; Hansen et al., 1980). Strata at the site are poorly exposed with Mississippian Madison Limestone forming the dip slope in the

Minor Fault Data Analysis – Yampa East

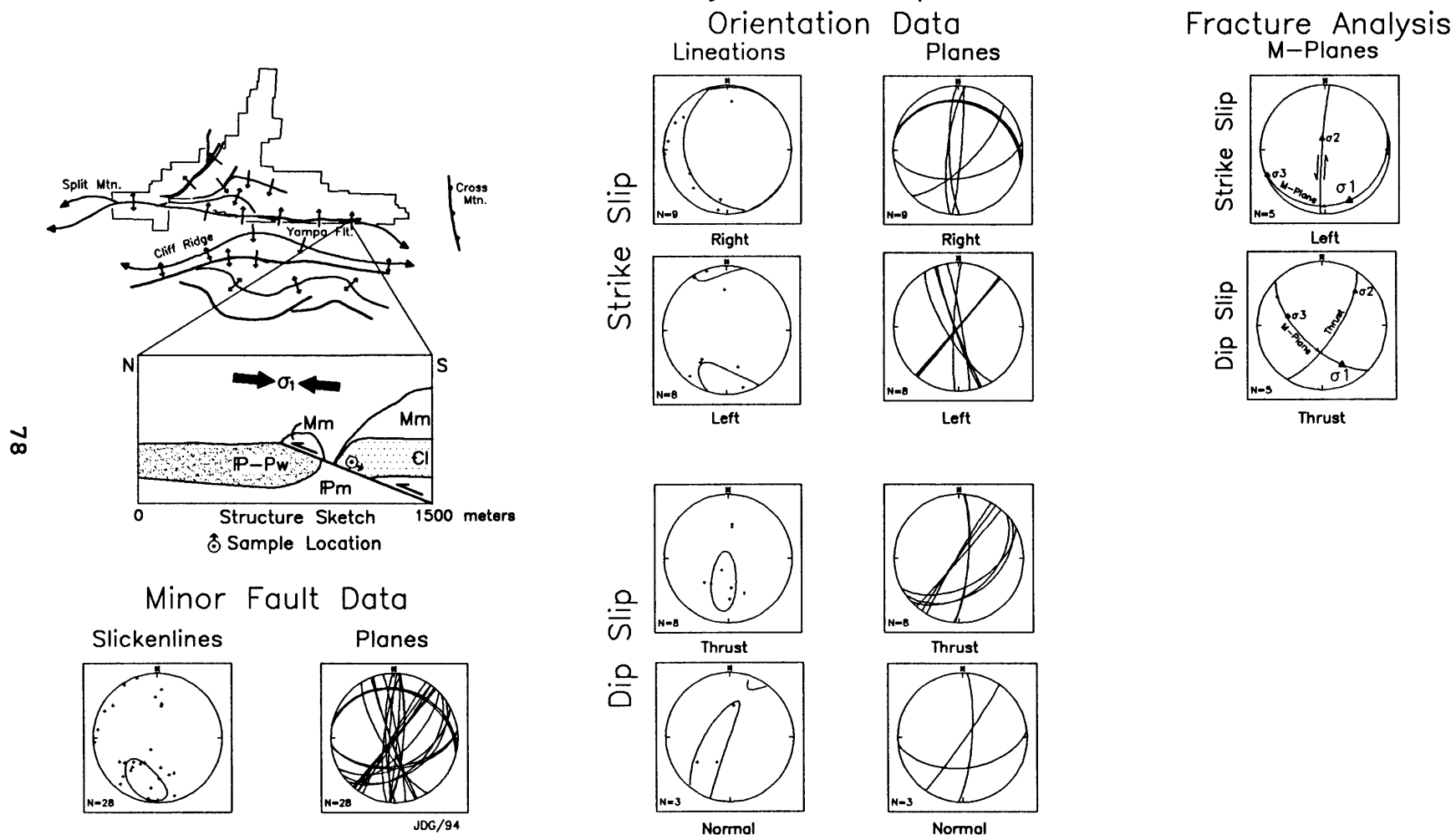


Figure 4.21 Site data summary. Ellipses represent 95% C.I. of E_1 (lineations). Solid arrows indicate apparent plunge of σ_1 in plane of section.

Table 4.20 Yampa Fault East

PALEOSTRESS TENSOR σ_1 ESTIMATES (n = 28)			
<u>METHOD</u>	<u>TREND-PLUNGE</u>	<u>SENSE</u>	<u>\$/PROB./EIGEN.</u>
Direct Inversion	285-01	All	0.75
Octahedra Method	036-02	All	40.3%
Slickenlines E_1	197-29	All	0.5245
M-Plane(s)	154-32	Thrust	
	155-14	Left	
Bedding Attitude	288-23 to 271-15		

forelimb of the fold. A klippe of Madison Limestone forms an isolated hill to the northwest (Fig. 4.21). The Yampa fault places the Madison strata over the Weber Sandstone, and the poorly exposed Weber Sandstone in the footwall is sharply folded into nearly vertical dips. The exposed Ladore Formation sandstones are high on the forelimb of the hanging wall with bedding attitudes ranging from 288-23 to 271-15. The 28 minor fault data are diverse (Fig. 4.21).

The direct inversion, octahedra, and slickenlines E_1 methods all display relatively poorly defined σ_1 estimates (Table 4.20). Direct inversion yields an oblate stress ellipsoid, while the octahedra method gives a low probability, and the slickenlines E_1 has a low eigenvalue. The M-plane constructions are similar, but the data sets are small and diverse. Overall, the results suggest a generally north-trending σ_1 of low plunge.

WOLF CREEK FAULT - MUD SPRINGS MONOCLINE

The Wolf Creek fault and Mud Springs monocline are generally east-west trending, south-vergent structures that parallel the Yampa fault about 8-10 km to the south (Rowley

Table 4.21 Wolf Creek Fault - Mud Springs Monocline

PALEOSTRESS TENSOR σ_1 ESTIMATES (n = 69)			
<u>METHOD</u>	<u>TREND-PLUNGE</u>	<u>SENSE</u>	<u>%/PROB./EIGEN.</u>
Direct Inversion	011-07	All	0.37
Octahedra Method	054-02	All	86.1%
Slickenlines E_1	190-23	All	0.8403
M-Plane(s)	019-02	Thrust	
	164-15	Left	
	022-10	Right	
Conjugate Faults E_2	170-00	Lateral	0.0262
Conjugate Striae E_1	182-03	Lateral	0.9561
Bedding Attitude	288-90		

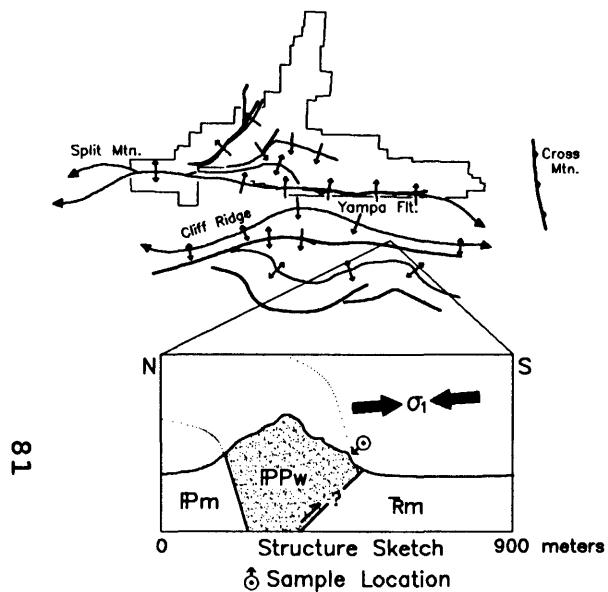
et al., 1985). To the west, the monocline curves toward the west-southwest and increases in relief to form the Section Ridge anticline. To the east, the Wolf Creek fault passes into a monocline which may merge with the south Yampa monocline to form the Elk Springs anticline in the subsurface (Stone, 1986b). The Mud Springs/Wolf Creek structure forms the southern boundary of the Yampa uplift block but displays less relief than the Yampa fault.

Wolf Creek Fault

The Wolf Creek fault site is located about 9.5 km south of the Yampa fault east site (Fig. 4.22; SW, SW, NE, SEC. 26, T5N, R101W, Moffat County, Colorado; Rowley et al., 1985). The hanging wall of the Wolf Creek fault exposes almost vertically-bedded Weber Sandstone (108-90 average; Table 4.21). The footwall is covered, but Rowley et al. (1985) mapped the footwall strata adjacent to the fault as Chinle Formation, and the Glen Canyon Sandstone crops out to the south. The Weber outcrop exhibited fractures and veins

Minor Fault Data Analysis – Mud Springs

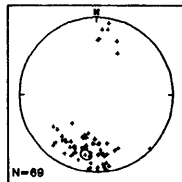
Orientation Data



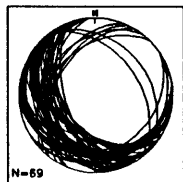
81

Minor Fault Data

Slickenlines

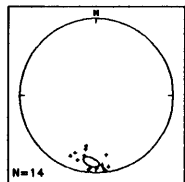


Planes

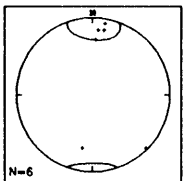


JDG/94

Lineations

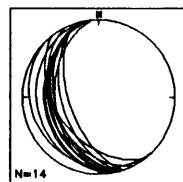


Right

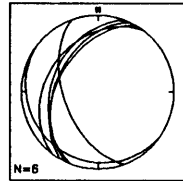


Left

Planes

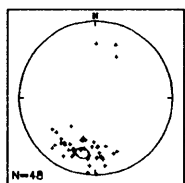


Right

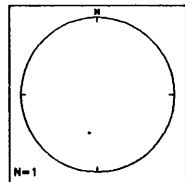


Left

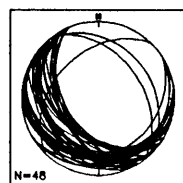
Strike Slip



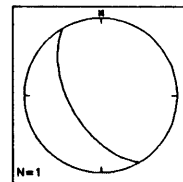
Thrust



Normal



Thrust

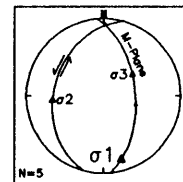


Normal

Dip Slip

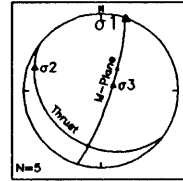
Fracture Analysis M-Planes

Strike Slip

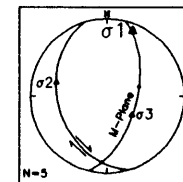


Left

Dip Slip



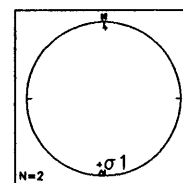
Thrust



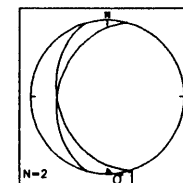
Right

Possible Conjugates

Strike Slip



Lineations



Planes

Figure 4.22 Site data summary. Ellipses represent 95% C.I. of E_1 (lineations). Solid arrows indicate apparent plunge of σ_1 in plane of section.

as well as local exposures of minor faults--many with highly weathered surfaces. Most of the minor faults displayed consistent attitudes with more diversity in the lineations.

With the exception of the left M-plane and conjugate constructions, the σ_1 estimates exhibit an overall north-northeast axial trend (Table 4.21). Direct inversion gives a prolate stress ellipsoid, and the octahedra method yields a high probability. The thrust and right M-planes exhibit close agreement, but the left M-plane and lateral conjugate constructions are diverse. The results suggest a σ_1 that trends 010-020° with a low to horizontal plunge.

CROSS MOUNTAIN

Cross Mountain is a north-northwest trending anticline that is bounded by Laramide thrust faults along the northeast and southwest margins (Rowley et al., 1985). The Cross Mountain structure is adjacent to the northeast margin of the Uinta arch and may represent a back-thrusted pop-up structure associated with the Uinta-Sparks boundary thrust (Ritzma, 1968; Gries, 1983). The anticline abuts the east-west trending Elk Springs anticline to the south.

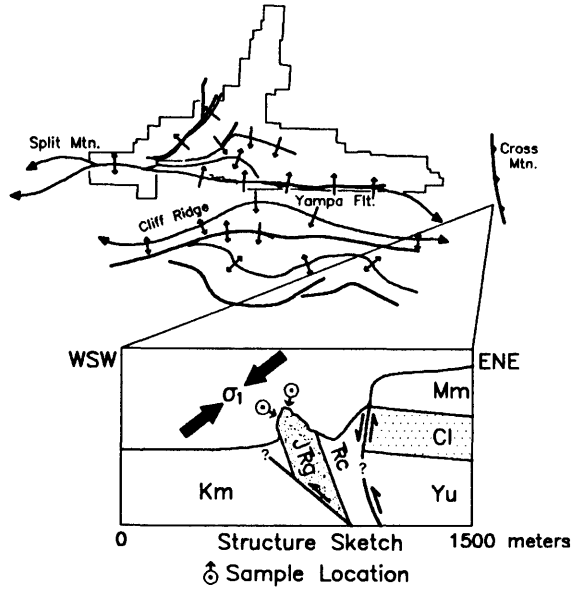
The Cross Mountain site is located on the west side of the anticline just south of the mouth of Cross Mountain canyon and west of the Deer Lodge Park road (SW, SW, SW, SEC. 23, T6N, R98W, Moffat County, Colorado; Dyni, 1968). Minor faults (n = 94) were found in the overturned limb of the west-southwest directed thrust fault (Table 4.22, Fig. 4.23). The overturned attitude of the undifferentiated

Minor Fault Data Analysis – Cross Mountain West

Orientation Data

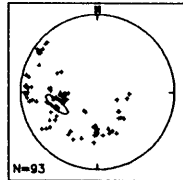
Fracture Analysis

M-Planes

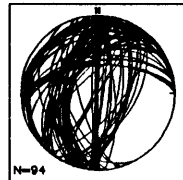


Minor Fault Data

Slickenlines

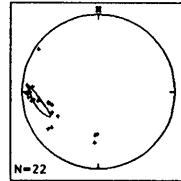


Planes

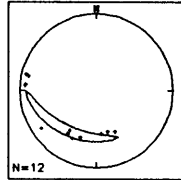


JDC/94

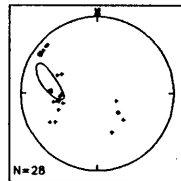
Lineations



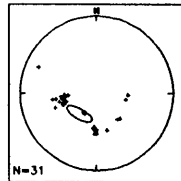
Right



Left

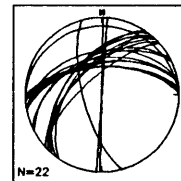


Thrust

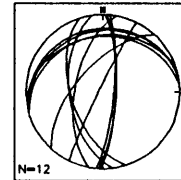


Normal

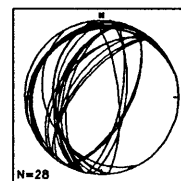
Planes



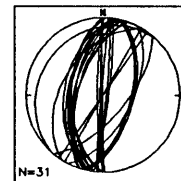
Right



Left



Thrust



Normal

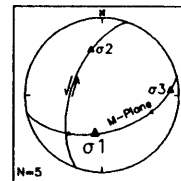
Strike Slip

Dip Slip

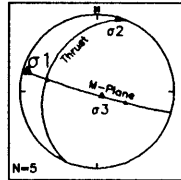
Strike Slip

Dip Slip

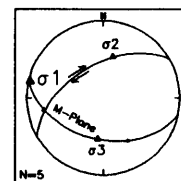
Dip Slip



Left



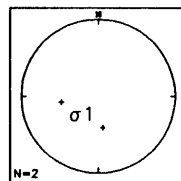
Thrust



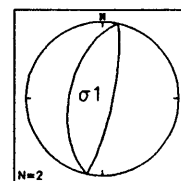
Right

Conjugate Minor Faults

Dip Slip



Normal



Normal

Figure 4.23 Site data summary. Ellipses represent 95% C.I. of E_1 (lineations). Solid arrows indicate apparent plunge of σ_1 in plane of section.

Table 4.22 Cross Mountain West

PALEOSTRESS TENSOR σ_1 ESTIMATES (n = 94)			
<u>METHOD</u>	<u>TREND-PLUNGE</u>	<u>SENSE</u>	<u>*/PROB./EIGEN.</u>
Direct Inversion	104-22	All	0.67
Octahedra Method	359-47	All	42.7%
Slickenlines E_1	252-43	All	0.6263
M-Plane(s)	286-06	Thrust	
	190-48	Left	
	282-02	Right	
Conjugate Faults E_2	282-78	Normal	0.1590
Conjugate Striae E_1	220-62	Normal	0.8207
Bedding Attitude	318-75 OT		

Jurassic Entrada and Glen Canyon Sandstones averaged about 318-75 OT.

The σ_1 estimates give diverse orientations (Table 4.22). With the exception of the octahedra and left M-plane, however, the σ_1 axial trends range from about 240° to 285°. The left M-Plane σ_1 estimate is similar to the northerly trend of the octahedra method, and the left lateral data probably contribute to the oblate stress ellipsoid in the direct inversion. The diversity of the data and results probably reflect the extreme deformation and overturning in the fault zone. The stress tensor estimates suggest a generally west to west-southwest oriented σ_1 during faulting at Cross Mountain.

Chapter 5

COMPOSITE PALEOSTRESS ANALYSES

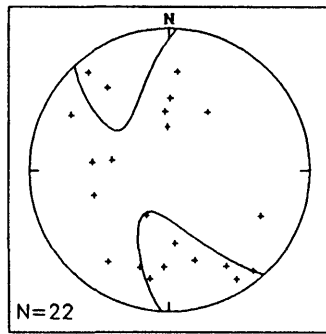
The purpose of the paleostress analysis was to determine overall Laramide σ_1 orientations in the study area as accurately as possible and attempt to differentiate local from regional components of the stress tensor(s).

Composites of the paleostress estimates from the 22 sample sites (Chapter 4) were used to approximate the overall σ_1 orientation(s). The composite σ_1 estimates were computed with eigenvectors from the combined data for each method from all 22 sites. To test for alternative σ_1 orientations, the site σ_1 estimates were also divided into two groups: east-west trending structures and those of all other orientations. Eigenvector data for each minor fault type at each site (i.e., left, right, thrust, normal) were combined into a single data set and analyzed with the direct stress inversion, octahedra, and slickenline eigenvector methods. Site slickenline results were compared to structural trends to test for structure perpendicular and flexural slip.

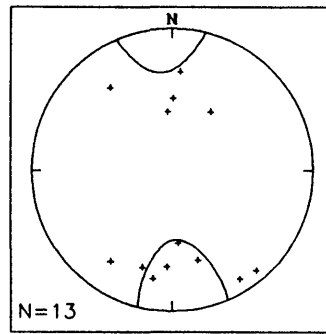
Slickenlines E_1 Stress Solutions

The eigenvectors computed from all 22 slickenlines E_1 estimates of σ_1 display a south-southeast E_1 orientation (162-06) with an eigenvalue of 0.4606 (Fig. 5.1). East-west

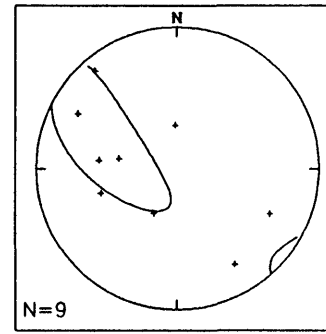
Dinosaur Area Slickenline Analysis σ_1 Estimates



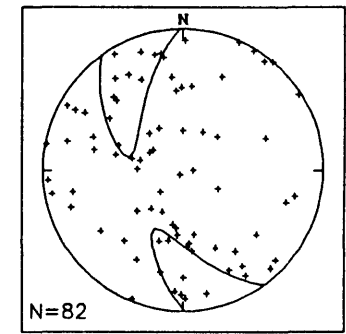
Each Site E1
E1: 162-06 0.4606



East-West Structures
E1: 176-09 0.5843



All Other Structures
E1: 290-42 0.5808



Fault Types E1
E1: 340-04 0.4088

98

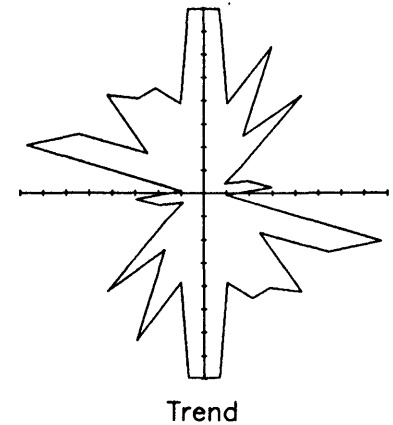
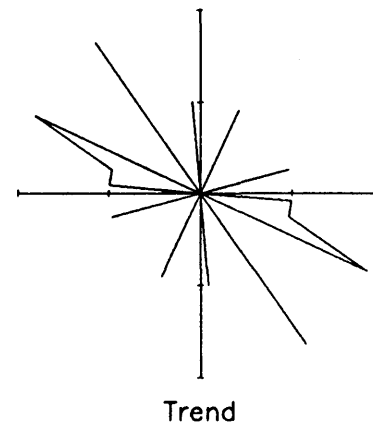
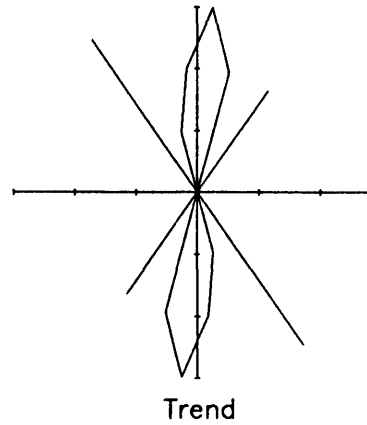
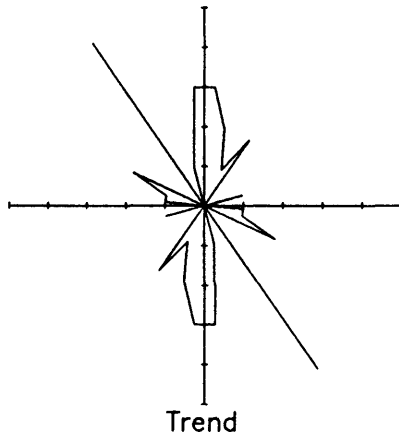
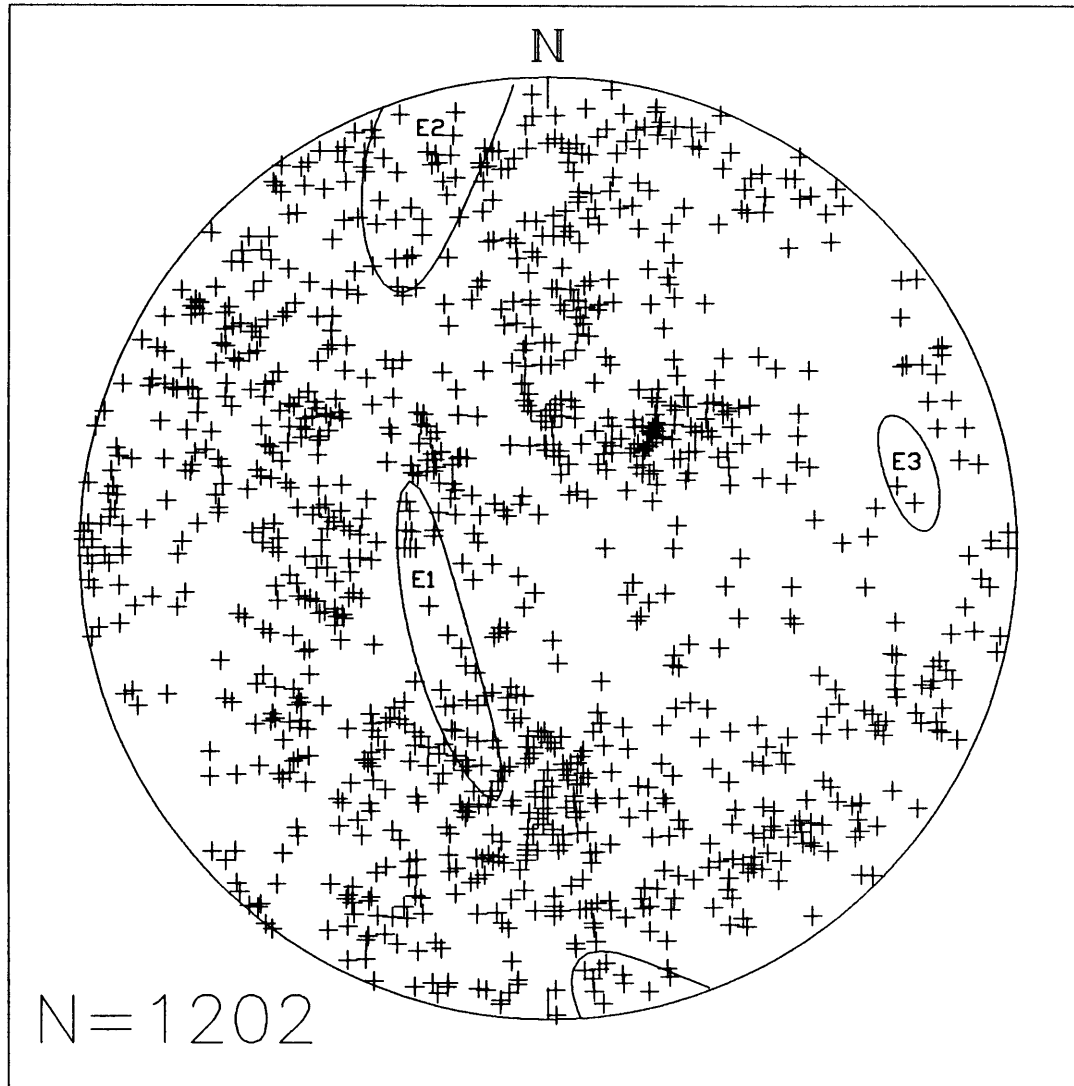


Figure 5.1 Composite slip vector estimate from slickenlines E_1 of 22 sample sites. Ellipses represent the 95% C.I. for composite E_1 .

trending structures exhibit a south-oriented E_1 (176-09) with a higher eigenvalue of 0.5843. Structures of all other trends yield a west-northwest E_1 orientation (290-42) with a similar eigenvalue of 0.5808. The composite eigenvectors for all of the 82 fault types slickenlines E_1 results in a north-northwest E_1 orientation (340-04) with a low eigenvalue of 0.4088. In addition, the eigenvectors of all 1202 slickenline orientations (Fig. 5.2) display high dispersion and a girdle distribution (comparable to an oblate stress ellipsoid) with even lower eigenvalues for E_1 (227-65, 0.3838) and E_2 (343-12, 0.3771). The orientation of E_2 (343-12) is similar to the other composite estimates for σ_1 and indicates that a significant portion of slip occurred parallel to the σ_1 estimates.

M-Plane Stress Solutions

The σ_1 estimate obtained from the eigenvectors of all 57 M-planes exhibits a north-northwest E_1 orientation (342-03) with an eigenvalue of 0.4754 (Fig. 5.3). East-west trending structures display a north-south E_1 orientation (177-07) with a higher eigenvalue of 0.5329. Structures of all other trends yield a northwest E_1 orientation (315-20) with an eigenvalue of 0.5040. When the M-plane and conjugate estimates (discussed below) are combined, the resulting orientation of E_1 is also toward the north-northwest (339-07) with an eigenvalue of 0.4580. The composite M-plane approximations for σ_1 are similar to the other composites.

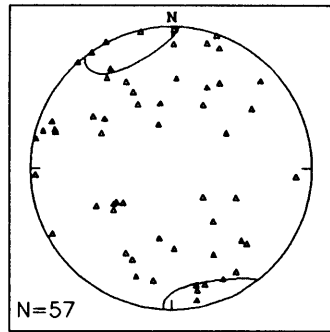


Slickenline Orientation Data
Dinosaur National Monument
Southeastern Uinta Mountains

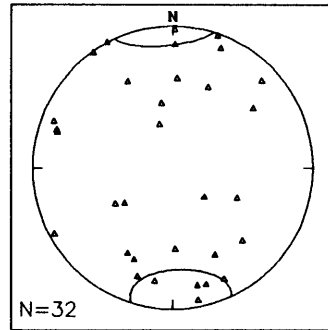
Eigenvector	Confidence Intervals (95%)	Eigenvalue
E1:	227-65	0.3848
E2:	343-12	0.3771
E3:	078-22	0.2381

Figure 5.2 Eigenvector analysis of 1202 slickenlines measured at 22 sample sites. Ellipses represent the 95% C.I. for noted eigenvectors.

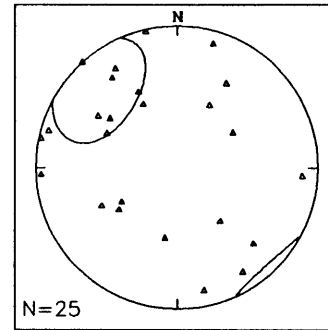
Dinosaur Area M-Plane σ_1 Estimates



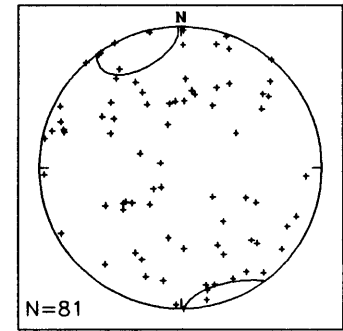
All M-Planes
E1: 342-03 0.4754



East-West Structures
E1: 177-07 0.5329



All Other Structures
E1: 315-20 0.5040



M-Planes and Conjugates
E1: 340-06 0.4544

68

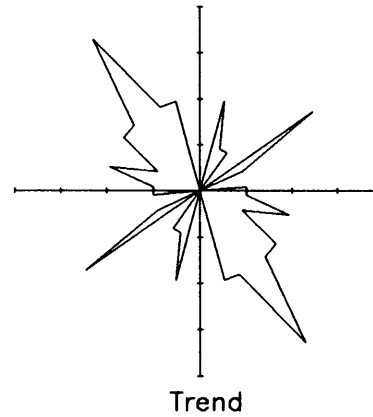
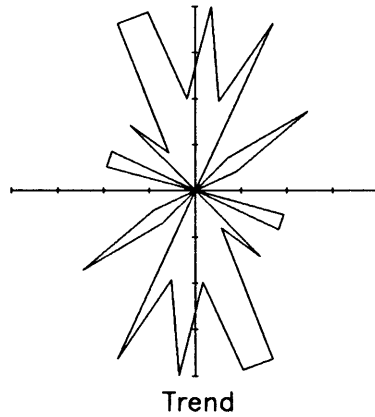
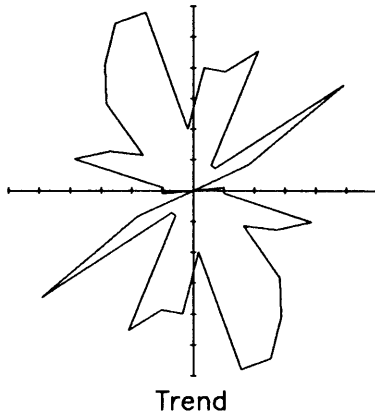


Figure 5.3 Composite stress tensor estimate for M-plane solutions of 22 sample sites. Ellipses represent the 95% C.I. for composite E_1 .

Conjugate Stress Solutions

Eigenvectors computed with all 24 conjugate estimates of σ_1 display a north-northwest E_1 orientation (339-26) with an eigenvalue of 0.4174 (Fig. 5.4). East-west trending structures exhibit a more northerly E_1 orientation (344-15) with a higher eigenvalue of 0.5618. Structures of all other trends give a west-southwest E_1 orientation of high plunge (240-67) with a higher eigenvalue of 0.5767. The high plunge results from the conjugate normal faults collected from Section Ridge and Cross Mountain anticlines.

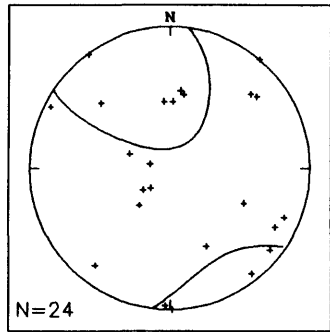
Combined M-Plane and Conjugate Stress Solutions

Since the criteria for constructing M-plane and conjugate σ_1 solutions are generally mutually exclusive at the same site, the results of the two fracture techniques are considered in combination. The eigenvectors from all 57 M-plane and 28 conjugate σ_1 estimates yield a north-northwest E_1 orientation (340-06) with an eigenvalue of 0.4544 (Fig. 5.5). East-west trending structures provide a more north-directed E_1 orientation (351-02) with a higher eigenvalue of 0.5256. Structures of all other orientations display a northwest-oriented E_1 (303-36) with an eigenvalue of 0.4530. The combined composite σ_1 estimates are similar to the other composite solutions.

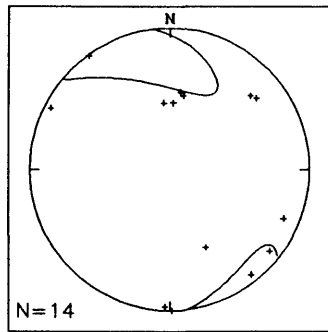
Direct Stress Inversion

The eigenvectors computed with all 22 direct stress inversion σ_1 estimates display a northwest oriented E_1 (322-06) with an eigenvalue of 0.4936 (Fig. 5.6). East-west

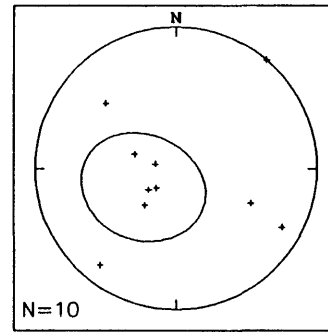
Dinosaur Area Conjugate σ_1 Estimates



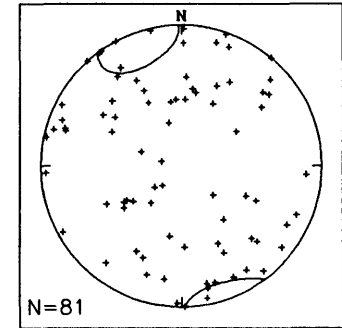
All Conjugates
E1: 339-26 0.4174



East-West Structures
E1: 344-15 0.5613

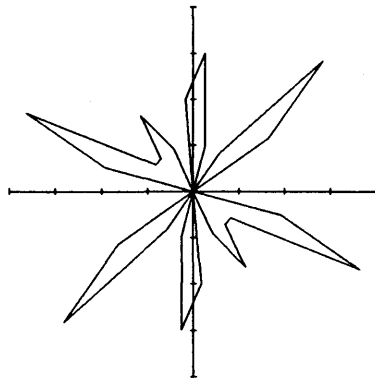


All Other Structures
E1: 240-67 0.5767

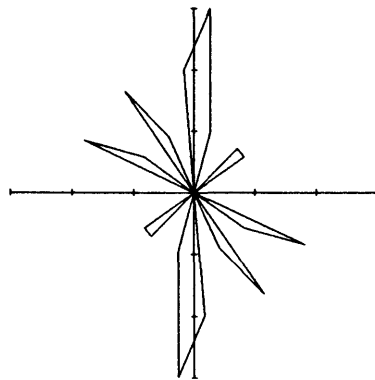


M-Planes and Conjugates
E1: 340-06 0.4544

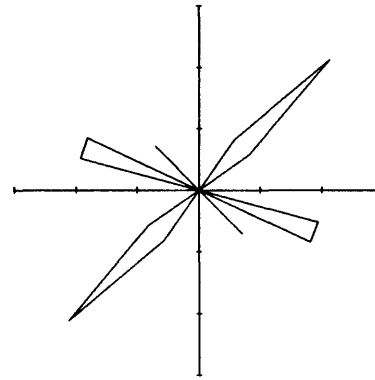
91



Trend



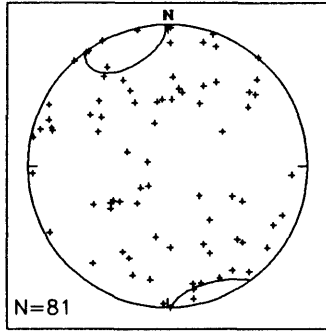
Trend



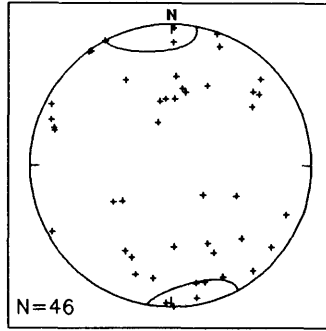
Trend

Figure 5.4 Composite stress tensor estimate for conjugate fault solutions of 22 sample sites. Ellipses represent the 95% C.I. for composite E_1 .

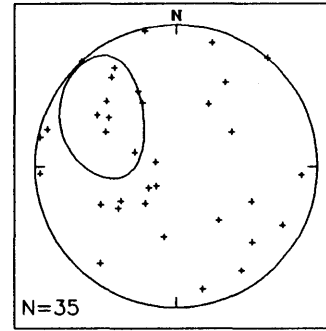
Dinosaur Area Combined M-Plane and Conjugate σ_1 Estimates



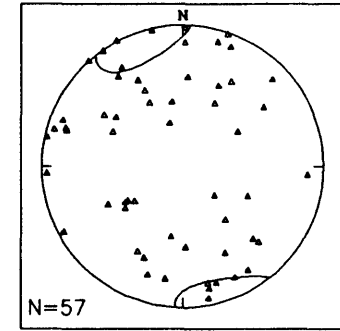
All σ_1 Estimates
E1: 340-06 0.4544



East-West Structures
E1: 351-02 0.5256

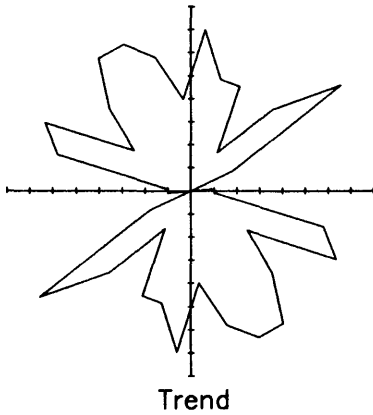


All Other Structures
E1: 303-36 0.4530

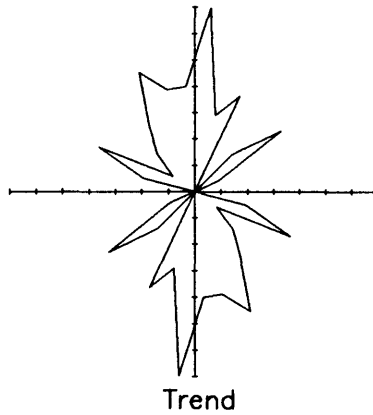


M-Planes
E1: 342-03 0.4754

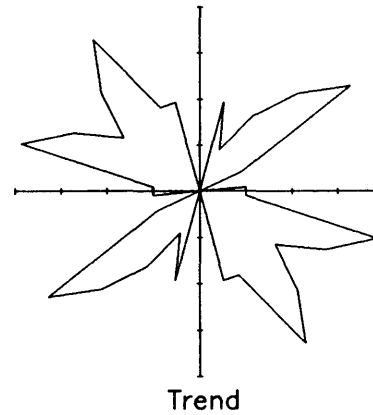
92



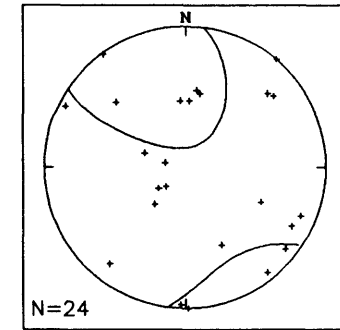
Trend



Trend



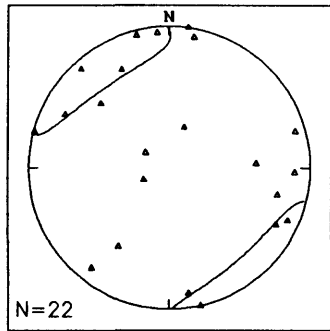
Trend



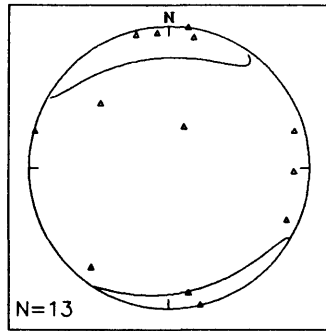
Conjugates
E1: 339-26 0.4174

Figure 5.5 Composite stress tensor estimate for M-planes and conjugates of 22 sample sites. Ellipses represent the 95% C.I. for composite E_1 .

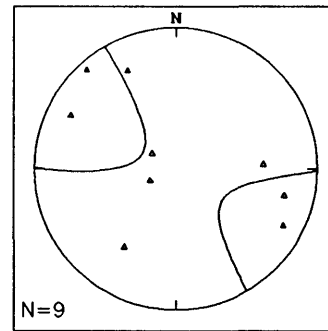
Dinosaur Area Direct Stress Inversions σ_1 Estimates



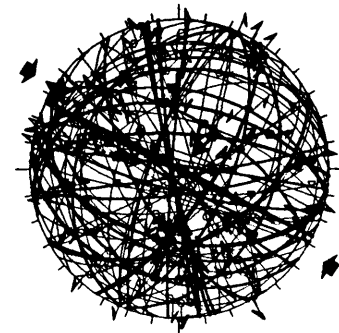
All Locations
E1: 322-04 0.4936



East-West Structures
E1: 349-05 0.5606

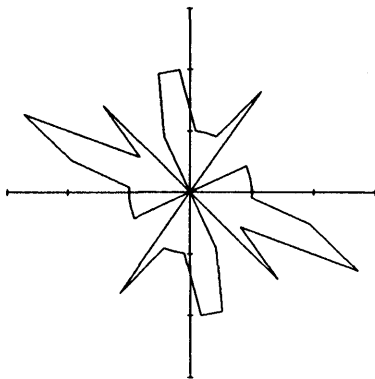


All Other Structures
E1: 300-06 0.5166

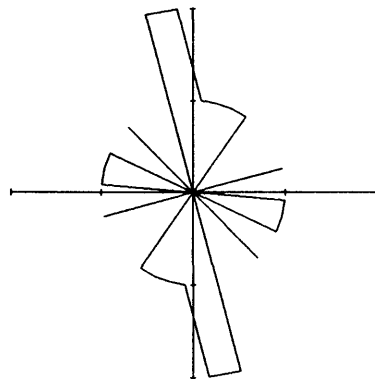


Site Fault Types (E1)
 σ_1 : 303-04
 σ_2 : 034-11
 σ_3 : 194-79

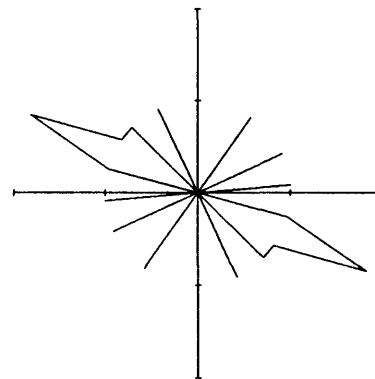
93



Trend



Trend



Trend

Figure 5.6 Composite stress tensor estimate for direct stress inversion of 22 sample sites. Ellipses represent the 95% C.I. for composite E_1 .

trending structures exhibit a more north-south E_1 (349-05) and a higher eigenvalue (0.5606). Structures of all other trends give a west-northwest E_1 (300-06) with an eigenvalue of 0.4936. Direct inversion of all the fault types from each site ($n = 82$) gives an oblate stress ellipsoid ($\Phi = 0.69$) with σ_1 oriented 303-04 and σ_2 oriented 034-11.

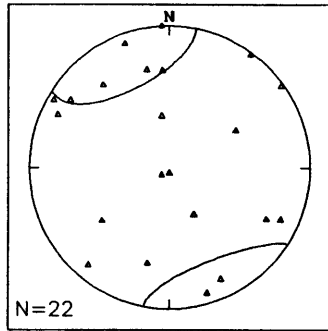
Octahedra Method Stress Composites

The eigenvectors computed with all 22 octahedra method σ_1 estimates exhibit a north-northwest oriented E_1 (336-05) with an eigenvalue of 0.4684 (Fig. 5.7). East-west structures display a more north-south E_1 (174-03) with a higher eigenvalue of 0.5372. Structures of all other trends produced a northwest E_1 orientation (315-31) with an eigenvalue of 0.4836. Applying the octahedra method to all the fault type data from each site results in a low probability (29.6%) with σ_1 oriented 306-19 and σ_2 oriented 047-28. The octahedra composite is similar to the others.

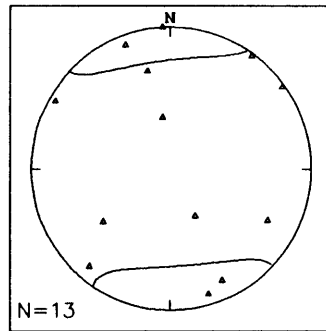
Interpreted Stress Solutions

The eigenvectors computed with the qualitative σ_1 interpretations from all 22 sites give an E_1 oriented 337-12 with an eigenvalue of 0.5922 (Fig. 5.8). East-trending structures produce a 353-02 σ_1 orientation with a higher eigenvalue (0.6776). Structures of all other trends give an E_1 of 308-30 with a slightly higher eigenvalue (0.6847). Although the E_1 orientations are similar to the other paleostress composites, the higher eigenvalues indicate less dispersion in the interpreted estimates.

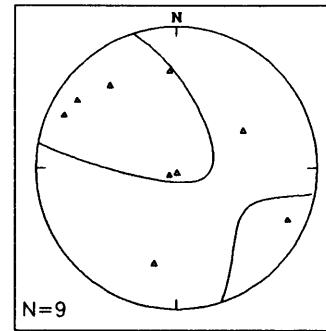
Dinosaur Area Octahedra σ_1 Estimates



All Locations
E1: 336-05 0.4684



East-West Structures
E1: 174-03 0.5372



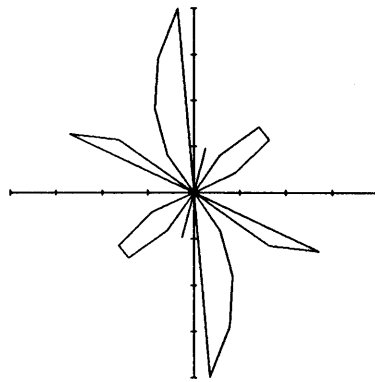
All Other Structures
E1: 315-31 0.4836



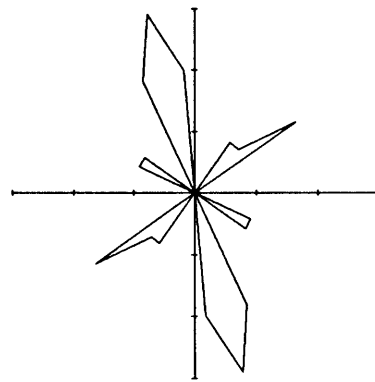
Site Fault Types (E1)

σ_1 : 306-19
 σ_2 : 047-28
 σ_3 : 187-55

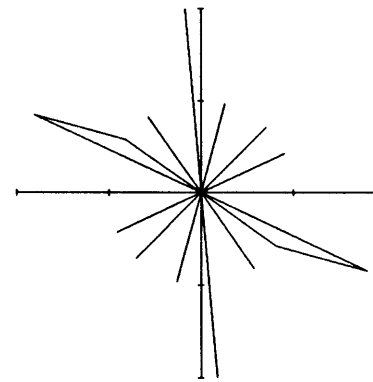
95



Trend



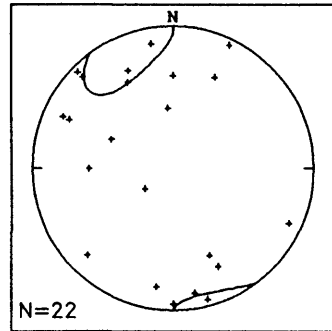
Trend



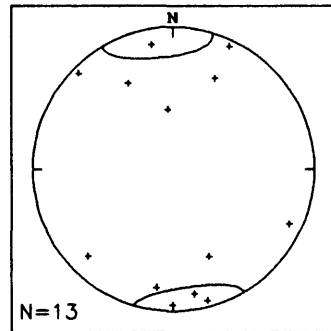
Trend

Figure 5.7 Composite stress tensor estimate for octahedra method of 22 sample sites. Ellipses represent the 95% C.I. for composite E_1 .

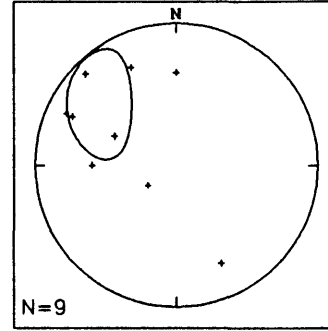
Dinosaur Area Interpreted σ_1 Estimates



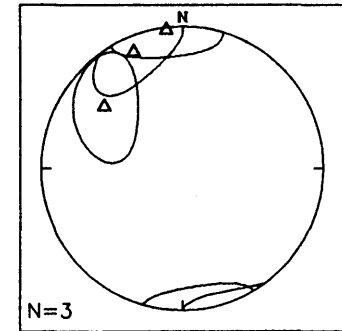
Each Site E_1
 E_1 : 337-12 0.5922



East-West Structures
 E_1 : 353-02 0.6776

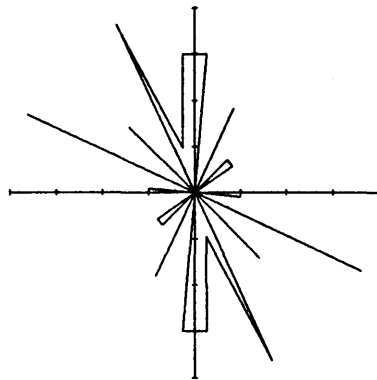


All Other Structures
 E_1 : 308-30 0.6847

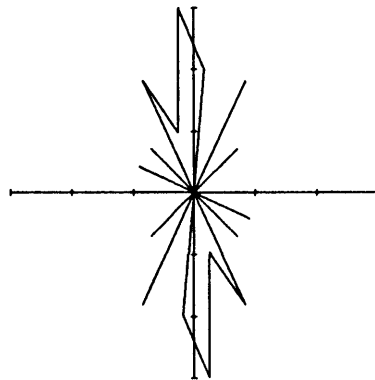


95% Confidence Intervals

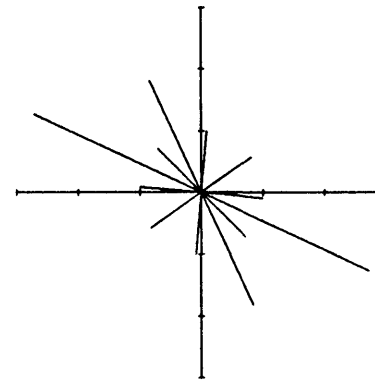
96



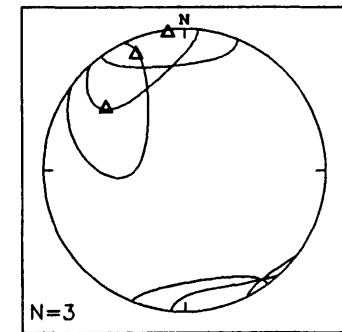
Trend



Trend



Trend



99% Confidence Intervals

Figure 5.8 Composite stress tensor estimate for best qualitative solutions of 22 sample sites. Ellipses represent the 95% C.I. for composite E_1 .

Comparison of Structural and Slip Orientations

Minor fault slip may result from both flexural-slip or inclined shear within and between strata during folding and/or from a more uniform regional slip direction. Uniform regional slip should produce generally unidirectional average slickenline trends regardless of structural trend. The flexural-slip mechanism predicts that predominant slip directions during deformation will be layer-parallel and normal to the fault strike/fold trend. Inclined shear should also have average slip normal to structural trends but need not be layer-parallel. In a two-dimensional (2-D) map view, flexural-slip and inclined shear should result in a 1:1 relationship between structural trends and normals to the average slip trends (i.e., the slickenline E_3 trend). In three dimensions (3-D), a common slip trend should occur for both predicted flexural-slip and average observed slip (i.e. slickenline E_1).

To test the possibility that flexural-slip or inclined shear due to local structural geometries caused the minor fault slip in the study area, 2-D comparisons between structural trends and slickenlines E_3 of each site were made (Figs. 5.9, 5.10). A 3-D comparison of site striae E_1 and predicted flexural-slip was also made (Fig. 5.11).

Linear regression between the structural trends (site bedding strikes) and site slickenlines E_3 (Fig. 5.9) gives a poor correlation between the two variables ($R^2 \approx 0.44$) and relatively large errors for the X coefficient ($X \approx 0.739 \pm$

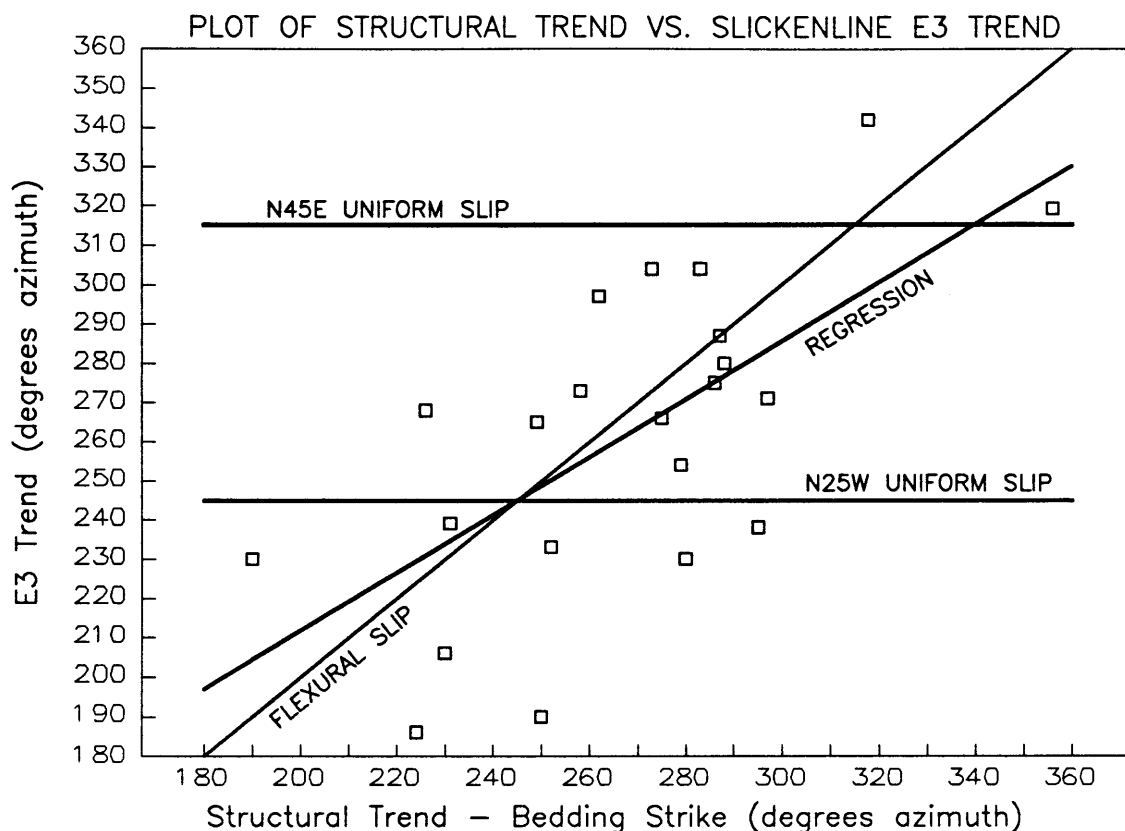


Figure 5.9 Graph of bedding strike vs. striae E_3 trend (see text).

0.19) and calculated Y value ($\approx \pm 30.9^\circ$). Regression between mapped major structural trends (Rowley et al., 1985; Hansen et al., 1983) and site slickenlines E_3 (Fig. 5.10) gives similar results but an even lower $R^2 \approx 0.26$. The regression lines on Figs. 5.9 and 5.10 plot between the 1:1 slope predicted for flexural slip and the horizontal line of 245° for overall north-northwest σ_1 suggested by the paleostress analyses. The results suggest that both regional slip and localized flexural-slip occurred during deformation.

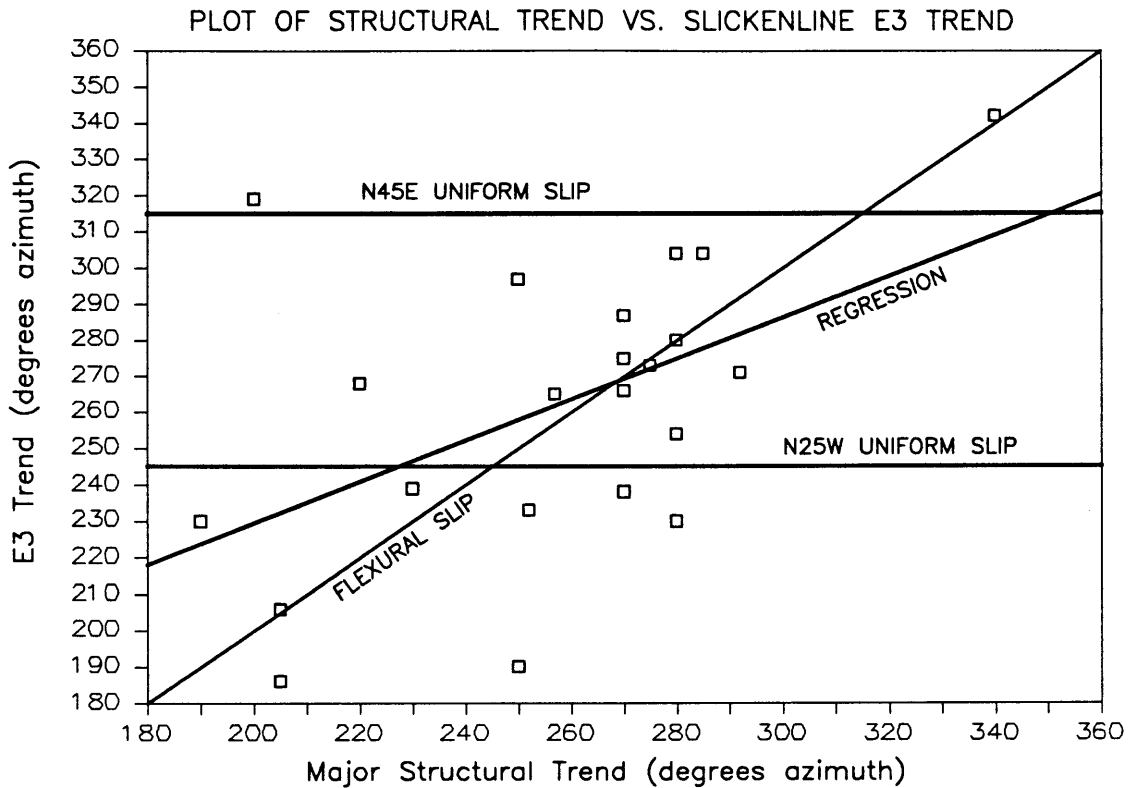


Figure 5.10 Graph of structural trend vs. striae E_3 trend (see text).

A comparison of the 95% confidence intervals for E_1 produced in ORIENT (Vollmer, 1989) from the site slickenlines E_1 and predicted flexural-slip orientations (from bedding attitudes) displays no overlap (Fig. 5.11). This indicates that flexural-slip did not predominate in the observed minor fault deformation. However, the predicted flexural-slip direction is similar to the E_1 of all the lineations (Fig. 5.4). In addition, the large confidence interval for the site slickenlines E_1 also suggests diverse and non-uniform slip (and stresses) in the study area.

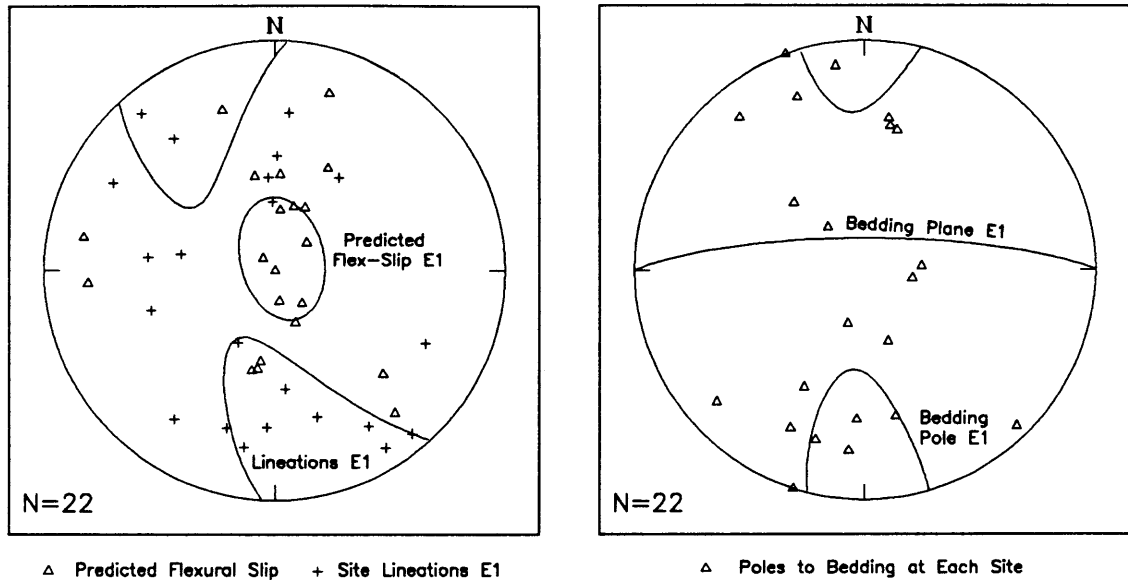


Figure 5.11 a) Stereonet of data and 95% confidence intervals of site slickenlines E_1 , and predicted flexural-slip (see text). b) Poles to bedding, 95% C.I. pole, and average bedding plane for study sites.

Discussion

The composite σ_1 estimates display good agreement between the various paleostress methods (Table 5.1). Eigenvector analysis of the site composites from the direct inversion, octahedra, slickenlines, and combined M-plane/conjugate methods gives an E_1 orientation of 335-02 with an eigenvalue of 0.9748. The composite for east-trending structures results in a more south-oriented E_1 of horizontal plunge (172-01) and an eigenvalue of 0.9893. In contrast, the composite for structures of other trends exhibits an E_1 attitude of 302-29 with an eigenvalue of 0.9286. The increased eigenvalues seen in the east-west

Table 5.1 Composite σ_1 Estimates - Dinosaur Area

Eigenvector Analyses of Paleostress Tensor Estimates
Composite E_1 Orientations

<u>PALEOSTRESS TECHNIQUE</u>	<u>SITE E_1 ESTIMATES</u>	<u>EAST-WEST STRUCTURES</u>	<u>ALL OTHER STRUCTURES</u>
22 Direct Inv.	322-04	349-05	300-06
22 Octahedra	335-05	174-03	315-31
22 Striae	162-06	176-09	290-42
57 M-Planes	342-03	177-07	315-20
28 Conjugates	339-26	344-15	240-67
82 Combined	340-04	351-02	303-36
Overall E_1 Eigenvalue	335-02 0.9748	172-01 0.9893	302-29 0.9286
Interpreted E_1 Eigenvalue	337-12 0.5922	353-02 0.6776	308-30 0.6847

composite are more than offset by the lower eigenvalues for the other sites composite. In addition, the 95% confidence interval for the interpreted σ_1 composite contains the E_1 of the east-west composite and vice versa (Fig. 5.8).

In contrast to the dispersion within and between the individual sites, the similarity of the site composites indicates an average north-northwest trending σ_1 of almost horizontal plunge for the study area. Comparison of structural and slip trends, however, indicate that a combination of local and regional stresses probably produced the observed strain. This observation is consistent with major Laramide deformation trends in the study area.

Chapter 6

STRUCTURE SURFACE MODELING

Structural modeling for part of the study area in Dinosaur National Monument consisted of construction of several cross sections, a structure surface on the top of the Pennsylvanian-Permian Weber Sandstone, and three-dimensional (3-D) restoration of the Yampa graben area (Fig. 6.1). The structural cross sections and 3-D restoration are discussed in the next chapter. Structure surface models provide tools to interpolate and visualize deformation not exposed at the surface. The structure surface and structure contour illustrations are based on strata elevation data obtained from geologic quadrangle maps, published and/or constructed cross sections, and linear projection along fold axes. The map data were digitized into a geographic information system (GIS) database for structure surface and contour generation. The models provide a good visualization of the geometry and complex relationships displayed at the junction of the Yampa, Red Rock, and Mitten Park structures.

COMPUTER-AIDED STRUCTURAL MODELING

The general procedure used in this study for the computer-aided structural modeling included data acquisition

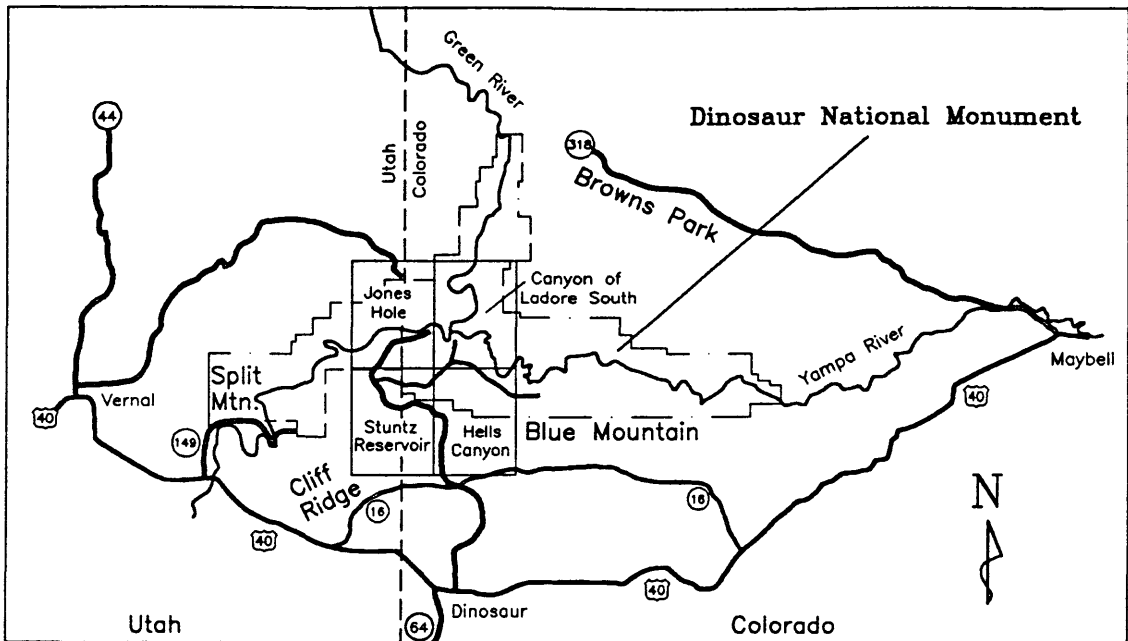


Figure 6.1 Location of Yampa graben area in Dinosaur National Monument (after Hansen and Rowley, 1985).

and preparation, data entry and spatial attributing, preprocessing and model construction, as well as graphics preparation and output. The ARC/INFO GIS provided a versatile platform with good data entry, manipulation, modeling, and graphics capabilities. Approximate project time expenditures consisted of data preparation (50%), data entry (20%), modeling (10%), and graphics output (20%). Although based on surface point data, the modeling could easily incorporate any type of elevation data, and a more integrated spatial database could be accommodated.

Data Acquisition and Preparation

Elevation data for the top of the Weber Sandstone came from four USGS 7.5 minute geologic quadrangle maps (Fig. 6.1): Jones Hole (Hansen, 1977a), Canyon of Lodore South (Hansen, 1977b), Stuntz Reservoir (Hansen and Rowley, 1980a), and Hells Canyon (Hansen and Rowley, 1980b). An overlay of each map traced strata tops, cross section lines, and fold axes (Fig. 6.2). The cross section lines provided Weber data over unexposed or eroded areas. Linear interpolation along syncline and anticline axes helped constrain areas of high relief. As mapped in the study area, the Weber Sandstone displays a fairly uniform thickness of about 300 m (1000 feet).

The several types of elevation data used in the structural modeling can be ranked by quality. The highest quality data consisted of mapped surface outcrops of the Weber Sandstone tops. Due to the generally uniform thickness of the Weber in the study area, outcrops of Weber bottoms provided good control in horizontal to gently-dipping strata. Structural cross sections gave top elevations that were as good as the interpretation on the section, and contributed more constrained data than did elevations projected vertically from mapped tops of other strata. The lowest quality data used in the modeling came from linear interpolation of data points along fold axes between outcrop and cross section elevations. The interpolation assumed uniform linear slopes between "known"

Weber Sandstone Tops - Yampa Graben Area Colorado and Utah

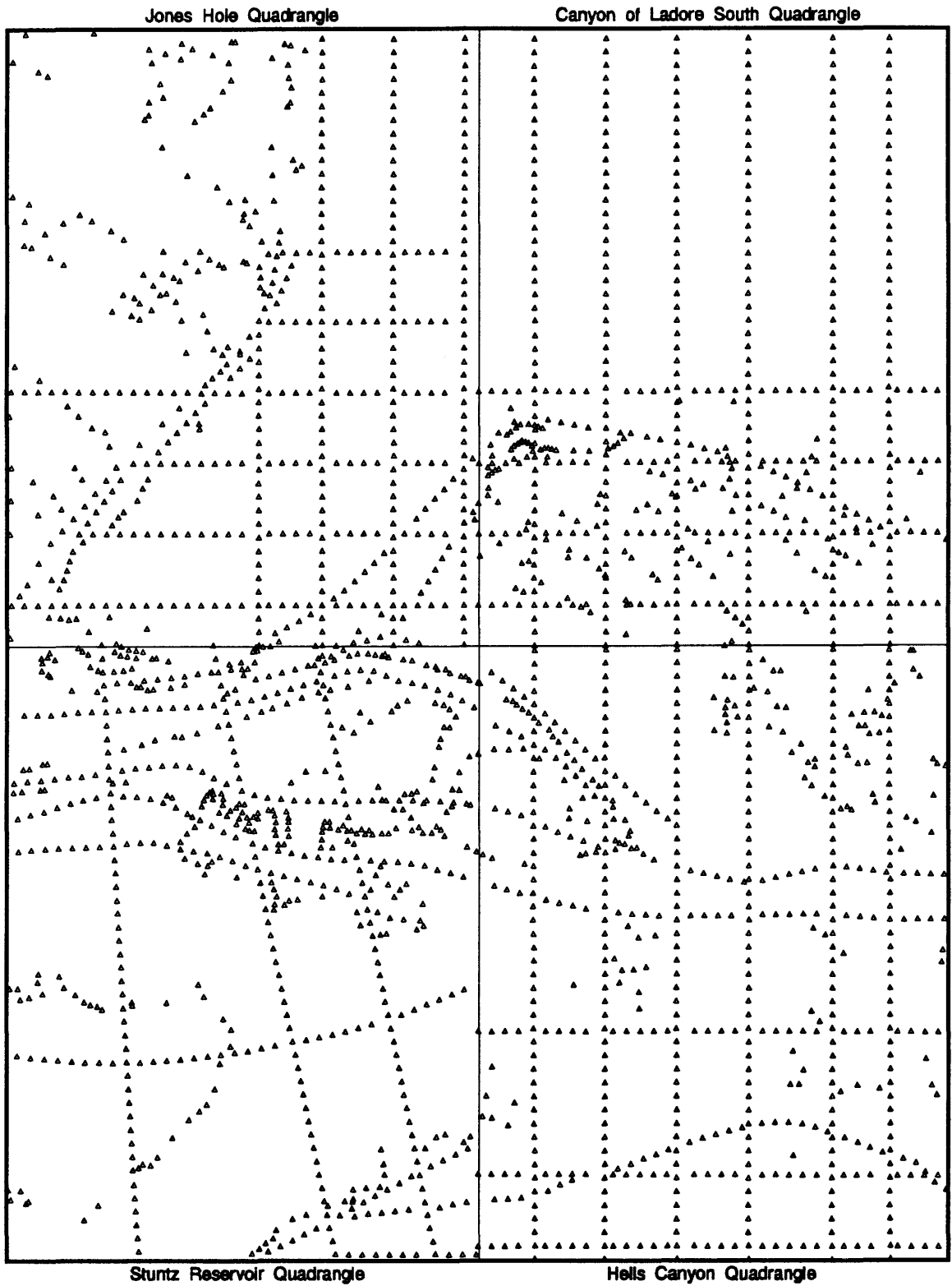


Figure 6.2 Weber data points for structure surface models.

points along vertical axial planes. Overlap of strata along thrust faults, such as the Yampa fault, was not represented in the data and only revealed by extreme vertical relief between data points and fold axes.

Data for the Yampa graben area consisted of 509 points from the Jones Hole quad, 539 points from the Canyon of Lodore South quad, 500 points from the Stuntz Reservoir quad, and 612 points from the Hells Canyon quad. The 2401 data points and quadrangle locations appear on Figure 6.2.

Data Entry and Spatial Attribution

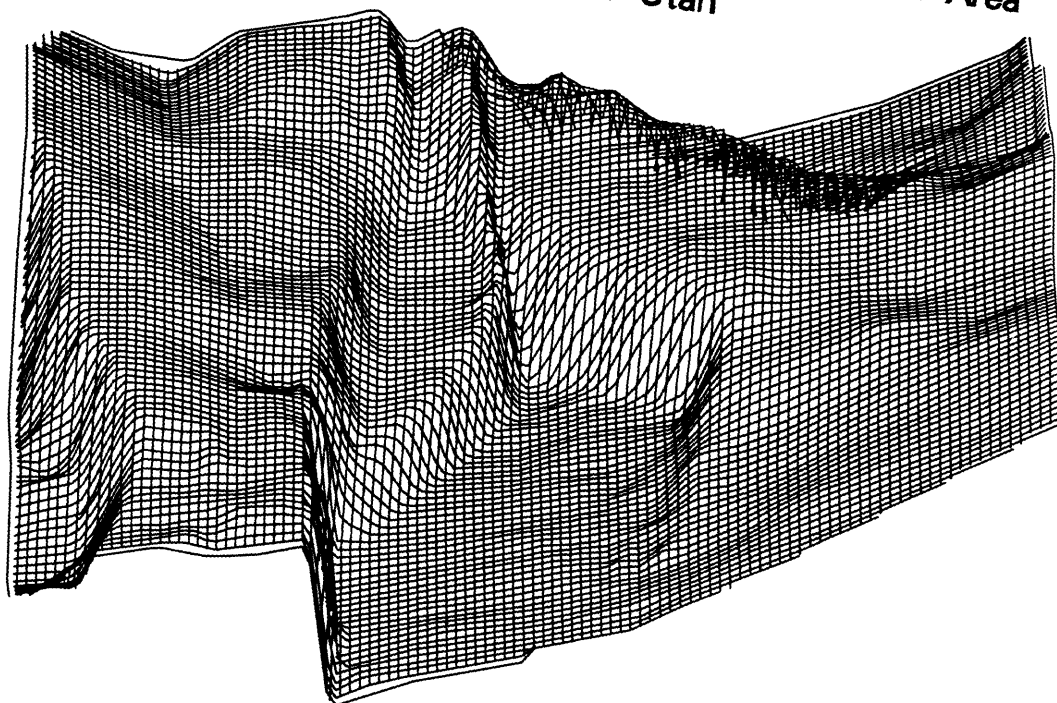
The geologic quadrangle overlays were digitized separately as point coverages in ARC/INFO. Each overlay contained corresponding tic numbers for common corners and unique series of point identification (ID) numbers. This gave every data point a unique ID number for digitizing and allowed points to be attributed with individual elevations.

Each point coverage was attributed in INFO from text file tables. The resulting point coverages consisted of map coordinates in digitizer inches with Weber top elevations in feet.

Preprocessing, Structural Modeling, and Graphics Output

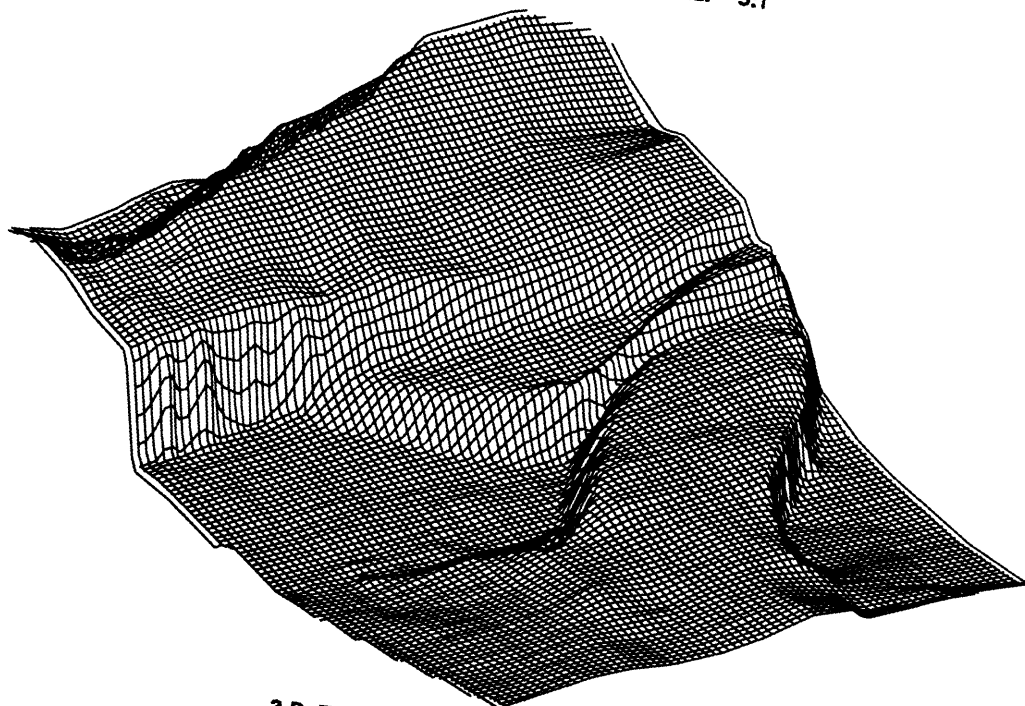
Preprocessing included projection and transformation of the coverages into Universal Transverse Mercator (UTM) coordinates (Zone 12) in ARC. The four coverages were combined into a single coverage (Fig. 6.2). Conversion of the appended coverage into a Triangular Irregular Network (TIN) created a 3-D representation for modeling and

Weber Sandstone Structure - Yampa Graben Area
Colorado and Utah



a)

3-D TIN View from S85E - V.E. 5:1



b)

3-D TIN View from N35E - V.E. 3:1

Figure 6.3 3-D views of the Yampa structure (see text).

projection (Figs. 6.3a, 6.3b). TIN creation produced some edge-effect errors along the outside boundaries of the map, but overall the results appear quite good.

Draping a fishnet surface over the TIN illustrated a well-defined structural surface that could be viewed from different azimuths, altitudes, distances, and vertical exaggerations. Figure 6.3a illustrates the Yampa graben structure viewed from S85E with a vertical exaggeration of about 5:1. Figure 6.3a also displays the trapdoor nature of the Yampa graben structure, the regional south-southwest dip of the strata, as well as the kink-folded Ruple Point anticline between the Red Rock and Mitten Park structures. In addition, the 3-D view illustrates the relatively narrow pop-up and anastomosing nature of the structures.

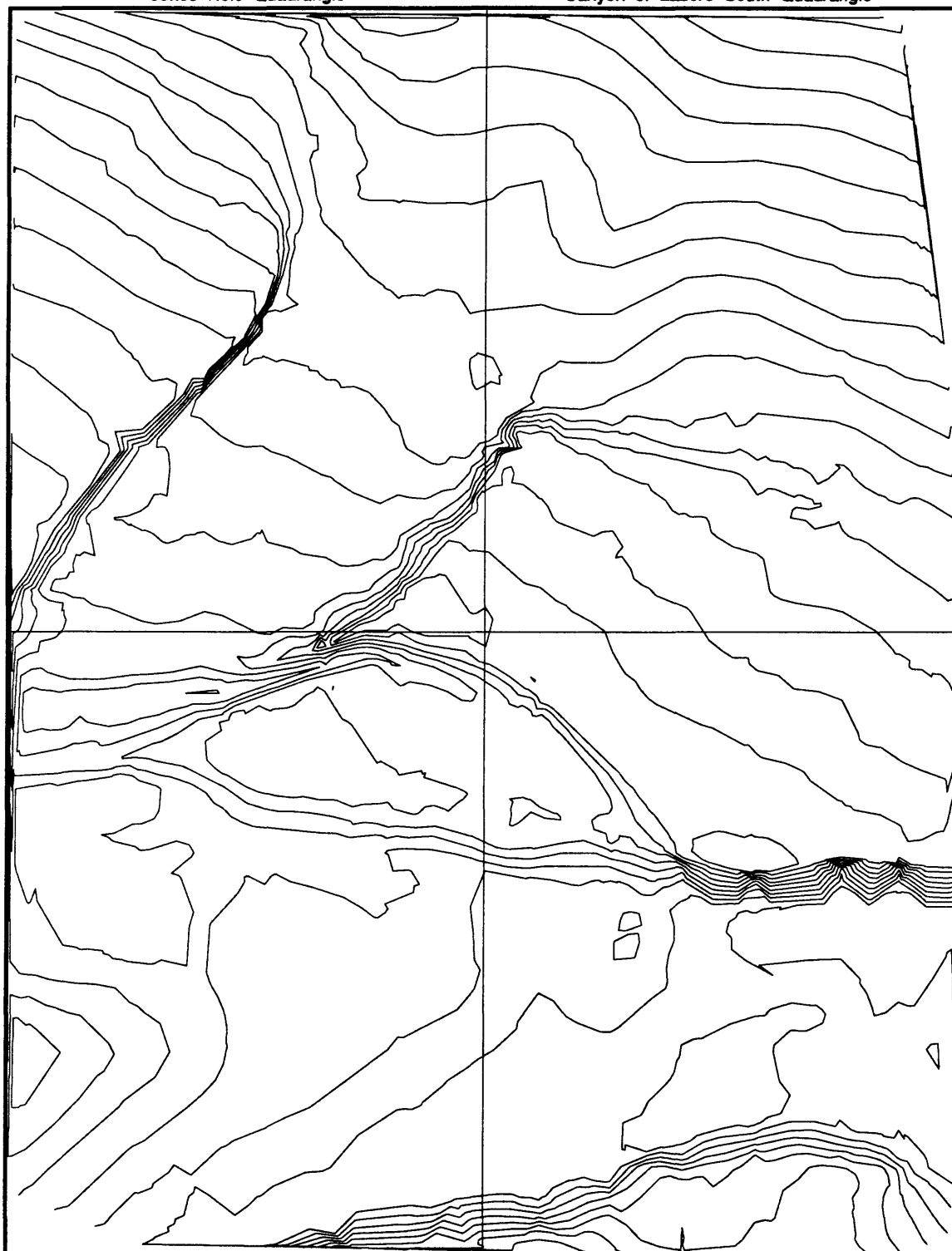
Figure 6.3b gives a second view of the Yampa graben structure viewed from N25E with a vertical exaggeration of about 3:1. This view illustrates the north-northeast trending Mitten Park block bounded by the Mitten Park (left) and Island Park (right) faults as well as the uniform overall uplift along the Yampa system to produce the Blue Mountain highland. The left side of Figure 6.3a and the top of Figure 6.3b shows the continuity of part of the Section Ridge and Mud Springs/Wolf Creek structure.

Conversion of the Yampa graben TIN in ARC to a contour line (arc) coverage provided quantitative definition of the qualitative 3-D projections (Fig. 6.4). Edge-effect errors appear enhanced in the contour coverage, but the arcs could

Weber Sandstone Structure - Yampa Graben Area Colorado and Utah

Jones Hole Quadrangle

Canyon of Lodore South Quadrangle



Stuntz Reservoir Quadrangle

C.I. 500 FT

Hells Canyon Quadrangle

Figure 6.4 Structure contour coverage from ARC/INFO.

be edited to resolve this problem. The contour coverage could be exported as a .DXF file and edited in AUTOCAD. The real world coordinates (in UTM) in the ARC coverage are useful for locating illustrated structural features.

In addition to the features discussed above, the structure contour map defines areas of structural closure. Subsurface anticlinal closures of reservoir rocks such as the Weber Sandstone provide prime targets for hydrocarbon prospects. Anticlinal closures are illustrated on Blue Mountain south of the Yampa fault, northwest of the Mitten Park/Warm Springs corner, and along the Ruple Point anticline. Anticlinal closure is also indicated on the eastern part of Split Mountain in the Stuntz Reservoir quad, but the map edge prevents complete definition of the structure. The structure contours also illustrate the Mitten Park anticlinal trend inverting into a syncline to the northeast. This change suggests that the attenuation of the bounding faults to the north may result from relative rotations of the blocks away from the synclinal axis to the northeast. Indeed, clockwise rotation of the eastern block(s) is indicated by the 3-D restoration in the following chapter.

Chapter 7

THREE-DIMENSIONAL RESTORATION

In contrast to the overall northeasterly shortening and estimated σ_1 observed elsewhere in the Laramide foreland (Molzer, 1993; Erslev, 1993; Wise and Obi, 1994; Selvig, 1994; Gregson and Erslev, 1994), analyses of minor fault data from the southeastern Uinta arch (Chapter 5) indicate a north-northwest σ_1 and shortening across the study area. To test the validity of these results, a three-dimensional (3-D) restoration on the top of the Weber Sandstone was constructed for the Yampa graben area of the surface model illustrated in Chapter 6.

Criteria for 3-D Restoration

Cross section balancing methods provide tests for the plausibility of 2-D structural interpretations under plane strain conditions. Plane strain constraints, however, are but one unique end member of possible fault/fold kinematics. Oblique- and strike-slip motions, which may be the dominant kinematic components in a system, are often not revealed on 2-D sections. In contrast, 3-D restoration provides a test for 2-D interpretations, illustrates the possibility of oblique- or strike-slip, and further restricts geometrically possible structural interpretations. Problems and

constraints for balancing a deformed surface are discussed by Gratier and Guillier (1993).

Most 2-D methods developed for cross section balancing were derived from 3-D properties (Dahlstrom, 1969), and ideally, balanced cross sections provide geometrically possible 2-D interpretations of 3-D structures (Suppe, 1983). Therefore, a set of balanced 2-D interpretations contains an approximation of structural deformation in 3-D. Indeed, a restored series of sequential cross sections constructed parallel to a uni-directional set of slip vectors will give a direct 3-D restoration (Gratier and Guillier, 1993). Since this is rarely the case, however, a network or grid of restorable sections is necessary to approximate the 3-D kinematics.

Method

The 3-D restoration of a deformed stratigraphic surface used in this study is a straight-forward process. An area with definable structural blocks is chosen along with a specific stratum for restoration. Sequential gridded cross sections are constructed and structural domains are defined. Stratum lines are unfolded to an undeformed length along each cross section in each structural domain. The deformed map view of structural domains and cross section lines are digitized in a CAD system at their map scale. The deformed line lengths are added to the original lengths to delineate the shape of the restored domain. The flattened domains are best fit along their borders using trial and error in the

CAD system. Areas of poor fit between domains are evaluated for more complete balancing (if desired). The process can be detailed or general as needed for discrete applications.

The final structural surface restoration results in a precise 3-D interpretation which tests the accuracy of 2-D interpretations, the validity of plane-strain assumptions, and the compatibility of independent strain data (e.g. the resolved stress tensor). The restored surface also gives an estimate of the finite displacement field of the structural domains (Gratier and Guillier, 1993).

Application to the Yampa Graben Structure

The Yampa graben is a compressional trap door structure that is bounded on three sides by the Warm Springs monocline on the north, the Mitten Park fault and monocline on the west, as well as the Yampa fault and Red Rock anticline on the south (Fig. 7.1). The structures are superimposed upon a generally south-southwest regional dip of 5° to 10°. Laramide thrust faults are exposed at Hell's Canyon (Yampa) and at the head of Whirlpool Canyon on the Green River (Mitten Park). With the exception of the intersection between the Yampa fault and Red Rock anticline, the border of the selected study area is relatively undeformed. The area is mapped on the Hells Canyon, Stuntz Reservoir, Jones Hole, and Canyon of Ladore South geologic quadrangles (Hansen and Rowley, 1980a, 1980b; Hansen, 1977a, 1977b). An orthogonal north-south, east-west cross section grid was chosen for the project that generally corresponded with Land

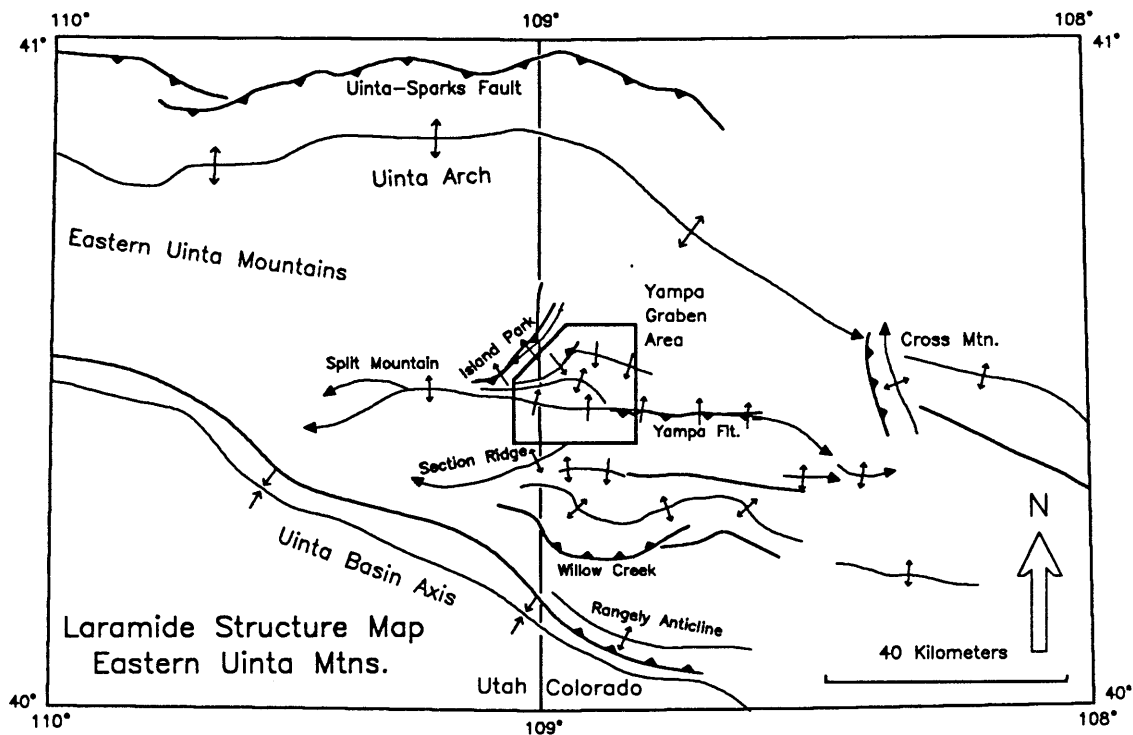


Figure 7.1 Structural location map of the Yampa graben study area and surrounding uplifted structures.

Office Survey section lines with the exception of an existing north-south cross section through Hell's Canyon (Fig. 7.2).

Twenty-six cross sections were constructed to cover the area using the top of the Weber Sandstone as the reference stratum. Many of the sections exhibited little structural relief and were drawn with only the Weber top. Other sections (e.g. the Yampa fault and Red Rock anticlines) required more rigorous interpretations. With the exception of a short northeast-trending segment paralleling the Mitten Park block, the final study area boundaries followed cross section lines (Fig. 7.2). The final project consisted of 10 north-south and 11 east-west cross sections (Figs. 7.3-7.6)

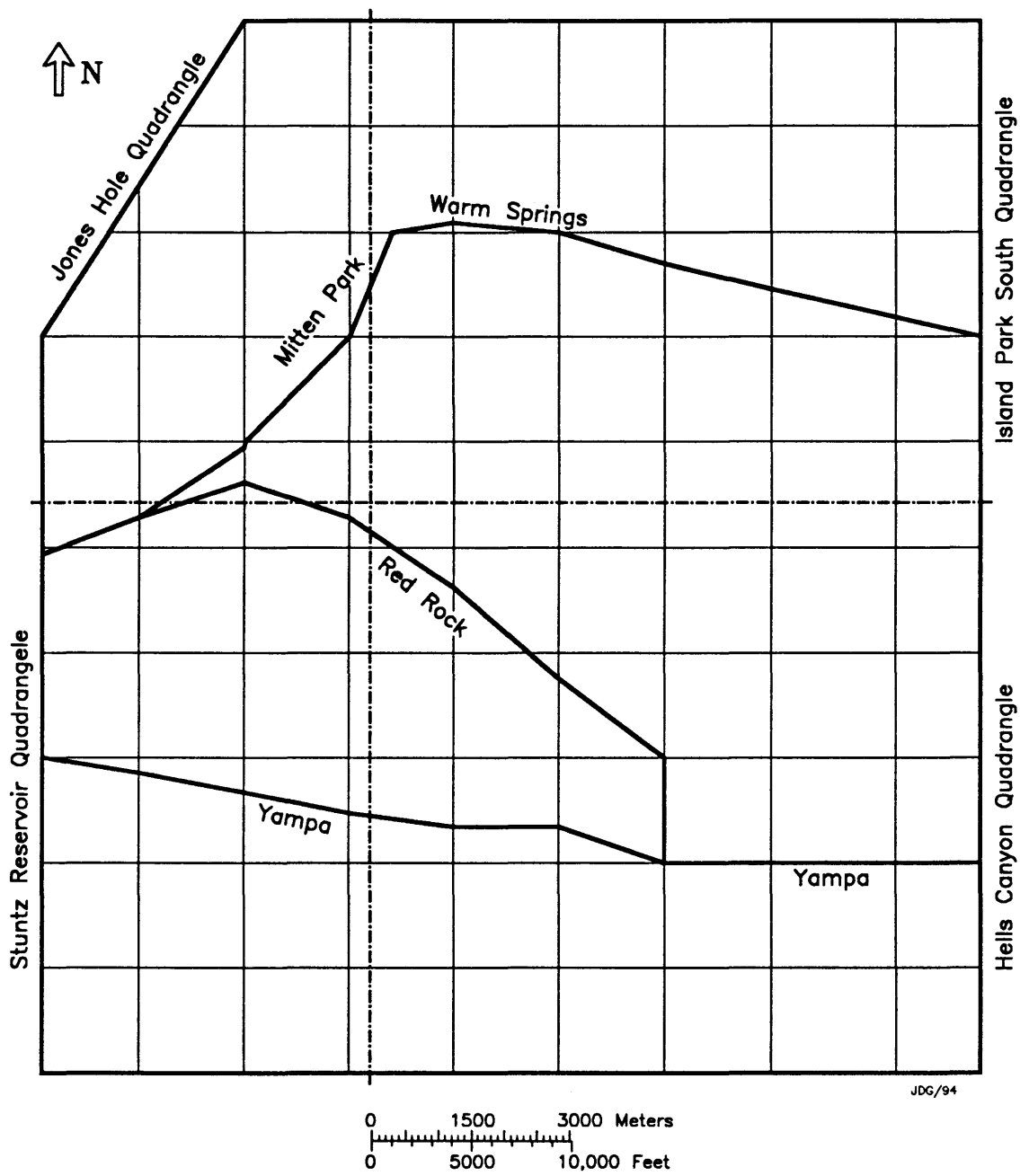


Figure 7.2 Structural domain boundaries and cross section grid used in the 3-D restoration of Yampa graben area.

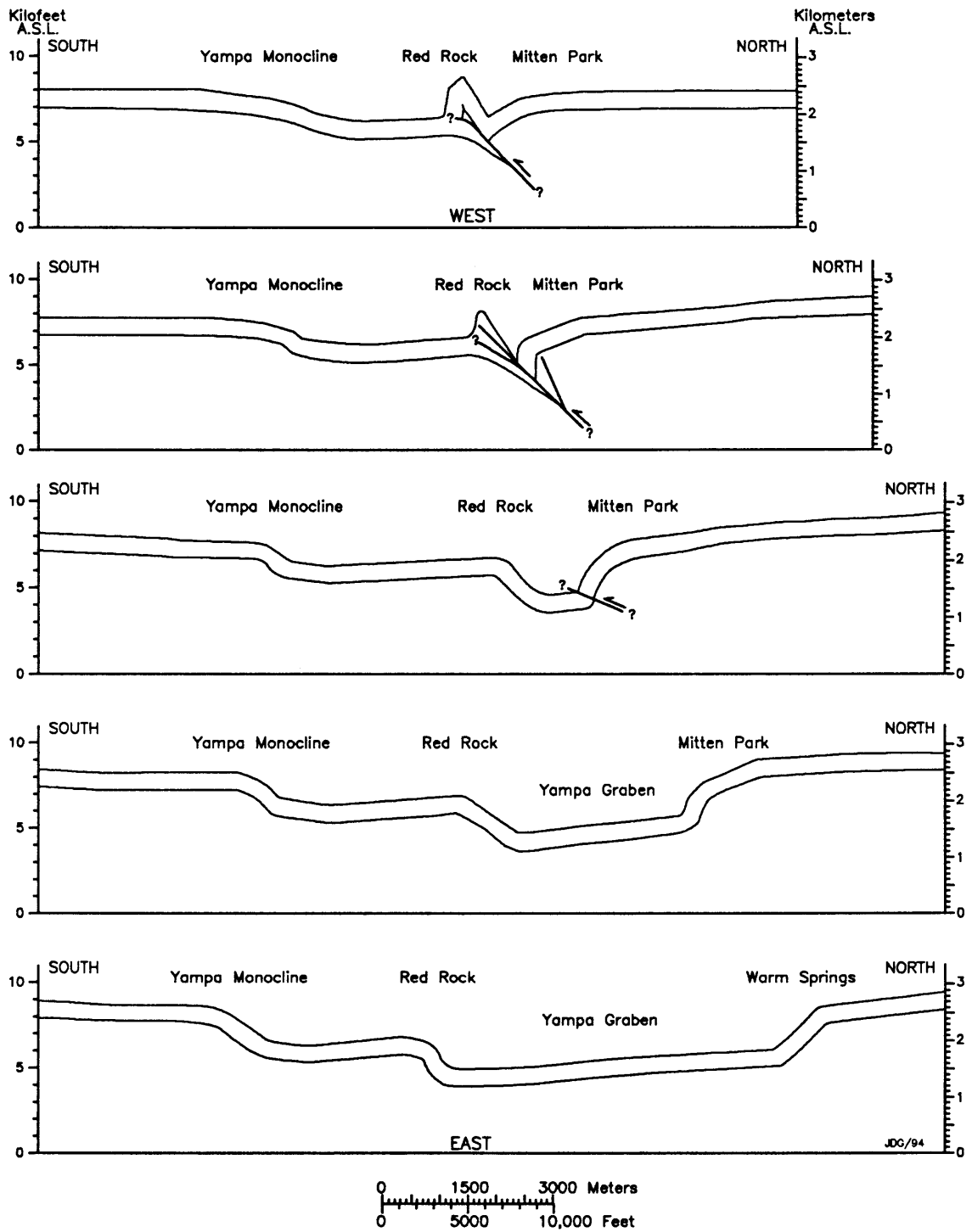


Figure 7.3 North-south structure sections of the Weber Sandstone in the western one-half of the Yampa graben area.

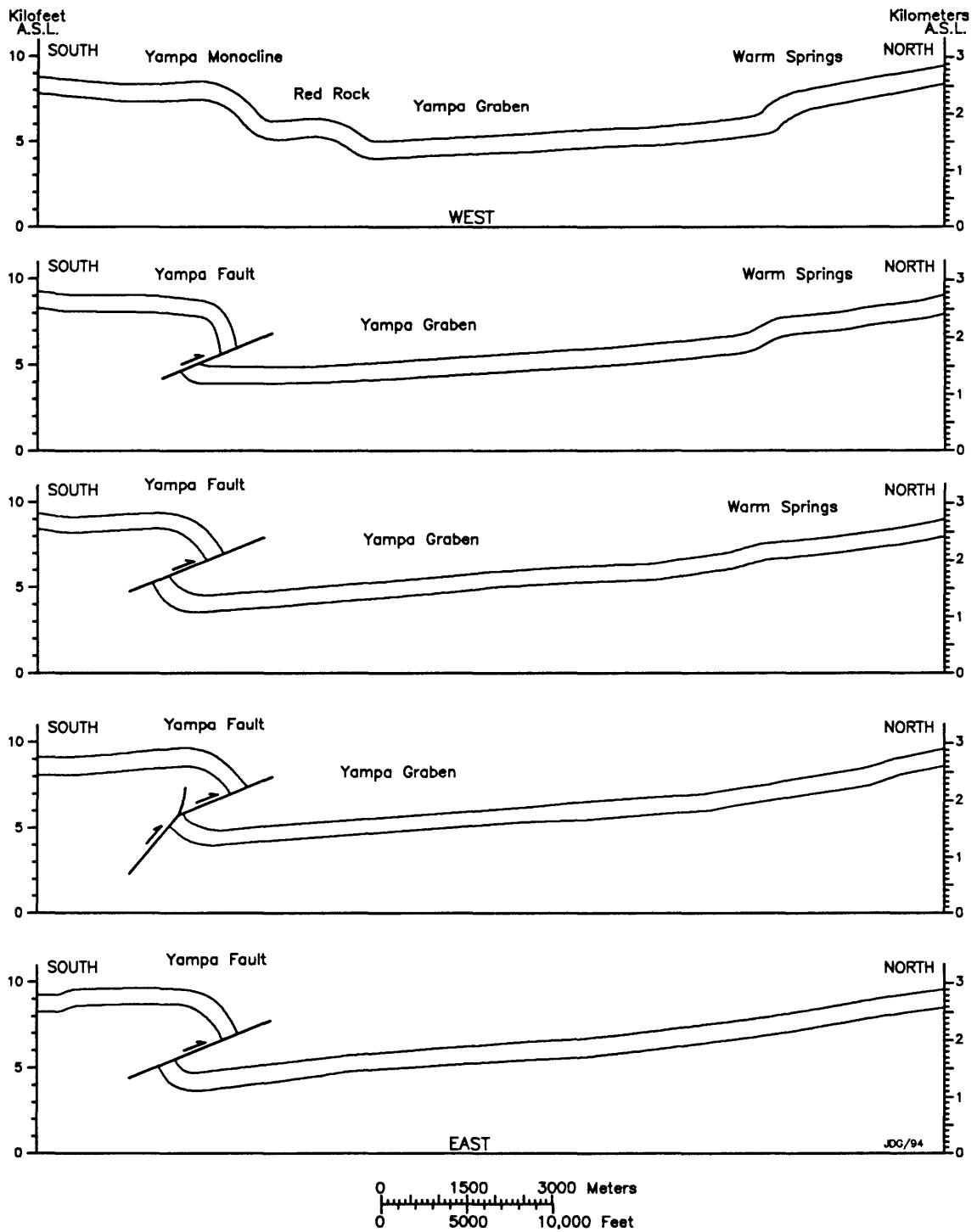


Figure 7.4 North-south structural sections of the Weber Sandstone in the eastern one-half of the Yampa graben area.

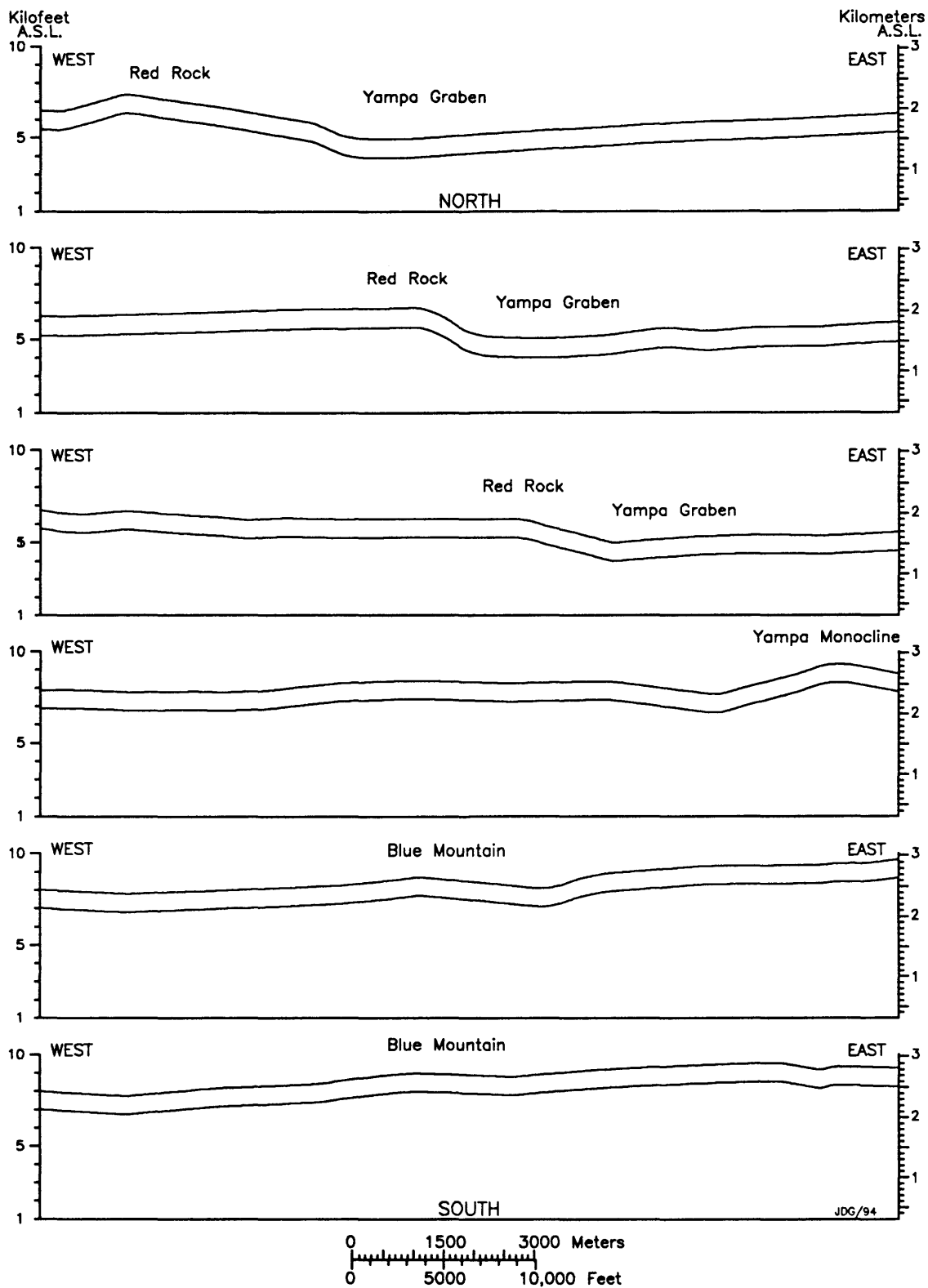


Figure 7.5 East-west structural sections of the Weber Sandstone in the southern one-half of the Yampa graben area.

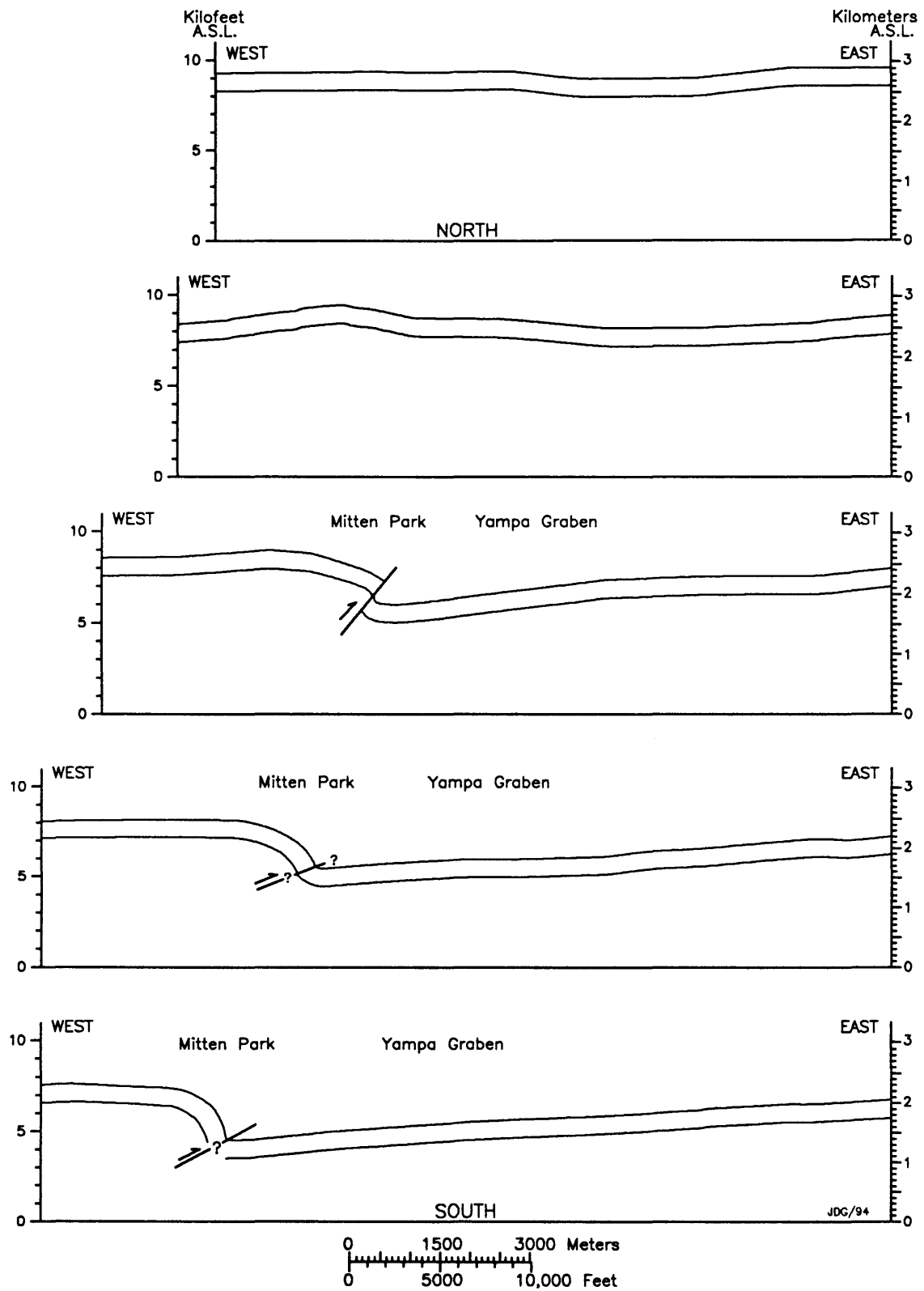


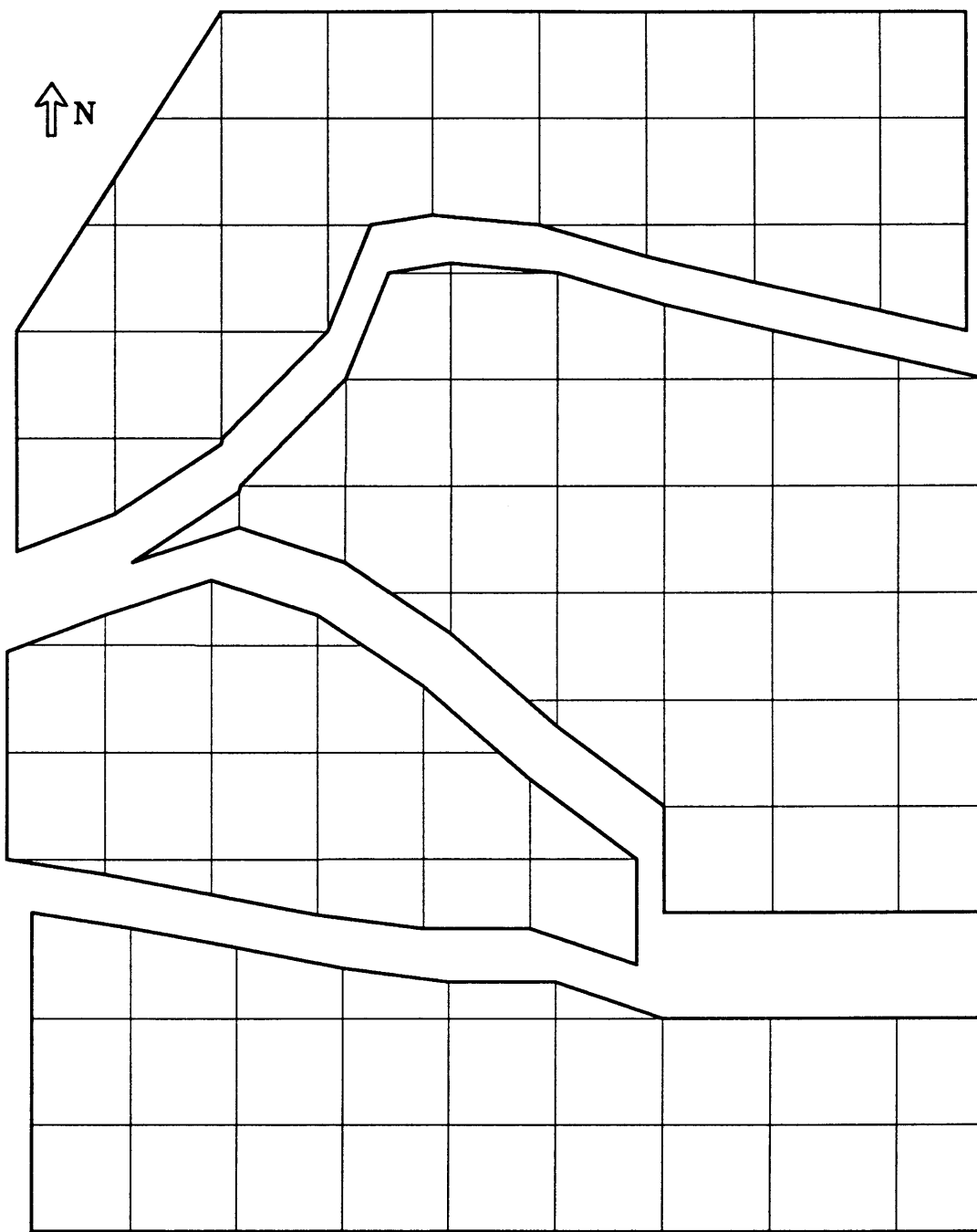
Figure 7.6 East-west structure sections of the Weber Sandstone in the northern one-half of the Yampa graben area.

in an area of about 87.5 square miles.

The project area consisted of four structural domains separated by faults or folds. The Yampa boundary followed the fault trace or the inflection line in the forelimb of the fold where the fault was not exposed. The Red Rock fold splays from the Yampa fault on the east and merges with the Mitten Park fold to the west. The west-northwest trending Warm Springs fold forms a structural corner at its intersection with the Mitten Park fault. The synclinal axes were chosen as the domain boundaries for these blocks to allow an easier transition between structures. The Warm Springs boundary continues from the Mitten Park boundary.

Initially, the project area, structural domains, and cross section grid were sketched and cut out before unfolding the individual domains (Fig. 7.7). After unfolding, the differences between deformed and restored line lengths were added to each domain boundary and resketched as individual blocks (Fig. 7.8). The domains were cut out and fitted into a north-south dip-slip interpretation (Fig. 7.9).

The north-south dip-slip interpretation presented immediate problems. A large gap appeared along the Red Rock anticline, and a smaller gap appeared along the Mitten Park and Warm Springs margins (Fig. 7.9). Revised 2-D interpretations could have corrected the Mitten Park/Warm Springs problems, but significant changes to the sections would have been required to close the Red Rock gap.



JDC/94

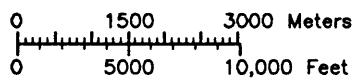


Figure 7.7 Deformed state structural domains in the Yampa graben area separated along faulted and folded boundaries.

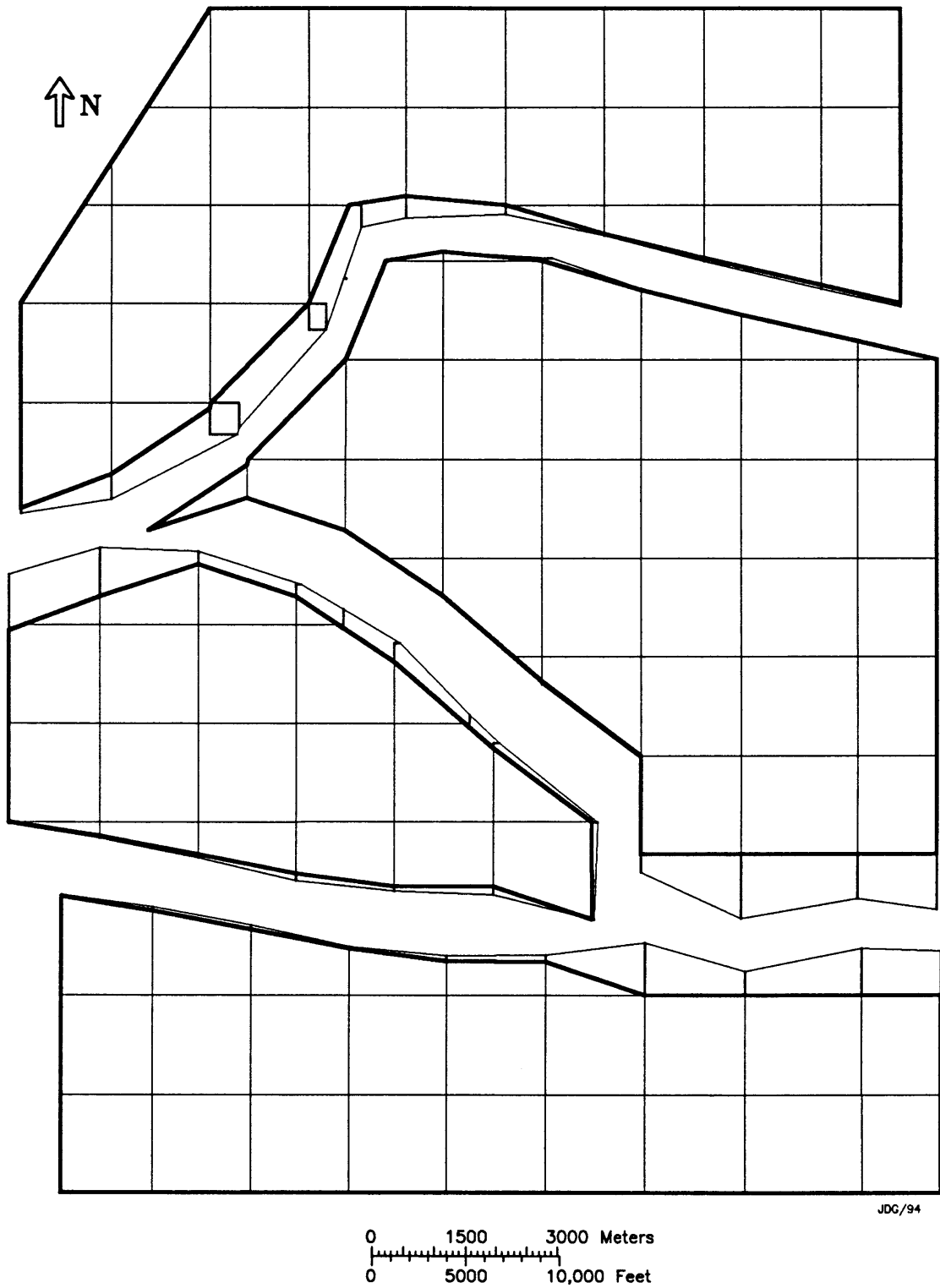
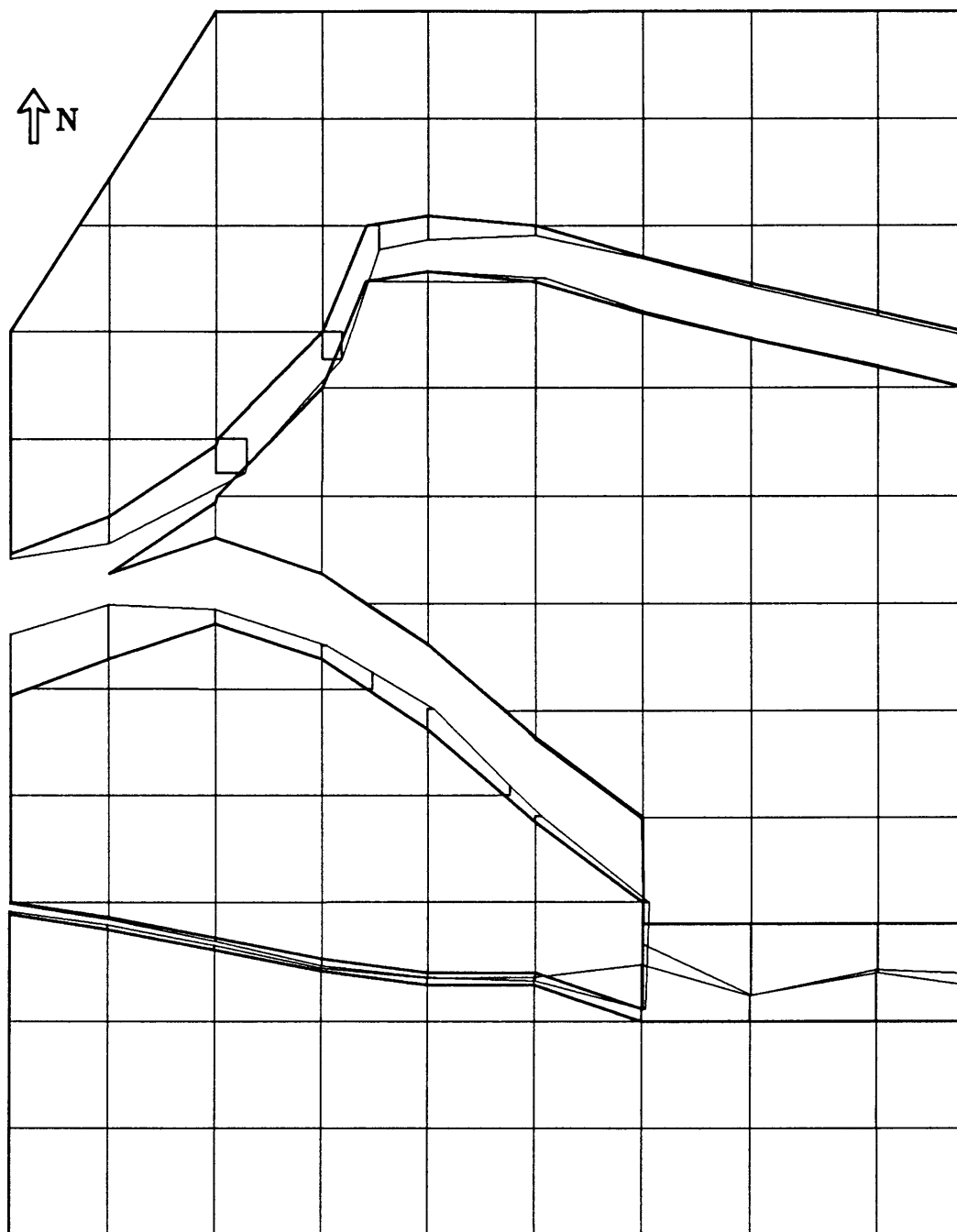


Figure 7.8 Restored state (flattened) structural domains.



JDG/94

0 1500 3000 Meters
 0 5000 10,000 Feet

Figure 7.9 North-south dip-slip interpretation.

With the southern domain fixed, the closest fit of the blocks required small counter-clockwise rotations of the northern domains and a northwestward oblique translation of the combined Red Rock/Yampa block (Fig. 7.10). This construction required the least revision of the 2-D interpretations and was consistent with stress tensors reduced from minor fault data (Chapter 5). The preliminary restoration reflected the usefulness of the 3-D balancing method, and the measurement data were tabulated for entry into an AutoCad drawing.

For entry into AutoCad, the cross section grid became a Cartesian coordinate system in map units and provided X,Y coordinates for drawing the model. The direct entry of drawing coordinates into AutoCad negated the need to hand draw an accurate base map for digitizing. Using measurements in map units directly from the 1:1 cross sections assured that the resulting restoration would be as accurate as the 2-D interpretation measurements.

After entry of the base map, the individual deformed domains were separated, and the domain boundaries were adjusted to a restored interpretation. Restoration of the flattened surface was similar to hand-fitting except that domain rotations could be precisely quantified. The southernmost domain, the Blue Mountain block, remained in its original orientation for a common reference frame.

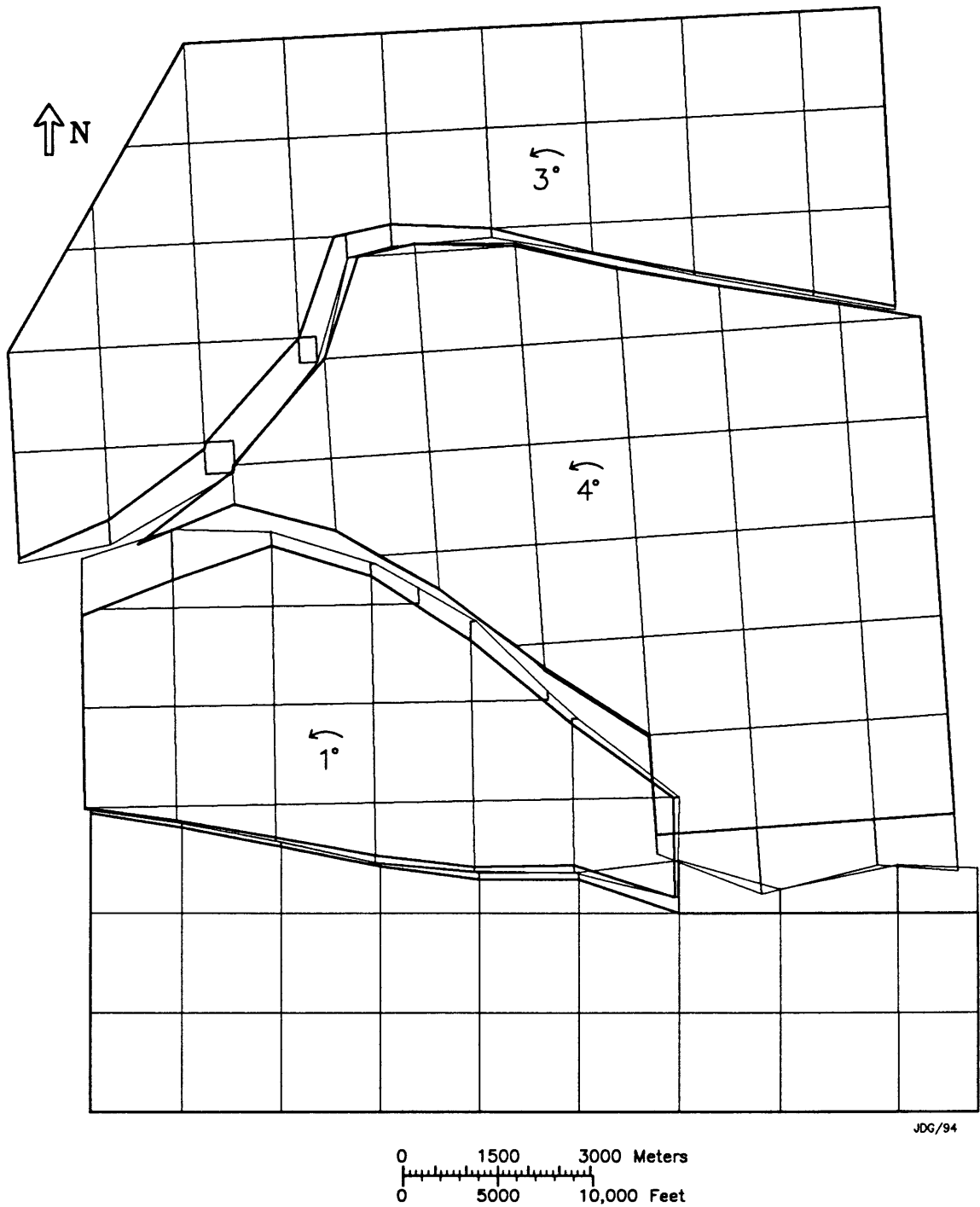


Figure 7.10 Right-lateral oblique-slip interpretation provides the best fit. Counter-clockwise rotations shown.

Discussion

Although not a perfect fit, the final restoration (Fig. 7.10) illustrates northwesterly contraction across the study area. The restoration corresponds well with the composite reduced stress tensors in the Dinosaur study area (Fig. 7.11). The composite estimates of σ_1 from minor fault analyses indicate a σ_1 of about 335-02 (Chapter 5). In addition, composite σ_1 trend estimates range from about 322° (direct inversion) to 342° (slickenlines and M-planes). In comparison, the slip trend from the 3-D restoration varies from about 312° (Warm Springs) to 340° (Yampa fault) in the mapped reference frame (Fig. 7.11). Relative rotations between structural domains might alter this estimate by as much as $\pm 5^\circ$. The 3-D restoration suggests that overall slip in the Yampa graben area closely paralleled the estimated σ_1 directions in the Yampa graben study area (Fig. 7.11).

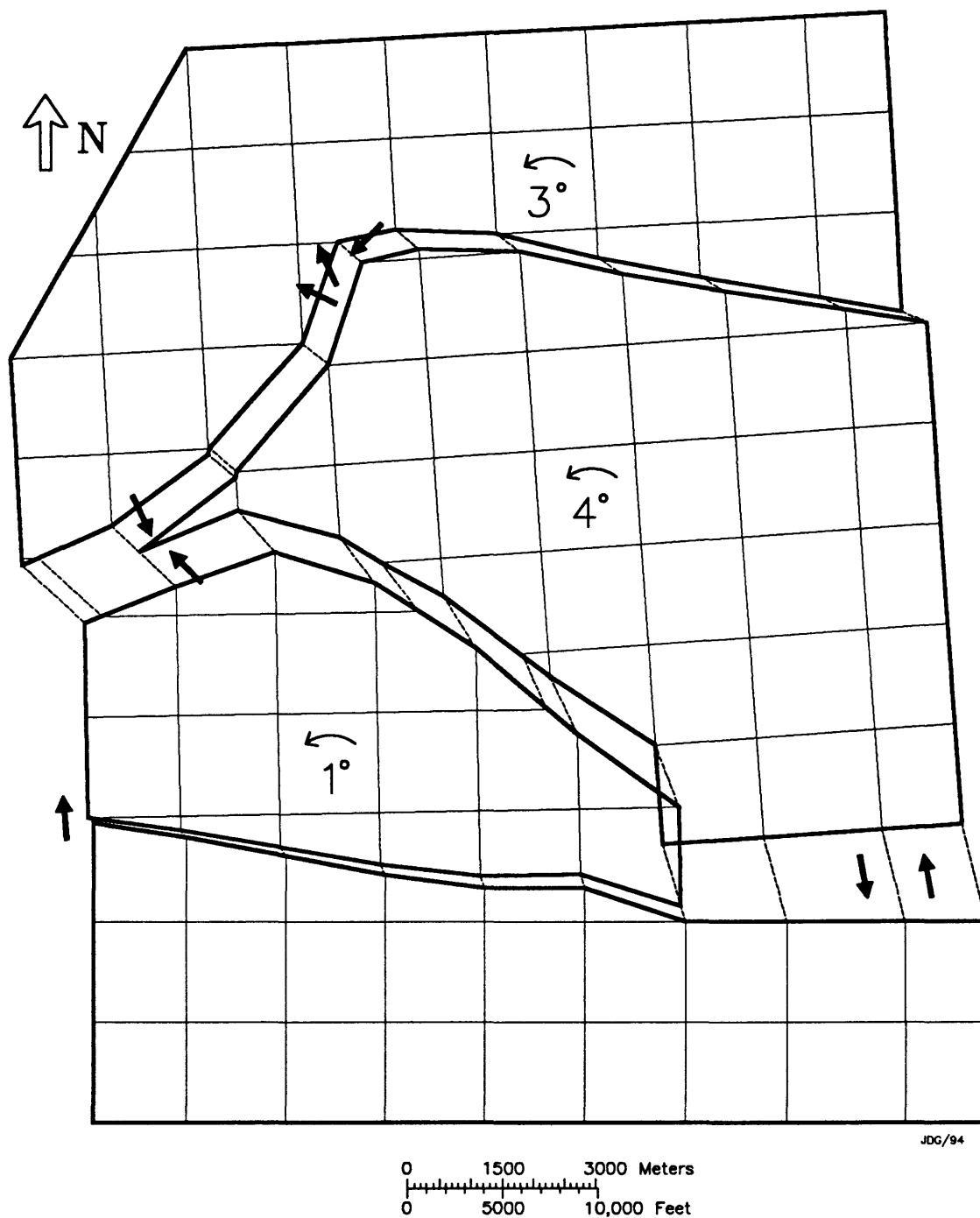


Figure 7.11 Final restoration of the Yampa graben area showing deformed domain boundaries, slip vectors, and resolved σ_1 directions between corresponding points.

Chapter 8

TECTONIC INTERPRETATIONS

Minor fault slip data, paleostress tensor estimates, and a 3-D restoration in the study area suggest that local Laramide structural trends resulted from overall north-northwest contraction. This north-northwest σ_1 direction differs from predictions of tectonic models, results of other kinematic studies in east-west structures, and deformation trends seen elsewhere in the Rocky Mountain foreland (Bergh and Snoke, 1993; Molzer, 1993; Paylor and Yin, 1993; Erslev, 1993). Yet Laramide structural trends along the Uinta-Sparks fault zone and stress estimates from the northern flank (Gregson and Erslev, 1994) are compatible with patterns expected for a northeast-southwest regional σ_1 — not the north-northwest σ_1 determined here (Fig. 2.1). Thus, the observed Laramide kinematics in the southeastern Uinta arch do not appear to be representative of the entire Uinta arch or the foreland in general and probably resulted from more localized processes. Possible causes for local stresses in the study area include bending in the thrust slab over a listric ramp, kinematic interplay between Laramide structures, and east-west compression from the Sevier thrust belt to the west.

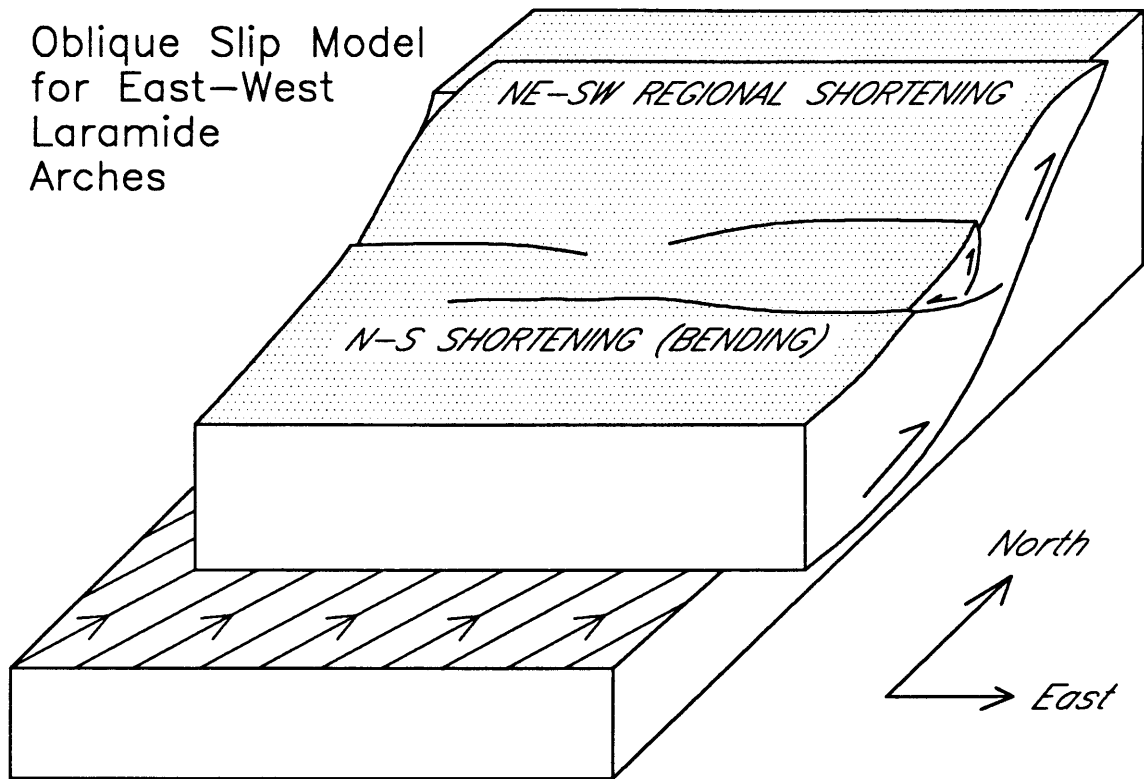


Figure 8.1 Compression in the backlimb due to bending in thrust slab (after Gregson and Erslev, 1994).

Hypothesis 1: Thrusting due to Bending in the Thrust Slab

For most of its length, the northern margin of the Uinta arch trends east-west. The structure verges northward and the 5-10° south-southwest dip of the backlimb strata suggests an underlying, south-dipping, listric master thrust (Figs. 2.1, 2.3). However, in the north-central arch near Flaming Gorge Reservoir, minor fault data indicate northeast oblique-slip across east-west structures (Gregson and Erslev, 1994). Northeast-southwest contraction is also suggested by the northwest trend of the Sparks thrust adjacent to the Sand Wash basin in the northeast Uintas

(Fig. 2.1) Northeast-directed thrusting on a south-dipping listric ramp could result in north-south compression in the monocline along the southern margin of the arch (Fig. 8.1). This model explains the north-south shortening across east-west faults along the southern Uinta arch boundary, but does not explain the north-northwest trending σ_1 and slip observed in the Dinosaur study area.

Hypothesis 2: Kinematic Interplay Between Laramide Structures

Kinematic interplay in Laramide structures includes development of transfer zones, back-thrusts, tear faults, fault imbrication, and possible stress reorientation along faults. East of Dinosaur National Monument, the northeast-verging frontal thrust of the easternmost Uinta arch (Sparks fault zone, Fig. 2.1) is juxtaposed against the southwest-verging frontal thrust of the White River uplift (Danforth Hills anticline/Axial arch, Figs. 2.1, 8.2) (Gries, 1983; Stone, 1986a, 1986b; Morel et al., 1986; Richard, 1986; Irwin, 1986). This juxtaposition may have resulted in a right-lateral transfer zone between the major basin-bounding thrusts. Figure 2.1 displays a complexly-deformed zone between the master thrusts at the Cross and Juniper mountains' pop-up structures.

Strike-slip faulting may locally reorient the regional stress field and strain patterns (Figure 8.3). For example, right wrenching across a north-northeast trending transfer zone could locally reorient σ_1 toward the north-northwest (Fig 8.3). Figure 8.4a schematically illustrates possible

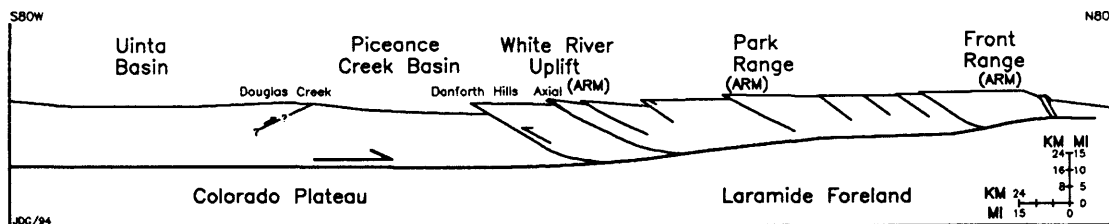


Figure 8.2 East-west crustal scale cross section across northern Colorado from the Uinta basin to east of Ft. Collins (based on interpretation of Erslev, 1993).

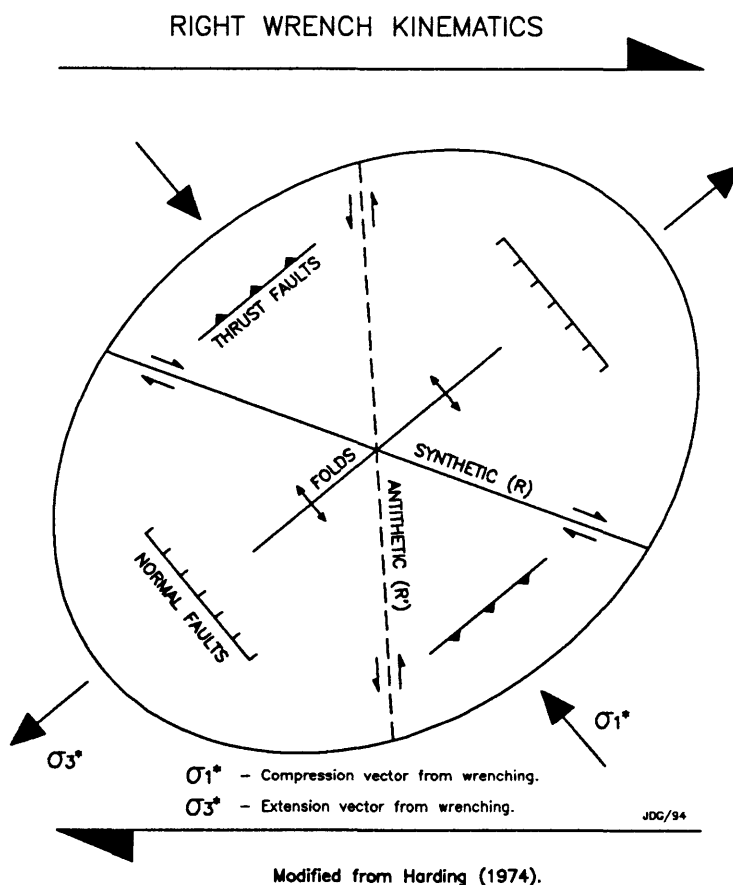
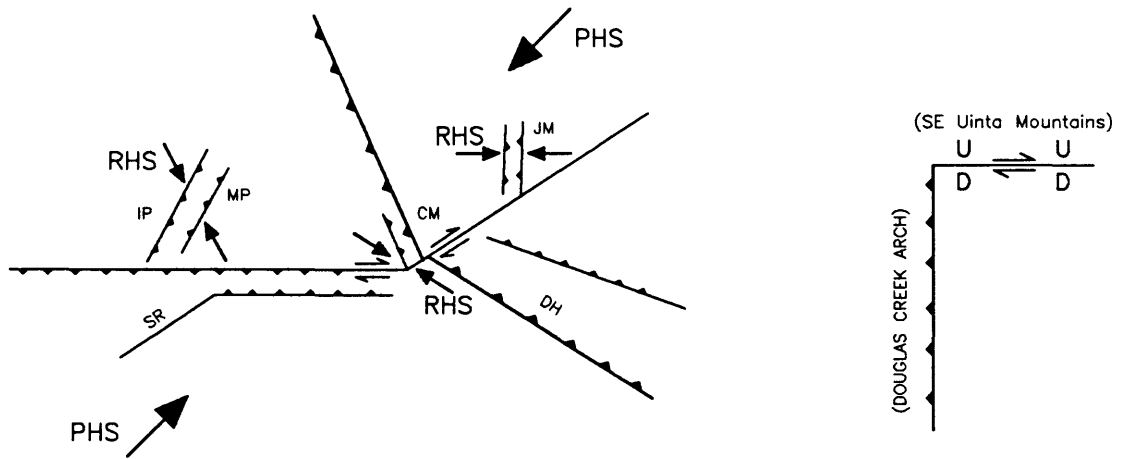


Figure 8.3 Strain ellipse illustrating deformation related to northwest-southeast σ_1 and right wrenching.



PHS—Principal Horizontal Stress RHS—Reoriented Horizontal Stress

a) Local stress reorientation in southeast Uinta Mountains.

b) Right wrench tear at end of thrust fault.

Figure 8.4. Hypothetical Laramide kinematics and tectonics in the southeastern Uinta Mountains. a) and b) Right wrench kinematics in the study area. Island Park (IP), Mitten Park (MP), Section Ridge (SR), Cross Mountain (CM), Juniper Mountain (JM), Danforth Hills (DH) (see text).

slip and stress reorientation in the southeastern Uinta arch due to localized right wrenching. Right-wrench separations and tear faults have been documented between the Beaver Creek and Pagoda thrust-faulted anticlines east of Juniper Mountain (Morel et al., 1986; Figure 2.1). The clockwise rotations on the 3-D restoration of the Yampa graben area are also suggestive of right slip (Chapter 7). In addition, early east-west shortening across the Douglas Creek arch, which may have coincided with uplift of the southeastern Uinta arch, also suggests a component of right slip along the southeastern Uinta margin (Figure 8.4b).

Hypothesis 3: Interaction with the Sevier Thrust Belt

During early Laramide time, the rising Uinta arch interacted with the Sevier thrust belt to the west (Beutner,

1977; Bradley and Bruhn, 1988; Kulik and Schmidt, 1988). Loading by the Sevier thrust belt may have slowed early uplift in the western Uintas, however, and could have contributed additional east-west compression to the Uinta arch. Bradley and Bruhn (1988) used fold axes, spaced cleavage, extension veins, and tension gash bands to determine two phases of folding in the Jurassic Twin Creek Formation of the Mount Raymond thrust adjacent to the northwestern Uinta arch. Based on resolved shortening directions ranging from 265° to 300° for phase I folds and from 343° to 010° for phase II folds, Bradley and Bruhn (1988) hypothesized two possible models for the evolution of the northwestern Uinta arch: 1) dextral wrench strain along the south end of the Hogsback thrust, and 2) dextral transpression along a south-dipping ramp that cut down along (and possibly joined) the northern Uinta boundary system.

The impingement of the Sevier thrusts from the west may have caused eastward translation of the Uinta structural block. Indenting by the Uinta block could have set up left- and right-lateral shear zones along the northern and southern arch boundaries, respectively. This tectonic geometry would have resulted in the respective northeasterly and northwesterly minor fault slip seen in the Uinta arch.

Discussion

This research did not provide unique tests of these hypotheses, and all three mechanisms discussed above may have contributed to the north-northwest shortening in the

study area. However, the effects of north-south compression from bending in the thrust slab combined with the transition in structural vergence between the Uinta and White River arches are favored due to the closer proximity of these processes relative to loading of the Uinta arch by the thrust belt farther to the west.

Implications for Laramide Tectonic Models

Multiple slip directions were not observed in the study area, and the results of this study are consistent with a single extended phase of Laramide contraction in the Dinosaur area. In addition, evidence in the literature for early Laramide deformation along the northern and southeastern Uinta arch as well as for coeval Laramide and Sevier thrusting in the northwestern Uintas (Hansen, 1986b; Johnson and Finn, 1986; Bradley and Bruhn, 1988) does not support models for multiple stress directions in the study area. The determination of north-northwest shortening and σ_1 for the Dinosaur area is not consistent with a left-lateral shear couple along this boundary (Sales, 1968, 1969). In addition, the north-northwest σ_1 trend is incompatible with clockwise rotation of the Colorado Plateau if the structural boundary is placed along the southern Uinta arch (Hamilton, 1988). However, rotation of the Colorado Plateau is still possible if the boundary is placed along the northern margin of the Uinta arch. In this case, the structural patterns generated by rotation of the Colorado Plateau about an Euler pole in central New Mexico

are similar to those generated by regional shortening toward the northeast (Fig. 1.3) (Hamilton, 1988; Brown, 1988; Erslev, 1993). Overall, the shortening, slip, and stress patterns in the eastern Uinta arch appear to be most consistent with localized deformation and stress reorientation during regional northeasterly shortening.

Chapter 9

CONCLUSIONS

Laramide structures in the Dinosaur area follow the east-west trend of the Uinta arch in a complex, anastomosing pattern. The predominant east-west structural grain and thrust geometries reflect north-south contraction in the study area (Berg, 1962; Gries, 1983; Powers, 1986). The Mitten Park, Island Park, and Section Ridge structures trend more southwest-northeast, however, and suggest a component of northwest-southeast shortening (Fig 1.4). Kinematic analyses of minor faults and a 3-D restoration in the Dinosaur area, the focus of this thesis, also indicate north-northwest shortening during Laramide deformation.

The following conclusions are based on the kinematics, surface geology, 3-D restoration, and field observations in the southeastern Uinta Mountains.

1. Eigenvectors of minor fault lineations indicate average shortening at 162-06 with a range from 176-09 (east-west trending structures) to 290-42 (other structures).
2. The composite σ_1 estimate from minor fault data was 335-02 and ranged from 322-04 for direct inversion to 342-03 for the average M-plane.

3. Minor fault slip and σ_1 axial trends average 338° but appear to be partially partitioned into north-south and northwest-southwest components perpendicular to structural trends.
4. Minor fault slip partitioning may be partly due to folding with flexural-slip and inclined shear perpendicular to structural trends.
5. The 3-D restoration indicates northwest to north-northwest shortening ($\approx 312-335^\circ$) and minor clockwise rotations across the Yampa, Red Rock, Mitten Park, and Warm Springs structures.
6. The right-oblique slip indicated by the 3-D restoration is not apparent on 2-D cross sections through the area.
7. Both the minor fault analyses and 3-D restoration indicate overall north-northwest Laramide σ_1 and shortening in the southeastern Uinta Mountains.
8. The north-northwest slip in the study area is not consistent with observations elsewhere in the foreland, including the north-central Uinta arch.
9. Hypotheses for localized north-northwest shortening in the Dinosaur study area include:
 - 1) north-south contraction from bending of the thrust slab over a south-dipping listric ramp during northeasterly thrusting,
 - 2) the complex transition in structural vergence between the Uinta arch and White River uplift, and/or

3) eastward translation of the Uinta block due to impingement of the Sevier thrusts from the west. Although present data are limited, a combination of hypotheses 1 and 2 appear to best explain the observed deformation. The slab-bending and right-wrench transfer zone hypotheses are consistent with northeasterly slip along the northern Uinta arch (Gregson and Erslev, 1994), with secondary processes responsible for the northwesterly slip along the southeastern margin. In addition, multiple slip directions are not seen in the Dinosaur area, and the resolved Laramide stresses are due to both regional and local effects, neither of which can be ignored in kinematic studies of foreland deformation.

Suggestions for Future Work

The hypotheses presented above are consistent with regional structures, a regional northeast-southwest σ_1 , and extended single-phase shortening during the Laramide. Additional detailed kinematic analyses are needed along the northeast, northwest, and southwest Uinta arch as well as other margins of the Colorado Plateau to further define the role of these structural units in Laramide tectonics. The slab-bending and right-wrench transfer zone hypotheses suggest predominant northeasterly slip all along the northern Uinta arch with north-south or northeasterly slip along the southwestern margin. In contrast, eastward translation of the Uinta block suggests northwesterly slip all along the southern arch margin. In either case, less

complex margins of the Colorado Plateau, such as the east-central and southeast White River uplift, should also record northeasterly slip.

Further insights into the kinematics of the north-northwest shortening in the study area could be tested with a 3-D restoration of the transition zone between the Uinta and White River arches. Detailed kinematic studies of other northeast trending and/or complexly deformed Laramide structures, such as the San Rafael, Hartville, Park/Gore Range, and northern Laramie arches, are also needed to more fully understand the reasons for the diversity in Laramide structural trends.

REFERENCES

- Allmendinger, R.W., J.W. Gephart, and R.A. Marrett, 1989, Notes on fault slip analysis: in A short course on quantitative interpretation of joints and faults, GSA, p. 1-68.
- Angelier, J., 1990, Inversion of field data in fault tectonics to obtain the regional stress--III. A new rapid direct inversion method by analytical means: *Geophysical Journal International*, v. 103, p. 363-379.
- _____, and P. Mechler, 1977, Sur une methode graphique de recherche des contraintes principales egalment utilisable en tectonique et en seismologie: La methode des diedres droits: *Bulletin de Societie Geologique de France*, v. 19, p. 1309-1318.
- Berg, R.R., 1962, Mountain flank thrusting in Rocky Mountain foreland, Wyoming and Colorado: *AAPG Bull.*, v. 46, no. 11, p. 2019-2032.
- Bergh, S.G., and A.W. Snoke, 1992, Polyphase Laramide deformation in the Shirley Mountains, south-central Wyoming foreland: *The Mountain Geologist*, v. 29, no. 3, p. 85-100.
- Beutner, E.C., 1977, Causes and consequences of curvature in the Sevier orogenic belt, Utah to Montana: in E.L. Heisey et al, eds., *Rocky Mountain thrust belt geology and resources*, WGA-MGS-UGS, p. 353-366.
- Bradley, M.D., and R.L. Bruhn, 1988, Structural interactions between the Uinta arch and the overthrust belt, north-central Utah; Implications of strain trajectories and displacement modeling: in C.J. Schmidt and W.J. Perry, Jr., eds., *Interaction of the Rocky Mountain foreland and the Cordilleran thrust belt*, GSA Memoir 171, p. 431-446.
- Brown, W.G., 1988, Deformational style of Laramide uplifts in the Wyoming foreland: in Schmidt, C.J., and W.J. Perry, Jr., eds., 1988, *Interaction of the Rocky Mountain foreland and the Cordilleran thrust belt*: GSA Memoir 171, p. 1-26.
- Bryan, P., and R.G. Gordon, 1990, Rotation of the Colorado Plateau: an updated analysis of paleomagnetic poles: *Geophysical Research Letters*, v. 17, p. 1501-1504.

- Bryant, B., and D.J. Nichols, 1988, Late Mesozoic and early Tertiary reactivation of an ancient crustal boundary along the Uinta trend and its interaction with the Sevier orogenic belt: in C.J. Schmidt and W.J. Perry, Jr., eds., Interaction of the Rocky Mountain foreland and the Cordilleran thrust belt, GSA Memoir 171, p. 411-430.
- Chapin, C.E., and S.M. Cather, 1983, Eocene tectonics and sedimentation in the Colorado Plateau - Rocky Mountain area: in J.D. Lowell, ed., Rocky Mountain foreland basins and uplifts, RMAG Guidebook, p. 33-56.
- Charlesworth, H., T. Villemin, and E.A. Erslev, 1993, Short course on some applications of IBM-PC compatible microcomputers in structural geology: Geological Association of Canada, 157 p.
- Cullins, H.L., 1968, Geologic map of the Banty Point Quadrangle, Rio Blanco County, Colorado: USGS Geologic Quadrangle Map GQ-703, scale 1:24,000.
- _____, 1969, Geologic map of the Mellen Hill Quadrangle, Rio Blanco and Moffat counties, Colorado: USGS Geologic Quadrangle Map GQ-835, scale 1:24,000.
- _____, 1971, Geologic map of the Rangely Quadrangle, Rio Blanco County, Colorado: USGS Geologic Quadrangle Map GQ-903, scale 1:24,000.
- Dahlstrom, C.D.A., 1969, Balanced cross sections: Canadian Journal of Earth Sciences, v. 6, p. 743-757.
- Davis, J.C., 1986, Statistics and data analysis in geology: New York, Wiley and Sons, 646 p.
- Dickinson, W.R., M.A. Klute, M.J. Hayes, S.U. Janecke, E.R. Lundin, M.A. McKittrick, and M.D. Olivares, 1988, Paleogeographic and paleotectonic setting of Laramide sedimentary basins in the central Rocky Mountain region: GSA Bull., v. 100, p. 1023-1039.
- Donath, F.A., 1970, Some information squeezed out of rock: American Scientist, v. 58, p. 54-72.
- Dupin, J.M., W. Sassi, and J. Angelier, 1993, Homogeneous stress hypothesis and actual fault slip: a distinct element analysis: Journal of Structural Geology, v. 15, no. 8, p. 1033-1044.
- Erslev, E.A., 1986, Basement balancing of Rocky Mountain foreland uplifts: Geology, v. 14, no. 3, p. 259-262.

Erslev, E.A., 1991, Trishear fault-propagation folding: *Geology*, v. 19, p. 617-620.

_____, 1993, Laramide basement tectonics: in C.J. Schmidt, R. Chase, and E.A. Erslev, eds., Laramide basement deformation in the Rocky Mountain foreland of the western United States, GSA Special Paper 280, p. 339-358.

_____, J.L. Rogers, and M. Harvey, 1988, The northeastern Front Range revisited: Compression and crustal wedging in a classic locality for vertical tectonics: in G.S. Holden, ed., GSA Field Trip Guidebook 1988, Colorado School of Mines Professional Contribution 12, p. 122-133.

_____, and J.L. Rogers, 1993, Basement-cover geometry of Laramide fault-propagation folds: in C.J. Schmidt, R. Chase, and E.A. Erslev, eds., Laramide basement deformation in the Rocky Mountain foreland of the western United States, GSA Special Paper 280, p. 339-358.

Goldstein, A., and S. Marshak, 1988, Analysis of fracture array geometry: in S. Marshak, and G. Mitra, eds., Basic methods of structural geology, Englewood Cliffs, Prentice-Hall, p. 249-267.

Gratier, J.P., and B. Guillier, 1993, Compatibility constraints on folded and faulted strata and calculation of total displacement using computational restoration (UNFOLD) program: *Journal of Structural Geology*, v. 15, nos. 3-5, p. 391-402.

Gregson, J.D., and E.A. Erslev, 1994, Heterogeneous Laramide deformation in Rocky Mountain foreland arches (abstract): AAPG Annual Convention Official Program, Vol. 3, p. 158.

Gries, R. 1983, North-south compression of Rocky Mountain foreland structures: in J.D. Lowell, ed., Rocky Mountain Foreland Basins and Uplifts, RMAG Symposium, p. 9-32.

Hamilton, W.B., 1981, Plate-tectonic mechanism of Laramide deformation: *University of Wyoming Contributions to Geology*, v. 19, p. 87-92.

_____, 1988, Laramide crustal shortening: in C.J. Schmidt and W.J. Perry, Jr., eds., Interaction of the Rocky Mountain foreland and the Cordilleran thrust belt, GSA Memoir 171, p. 27-39.

Hansen, W.R., 1955, Geology of the Flaming Gorge Quadrangle, Utah-Wyoming: USGS Geologic Quadrangle Map GQ-75, scale 1:24,000.

_____, 1977a, Geologic map of the Jones Hole Quadrangle, Uinta County, Utah, and Moffat County, Colorado: USGS Geologic Quadrangle Map GQ-1401, scale 1:24,000.

_____, 1977b, Geologic map of the Canyon of Ladore South Quadrangle, Moffat County, Colorado: USGS Geologic Quadrangle Map GQ-1408, scale 1:24,000.

_____, 1986a, Neogene tectonics and geomorphology of the eastern Uinta Mountains in Utah, Colorado, and Wyoming: USGS Prof. Paper 1356, 78 p.

_____, 1986b, History of faulting in the eastern Uinta Mountains, Colorado and Utah: in D.S. Stone, ed., New interpretations of northwest Colorado geology, RMAG, p. 229-246.

_____, and P.E. Carrera, 1980, Geologic map of the Tanks Peak Quadrangle, Moffat County, Colorado: USGS Geologic Quadrangle Map GQ-1534, scale 1:24,000.

_____, P.E. Carrera, and P.D. Rowley, 1980, Geologic map of the Haystack Rock Quadrangle, Moffat County, Colorado: USGS Geologic Quadrangle Map GQ-1535, scale 1:24,000.

_____, P.E. Carrera, and P.D. Rowley, 1983, Geologic map of Dinosaur National Monument and vicinity, Utah and Colorado: USGS Miscellaneous Investigations Map I-1407, scale 1:50,000.

_____, and P.D. Rowley, 1980a, Geologic map of the Stuntz Reservoir Quadrangle, Utah-Colorado: USGS Geologic Quadrangle Map GQ-1530, scale 1:24,000.

_____, and P.D. Rowley, 1980b, Geologic map of the Hells Canyon Quadrangle, Moffat County, Colorado: USGS Geologic Quadrangle Map GQ-1536, scale 1:24,000.

Harding, T.P., 1974, Petroleum traps associated with wrench faults: AAPG Bull., v. 58, p. 1290-1304.

Irwin, C.D., 1986, Upper Cretaceous and Tertiary cross sections, Moffat County, Colorado: in D.S. Stone, ed., New interpretations of northwest Colorado geology, RMAG, p. 151-156.

- Johnson, R.C., and T.M. Finn, 1986, Cretaceous through Holocene history of the Douglas Creek arch, Colorado and Utah, in D.S. Stone, ed., New interpretations of northwest Colorado geology, RMAG, p. 77-96.
- Kulik, D.M., and C.J. Schmidt, 1988, Region of overlap and styles of interaction of Cordilleran thrust belt and Rocky Mountain foreland: in C.J. Schmidt and W.J. Perry, Jr., eds., Interaction of the Rocky Mountain foreland and the Cordilleran thrust belt, GSA Memoir 171, p. 75-98.
- Lisle, R.J. 1987, Principal stress orientations from faults: an additional constraint: Ann. Tectonicae 1, p. 155-158.
- Molzer, P.C., 1993, Oblique slip in east-west Laramide foreland arches: unpublished M.S. thesis, Colorado State University, 156 p.
- Morel, J.A., P.H. Bursk, and D.L. Dlouhy, 1986, An interpretation of the subsurface structural style of the Beaver Creek anticline, Moffat and Routt Counties, Colorado: in D.S. Stone, ed., New interpretations of northwest Colorado geology, RMAG, p. 195-202.
- Paylor, E.D., II, and A. Yin, 1993, Left-slip evolution of the North Owl Creek fault system, Wyoming, during Laramide shortening: in Schmidt, C.J., R.B. Chase, and E.A. Erslev, eds., 1993, Laramide basement deformation in the Rocky Mountain foreland of the western United States: GSA Special Paper 280, p. 229-242.
- Perry, W.J., Jr., D.J. Nichols, T.S. Dyman, and C.J. Haley, 1992, Sequential Laramide deformation of the Rocky Mountain foreland of southwestern Montana, Wyoming, and north-central Colorado: USGS Bull. 2012, 14 p.
- Petit, J.P., 1987, Criteria for the sense of movement on fault surfaces in brittle rocks: J. Str. Geol., v. 9(5/6), p. 597-608.
- Pollard, D.D., S.D. Saltzer, and A.M. Rubin, 1993, Stress inversion methods: are they based on faulty assumptions?: Journal of Structural Geology, v. 15, no. 8, p. 1045-1044.
- Powers, R.B., 1986, The Willow Creek fault, eastern Uinta Mountains—geologic analysis of a foreland subthrust play: in D.S. Stone, ed., New interpretations of northwest Colorado geology, RMAG, p. 183-190.

- Richard, J.J., 1986, Interpretation of a seismic section across the Danforth Hills anticline (Maudlin Gulch) and Axial arch in northwest Colorado: in D.S. Stone, ed., New interpretations of northwest Colorado geology, RMAG, p. 191-195.
- Ritzma, H.R., 1969, Tectonic resume, Uinta Mountains: in J.B. Lindsey, ed., Geologic Guidebook of the Uinta Mountains, p. 57-63.
- _____, 1971, Faulting on the north flank of the Uinta Mountains, Utah and Colorado: in A.R. Renfro, ed., Wyoming Tectonics Symposium, 23rd Field Conf., Wyoming Geological Association, p. 145-150.
- Robbins, E.A., 1987, Laramide structural geometry of the northwestern Beartooth Mountains, Montana: M.S. Thesis, Colorado State University, Fort Collins, Colorado.
- Rowley, P.D., J.R. Dyni, W.R. Hansen, and G.N. Pipiringos, 1979, Geologic map of the Indian Water Canyon Quadrangle, Moffat County, Colorado: USGS Geologic Quadrangle Map GQ-1516, scale 1:24,000.
- Rowley, P.D., and, W.R. Hansen, 1979, Geologic map of the Split Mountain Quadrangle, Uintah County, Utah: USGS Geologic Quadrangle Map GQ-1515, scale 1:24,000.
- Rowley, P.D., D.M. Kinney, and W.R. Hansen, 1979, Geologic map of the Dinosaur Quarry Quadrangle, Uintah County Utah: USGS Geologic Quadrangle Map GQ-1513, scale 1:24,000.
- Rowley, P.D., W.R. Hansen, O. Tweto, and P.E. Carrara, 1985, Geologic map of the Vernal 1° X 2° quadrangle, Colorado, Utah, and Wyoming: USGS Misc. Inv. Series Map I-1526, scale 1:250,000.
- Sales, J.K., 1968, Crustal mechanics of Cordilleran foreland deformation: A regional and scale model approach: AAPG Bull., v. 52, no. 10, p. 2016-2044.
- _____, 1969, Regional tectonic setting and mechanics of origin of the Uinta uplift: in J.B. Lindsey, ed., Geologic Guidebook of the Uinta Mountains, p. 65-78.
- _____, 1971, Structure of the northern margin of the Green River basin, Wyoming: in A.R. Renfro, ed., Wyoming Tectonics Symposium, 23rd Field Conf., Wyoming Geological Association, p. 85-102.
- Selvig, B.W., 1994, Kinematics and structural models of faulting adjacent to the Rocky Flats Plant, central

Colorado: unpublished M.S. thesis, Colorado State University, 133 p.

Steiner, M.B., 1983, Mesozoic apparent polar wander and plate motions of North America: in M.W. Reynolds and E.D. Dolly, eds., Mesozoic Paleogeography of the West-Central United States, SEPM, p. 1-11.

Stone, D.S., 1986a, Seismic and borehole evidence for important pre-Laramide faulting along the Axial Arch in northwest Colorado: in D.S. Stone, ed., New interpretations of northwest Colorado geology, RMAG, p. 19-36.

_____, 1986b, Geology of the Wilson Creek Field, Rio Blanco County, Colorado: in D.S. Stone, ed., New interpretations of northwest Colorado geology, RMAG, p. 229-246.

_____, 1986c, Rangely field summary: 2. Seismic profile, structural cross section, and geochemical comparisons: in D.S. Stone, ed., New interpretations of northwest Colorado geology, RMAG, p. 226-228.

_____, 1993a, Tectonic evolution of the Uinta Mountains: palinspastic restoration of a structural cross section along longitude 109° 15', Utah: Misc. Pub. 93-8, Utah Geol. Survey, 19 p., 3 plates.

_____, 1993b, Basement-involved thrust-generated folds as seismically imaged in the subsurface of the Rocky Mountain foreland: in Schmidt, C.J., R.B. Chase, and E.A. Erslev, eds., 1993, Laramide basement deformation in the Rocky Mountain foreland of the western United States: GSA Sp. Paper 280, p. 271-317.

Suppe, J., 1983, Geometry and kinematics of fault-bend folding: American Jour. of Science, v. 283, p. 684-721.

Villemin, T., and H. Charlesworth, 1991, Stress Version 1.6 (computer program): Dept. of Geol., Univ. of Alberta, Edmonton, Alberta.

Vollmer, F.W., 1989, Orient Version 1.2 orientation data analysis program user's manual: Kingston, New York, St. Univ. of N.Y., 26 p.

_____, 1993, Slick Contour 1.2 (computer program): Crestline Software.

Wise, D.U., and C.M. Obi, 1994, Laramide basement deformation in an evolving stress field, Bighorn Mountain front, Five Springs area, Wyoming: Reply: AAPG Bull. v. 78, no. 4, p. 652-655.

APPENDIX

Data from this thesis is available on 3.25 inch disks in LOTUS format and may be obtained from:

Dr. Eric A. Erslev
Department of Earth Resources
Fort Collins, CO 80523
(303) 491-5661